2022

Formulation, Structure, and Applications of Therapeutic, Amino Acid, and Water-Based Deep Eutectic Solvents

MD Sajjadur Rahman

FORMULATION, STRUCTURE, AND APPLICATIONS OF THERAPEUTIC, AMINO ACID, AND WATER-BASED DEEP EUTECTIC SOLVENTS

BY

MD SAJJADUR RAHMAN

A dissertation submitted in partial fulfilment of the requirements for the

Doctor of Philosophy

Major in Chemistry

South Dakota State University

2022

DISSERTATION ACCEPTANCE PAGE
MD SAJJADUR RAHMAN

This dissertation is approved as a creditable and independent investigation by a candidate for the Doctor of Philosophy degree and is acceptable for meeting the dissertation requirements for this degree. Acceptance of this does not imply that the conclusions reached by the candidate are necessarily the conclusions of the major department.

Douglas Raynie
Advisor Date

Douglas Raynie
Department Head Date

Nicole Lounsbery, PhD
Director, Graduate School Date

ACKNOWLEDGEMENTS

I am grateful to Almighty for taking the front seat of my Ph.D. education in the United States. There are literally a number of people involved in the fulfillment of this dissertation work. List they remain unnoticed. I would like to devote some space here to acknowledge their valuable contribution.

I would like to express my gratitude to my advisor, Dr. Douglas E Raynie for sharing his vast knowledge in analytical chemistry and for his never-ending support and encouragement all through. His strong belief in science combined with a systematic approach, tremendous enthusiasm, and convivial criticism has been of great help and a real inspiration to me. I would like to thank the members of my graduate committee, Dr. Brian Logue, Dr. Fathi Halaweish, and Dr. Andrea Bjornstad for their encouragement, useful comments, remarks, and engagement through the entire learning process. Besides, I would like to express my gratitude to my advisor for the computational studies, Dr. Mohammad A. Halim, Assistant Professor of Chemistry and Biochemistry, Kennesaw State University, Georgia, USA for his endless support, encouragement and mentoring me for such a long time.

I find no words to express my thanks to my wife Hazera Khatun Koly, who has encouraged and supported me through these tough times nothing could have been possible without her affection and encouragement.

I am forever indebted to my parents Mr. Md. Daudur Rahman and Mrs. Asma Rahman for their encouragement, prayers, and support throughout my education. I am thankful to my siblings Samsun Naher Laboni and Nafia Rahman for your endless love and support.

I would also want to thank the Department of Chemistry and Biochemistry of the South Dakota State University for giving me the chance and supporting me financially throughout my studies. Also, I appreciate the Department of Pharmacy and Ag. Engineering for granting me access to their instruments. I thank Dr. Brian Logue for the financial awards for research excellence. A special thanks to SGS North America, SD Ag lab, SODAK Inc., Brookings for giving me practical training through internships.

CONTENTS

LIST OF FIGURES

extracted from their residues are depolymerized using CuO oxidation

LIST OF TABLES

ABBREVIATIONS

AADES	Amino acid-based deep eutectic solvents
Arg	Arginine
ASP	Aspirin
AA	Acetic Acid
cP	Centipoise
ChCl	Choline Chloride
π^*	Dipolarity/polarizability parameter
°C	Degree centigrade
DES	Deep eutectic solvents
DMSO	Dimethyl Sulfoxide
DMSO-d6	Deuterated dimethyl sulfoxide
DFT	Density functional theory
EPA	Environmental Protection Agency
FTIR	Fourier transformed infra-red
T_f	Freezing temperature
g	Gram
T_g	Glass transition temperature
Glu	Glutamic Acid
HBA	Hydrogen bond acceptor
HBD	Hydrogen bond donor

α	Hydrogen bond donor acidity
β	Hydrogen bond accepter basicity
ILs	Ionic liquids
Kg	Kilogram
Kcal	kilocalories
kJ	kilojoules
mg	Milligram
µl	Microliter
M	Molar
m_p	Melting point
T_m	Melting temperature
mL	milliliter
Men	Menthol
MD	Molecular Dynamics
λ_{max}	Maximum absorption wavelength
MTT	3-(4,5-dimethylthiazol-2-yl)-2,5-diphenyl-2H-tetrazolium bromide
%	Percentage
Pa	Pascal
^{1}H-NMR	Proton nuclear magnetic resonance
PBS	Phosphate buffered saline
QM	Quantum Mechanics
RDF	Radial Distribution Functions

THEDES	Therapeutic deep eutectic solvents
WDES	Water-based deep eutectic solvents

ABSTRACT

Formulation, Structure, and Applications of Therapeutic, Amino Acid, and Water-Based Deep Eutectic Solvents

MD SAJJADUR RAHMAN

2022

In the design of greener chemicals, deep eutectic solvents (DESs) are considered as one of the most versatile alternative solvents with widespread applications. DESs have the advantages of being nonflammable with negligible vapor pressure compared to traditional solvents. They share many characteristics of ionic liquids, but DESs are cheaper to formulate, typically nontoxic, recyclable, biodegradable, and are suitable for use with biological systems. In my Ph.D. research, three types of emerging and unconventional types of DESs, namely therapeutic DES (THEDES), amino acid-based DES (AADES), and water-based DES (WDES), have been investigated. To formulate these DES easily available and cheaper chemicals, such as water, choline chloride, menthol, aspirin, glutamic acid, arginine, and glycerol, were used. Besides formulation, experimental structural characterization, and rigorous computational studies, some of their preliminary applications have been explored to understand their potential area of applications. Formulation for poorly soluble drugs as THEDESs could enhance their solubility significantly and AADES were used to selectively depolymerize lignin. A complete characterization of WDES and solubility of salt or drug was explored. The structures and

structural properties of the DES studied were explored rigorously, as these insights can help to make them more effective. The major aim of the research projects was to find out the gaps of the DES research and provide a solid background for future research. Combining the molecular dynamics (MD), density functional theory (DFT), spectroscopic (Raman, IR, and VCD) techniques, solvatochormism, cheminformatics, and chromatographic techniques helped to understand the behavior and potential of the studied formulations. For example, atom-atom radial distribution functions (RDFs) based on MD simulation reveal that hydrogen bonds are formed between Cl-…HOCh+ and Cl-…HOCOOH of the THEDES, where Cl- works as a bridge between ASA and Ch+. Cation-anion electrostatic attractions are disrupted by highly interconnected hydrogen bonds. Non-salt HBA-HBD THEDES (1:1 L-Menthol: acetic acid) is also explored and found that their depression of melting point is mainly because of long network of hydrogen bond. Since menthol is a chiral molecular, VCD was found as a good tool to understand the behavior of chiral molecule-based DES. Melting points of WDESs (1:3 and 1:4 choline chloride: H_2O) were found significantly low, -79.21 and -79.25 °C, respectively. TGA study proved that water could be relatively stable at a higher temperature when it forms the DESs. Solvent selectivity triangle (SST) of Kamlet-Taft parameters proved that the DESs possess similar solvatochromic properties to ionic liquids. A simple analytical method was developed employing ion chromatography and atomic absorption spectroscopy to investigate the solubility of sodium halides, alkali chlorides, and cobalt chloride in the studied water-based DESs. Solubility trends of the metal halides in both DESs were found same, NaCl > NaBr > NaI > NaF for sodium halides and LiCl > NaCl > KCl for alkali metal chlorides. Solubilities of the studied drug molecules such as aspirin were found to be

1.3 to 6.7 times higher in the solvents than their solubilities in water. Cell viability assay of the WDES1 (1:3 ChCl:H_2O) compared to dimethyl sulfoxide (DMSO) against HEK293 cell line proved that the solvent is applicable to the biological system. The eutectic points of the formulated AADESs were -0.14°C for Glu-Gly and -1.36°C for Arg-Gly. FT-IR, ^{1}H-NMR spectroscopy, and mass spectrometry studies found that Glu-Gly formed ester impurities. However, mass spectrometry showed that the impurities are negligible. TGA revealed that both DESs could be applied up to 150-160°C without losing weight, while Glu-Gly could be used up to 200°C. AADESs are excellent pretreatment media for biomass, lignin was treated as a model biomass in this study with the formulated AADESs to determine their reaction products. It was found that Arg-Gly can isolate only one monomeric compound (4-methyl benzaldehyde), while Glu-Gly can isolate three monomeric compounds. Oxidative depolymerization of the lignin residues validated the outcomes obtained from the AADES-lignin reactions. Overall, this work helped to understand how to formulate novel DESs, their wide variety of characterizations, and possible application.

CHAPTER ONE

BACKGROUND AND PROBLEM STATEMENT

1. Background and Introduction

1.1. Problem Statement

General Assembly of United Nations (UN) announced a Millennium Declaration on 8 September 2000 [1]. Among the eight key objectives of the declaration, the fourth objective was to "protect our common environment". If we want to ensure in the improvement of the standard of life and achieve sustainable growth against increasing population, urbanization, industrialization, climate change, scarcity of resource, practicing green chemistry principles in each field is inevitable. The government of the USA took it seriously even before the UN declaration. Green chemistry practice officially began in the USA from 1990 by initiating the Pollution Prevention Act 1990 (42 U.S.C. §13101 et seq) [2]. The main aim was to prevent pollution at the source not just treat the wastes materials. In 1995, former President Bill Clinton introduced the Presidential Green Chemistry Challenge Awards based on five (later changed to six) award categories: Greener Synthetic Pathways, Greener Reaction Conditions, the Design of Greener Chemicals, Small Business, Academic, and Climate Change (or the reduction of greenhouse gas emissions. In 2009, President Obama appointed Dr. Paul Anastas to lead the US Environmental Protection Agency (EPA)'s Office of Research and Development. Previously, Dr. Anastas and Dr. John Warner proposed 12 green chemistry principles in 1996: pollution prevention; atom

economy; less hazardous chemical synthesis; design of safer chemicals; the use of safer solvents and auxiliaries; design for energy efficiency; use of renewable feedstocks; reduction of derivatives; catalysis; design for degradation; real-time analysis for pollution prevention; and inherently safer chemistry for accident prevention in their book “Green Chemistry: Theory and Practice” [3].

Solvents are ubiquitous in almost all industrial products, including paints, coatings, adhesives, as raw material for product synthesis, as reaction media, and for equipment cleaning. The following examples can provide more understanding of the use of solvents. It was reported in 2005 that solvents constituted about 80-90% of non-aqueous mass of materials to make an active pharmaceutical ingredient (API) [4]. But such solvents could have many intrinsic drawbacks, such as accumulation in the atmosphere, high toxicity, flammability, non-biodegradability, and persistency. Besides, these solvents could be unsuitable for high temperature applications or require expensive instrumentation. Another huge demand of solvent is in the market of recycling of spent Li-ion batteries [5]. Big company like Tesla has recently launched a such recycling project. Each industry can use green chemistry principles to make production or recycling sustainable and eco-friendly, which is even more economical. The following figure illustrates how green chemistry practices are related to achieve sustainable society.

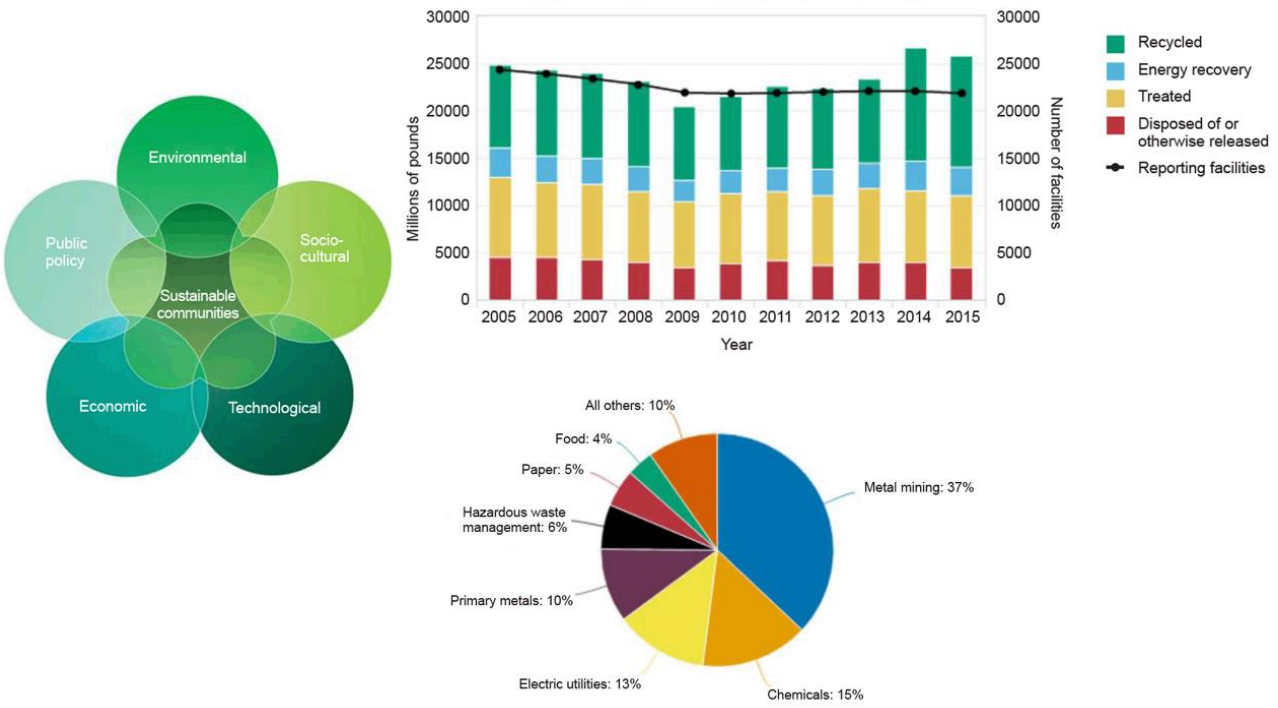

Figure 1.1. Left figure: Five domains of sustainable development reported by ECOStep: The Five Domains of Sustainability is a concept of W. Cecil Steward, FAIA, © 2017 Joslyn Institute for Sustainable Communities [6]. Top right corner: production-related waste managed by facilities reporting to TRI over 2005–2015 and below right corner: Total disposal or releases by industrial sector in the USA in 2015: 3.36 billion pounds (1.5 million tons) reported by US EPA's 2015 TRI National Analysis [7].

Another example of a problem related to solvent: 826 million pounds [375,000 tons] of hazardous chemicals and solvents are eliminated each year, enough to fill almost 3800 railroad tank cars or a train nearly 47 miles [75 km] long. But we have seen green chemistry practices, too, in the recent years. In 2010, Sherwin-Williams claimed that the manufacture of high-performance (greener) paint helped to eliminate over 800,000 pounds (360 tons) of VOCs (volatile organic compounds).

To solve such problems, formulation of greener solvents, such as ionic liquids and deep eutectic solvents (DESs), have been considered most promising nowadays. Between them DES is a comparatively newer type and more benign. Their classification and applications are yet to be explored a lot. In this research, we have re-structured and extended the existing classification. Detail formulation, structure, and some potential applications of water-based (WDES), therapeutic (THEDES), and amino acid-based (AADESs) have been explored. Our research group have done in-depth research on the WDES along with only a few research groups all over the world. Besides, we have classified AADES separately for the first time and define THEDES clearly so that future researchers can clearly understand and can improve their potential substantially to make them industrially more applicable.

1.2 Deep Eutectic Solvents

1.2.1 Definition

A homogeneous mixture which obtains a melting point lower than their individual components, typically using noncovalent interactions, at a certain molar ratio, is called eutectic system [8]. In 1884, Guthrie first named this system as eutēxia (a Greek word which means wellmelting) or eutectics. Since eutectics have been used for a long period, it has been referred to with different names in various areas of research and industries. They are called eutectic mixtures in pharmaceuticals [9], phase change materials (PCM) in the field of thermal energy storage devices or building materials [10–12], eutectic alloys for metallurgy [13], deep eutectic solvents (DES) [14] or low transition temperature mixtures (LTTM) [15] in green chemistry.

DESs are typically comprised of a hydrogen bond acceptor (HBA) and a hydrogen bond donor (HBD). Strong nonbonding interactions, such as dipole, hydrogen bond, alkyl-alkyl interactions, halogen bonds, and Van der Waals forces, exist among the HBA and HBD molecules, which lead to a significant depression of the melting point and inhibit the crystallization process [16]. Smith et al. (2014) described DESs by a general formula, $Cat^{+}X^{-}zY$ [17], where Cat^{+} refers to the cation of different organic salts (typically choline cation), and X^{-} refers to the anions (typically Cl^{-}) of the salt or Lewis base, Y refers to a Lewis or Brønsted acid or HBD (e.g., urea), and z refers to the number of HBD molecules.

1.2.2 Classification

The DES classification system could be extended by including the emerging and unconventional types of DES in the manner shown in **Table 1.1.**

Table 1.1 Classification of the deep eutectic solvents.

Types	General Formulas	Examples
1.	$Cat^{+}X^{-}$: Metal halides	1:2 ChCl: $FeCl_3$
2.	$Cat^{+}X^{-}$: Metal Halides hydrate	1:2 ChCl: $CrCl_3.6H_2O$
3.	$Cat^{+}X^{-}$: HBD	1:2 ChCl: H_2NCONH_2
4.	Metal Chloride: HBD	1:3 $ZnCl_2$: CH_3CONH_2
5.	Nonsalt HBA: HBD	1:1 Citric Acid: Sucrose
6	API* as HBA or HBD (THEDES)	1:1 ChCl: Phenylacetic acid, 3:1 DL-Menthol: Ibuprofen

7	Amino Acid as HBA or HBD (AADES)	1:1 Betaine: L-Histidine, 2:5 L-proline: Glycerol

*API= Active Pharmaceutical Ingredients

Smith *et al.* considered organic salts as the major hydrogen bond acceptors (HBAs) in their classification, and among them, Type 3 has been studied most [17]. DESs belonging to Types 5-7 are comparatively new. However, two emerging types of DESs (e.g., THEDES and AADES) will be discussed in this review. They could be considered as Type 3 or 5, but their specific and widespread applications demand to make separate categories for them. This will also help to track their evolving applications. WDESs could be considered as type 3. Only one group have been working with WDES except us, [18] we published our article at first on this type of DES [19]. Therefore, only a few articles have been found on similar DES [20].

1.2.2.1 Water-Based DES

We explored whether water could be used as a sole hydrogen bond donor to form DES. Therefore details of this kind of DES could not be found so much in articles. Our two articles [19,21] and the paper published by Triolo *et al.* [18] have explained most of the structural properties of choline chloride (ChCl) and water-based DESs. Use of greener chemicals, sustainable technologies, and industrial compliance are the major tools to build a world safer. Alternative solvents could play a major role to make the dream in reality

[22]. Organic solvents have been used for centuries and are typically toxic to the environment. In the last few decades, some greener alternative solvents have emerged and among them ionic liquids (ILs) show excellent qualities. Although ILs show a great promise, its toxic nature and expensive formulation make it difficult to use on a large scale [22–26]. To overcome the drawbacks, the idea of deep eutectic solvents (DESs) has been emerged in the past two decades [27–31]. Deep eutectic solvents show-a lot of promise in various fields, such as chemistry, material science, physics, and pharmaceutical science. It has the advantages of being nonflammable with negligible vapor pressure compared to the molecular solvents and shares many beneficial qualities of ILs at the same time [32]. DESs are also cheaper to formulate, nontoxic, highly pure, easily recyclable, and biodegradable [33]. Although DESs are environmentally benign and considered as one of the most versatile alternative media nowadays, detailed knowledge of their miscibility, polarity, and solvation behavior are yet to be explored. High viscosity and disruption of the eutectic environment by water dilution cause the major problems to use them on a large scale [34].

Recent studies reported that water has some unique effects on the physicochemical behavior and chemical structures of DES. If water is added to a DES system at higher mole fraction (e.g., >25%), both HBA and HBD of the DES get hydrated and show higher diffusivity, and the water molecules dominate the hydrogen bond formation with the constituents of the DES which eventually dampens the DES system [35]. Another study strengthened the claim that the water molecules make stronger interactions to the components of a DES than the interactions among themselves (e.g., water-water) or among the DES-DES clusters [36]. Viscosity of a DES typically decreases dramatically with the addition of a small amount of water. For instance, Savi *et al.* quantified that when

approximately 10% of water is added to the 5:1 lactic acid: glucose DES, viscosity of the DES decreases to 85.9% [37]. Therefore, it is inevitable to understand the role of water in field of DES.

To solve the problems, we formulated a novel type of DES where water is used as a sole hydrogen bond donor. These DESs can be called as water-based DESs (WDESs). Until now, only Yizhak Marcus [38] (2017) claimed that some aqueous salt hydrates should be considered as DES. Asare [39] (2018) proved that water can be a sole hydrogen bond donor (HBD) to form DES with ChCl. In this study, we have focused only on the combinations of 1:3 (WDES1) and 1:4 ChCl:H_2O (WDES2).

Thermal behavior of a DES is crucial to know because it helps to estimate the range of its applicability [40]. To measure the eutectic point and thermal stability of the solvents, differential scanning calorimetry (DSC) and thermal gravimetric analysis (TGA) techniques have been widely used [41]. Solvatochromism plays an important role to select a proper alternative solvent for a specific application [42]. Similar to an organic solvent, a DES system is hard to describe only by dielectric constant or dipole moment because it possesses many interactions, such as double ionic effect, hydrogen bonding, halogen bonding, π-π interactions, and van der Waals forces [43–45]. Since most of the available methods allow to examine only one major type of interaction, a range of different probes are required to get a clear insight of the strength of solute-solvent interactions in a DES system. Solvatochromic technique can determine some important properties, such as transition energy (E_T^N), hydrogen bond donor acidity (α), hydrogen bond acceptor basicity (β), and polarizability (π*) of such binary phase solvents at the same time through

measuring the solvatochromic responses of several ultraviolet-visible (UV-Vis) absorbance probes [43],[46–48].

Solvatochromism helps to understand the solvation of the DESs, but solubility of ionic compounds in DESs has not been investigated a lot. Only a few works have been published based on metal oxide and sodium salt solubility in some DESs using two methods, e.g. inductively coupled plasma-atomic emission spectroscopy (ICP-AES) [49,50] and shake-flask method [51]. In this study, a simple solubility determination technique has been developed using ion chromatography (IC) and flame atomic absorption spectroscopy (FAAS) to determine the solubility of sodium halides, alkali chlorides, and $CoCl_2$ in the WDESs. Besides the solvatochromism, solubility results could help to understand extractability using WDESs. Several studies on metal extraction, such as Li and Co extraction from Li-ion battery waste [5], extraction of Co and Fe from NdFeB magnets [52], dissolution and recovery of electrum, native Te, tellurobismuthite, galena, and chalcopyrite [53], and extraction of metal salts and oxides from incinerated sewage sludge and ash [54] using DESs have been reported. Therefore, it has already been established that certain types of DESs could be the excellent extraction media for the specific metal recycling process.

FT-IR and Raman spectroscopic methods are the two renowned, efficient, and available tools to observe the nonbonding interactions including H-bonding among the components, to prove the successful formation of DES, and to determine the water content in a DES [45,55]. However, measuring Raman responses for the samples having water in it could be challenging. In this study, optimization of the Raman spectroscopic method for the WDESs

has been explored. Molecular dynamics simulation, being a highly effective toolbox in the world of molecular modeling, can track the motion of individual atoms as well as can explain their arrangements, orientations and movement of chemical structures with extreme details [56]. MD simulation act as a bridge between the atomic world to the macroscopic world of the laboratory. The interactions among the molecules can be predicted and the insights behind bulk measurements can also be revealed [57]. Besides, DFT-based IR and Raman spectroscopy, quantum chemical calculation, and exploring nonbonding interactions of the optimized cluster structures of the DESs can add deeper understanding of the mechanism of formation [58].

Poor drug solubility in the aqueous medium is one of the major challenges for the formulation scientists [59]. Solubility could play a vital role to achieve optimum drug concentration at the target site and obtain the intended pharmacological responses [59]. Since a lot of oral drugs or drug candidates are poorly soluble in a biological system, scientists have been trying to overcome the problem by employing many techniques, such as chemical modifications of drug [59], solid dispersion, particle size reduction, crystal engineering, salt formation, use of surfactant, and complexation [60]. Formulation and delivery of the poorly soluble drugs using DES technology have shown excellent performance [61]. Although extensive studies should have been conducted, lab scale reports have already proved high potentiality of these approaches. Besides the qualities of the WDESs stated earlier, they also show high thermal stability and higher polarizability [62]. Overall, the studied solvent showed a lot of promise for the pharmaceutical and biological applications.

Along with the experimental insights molecular modeling can immensely help to understand a new chemical environment. Molecular dynamics simulation, being a highly effective toolbox in the world of molecular modeling, can track the motion of individual atoms as well as explain their arrangements, orientations, and movement of chemical structures with extreme details [56]. MD simulation acts as a bridge between the atomic world to the macroscopic world of the laboratory. The interactions among the molecules can be predicted and the insights behind bulk measurements can also be revealed [57].

Since very few studies have been published on this kind of DES, we looked into WDESs as much as possible in this thesis work. The overall objectives and questions of this study are (i) to get overcome the difficulties related to high viscosity of DES and to answer the questions, such as why water disrupts or disturbs a eutectic environment or can water be a sole hydrogen bond donor (HBD) to form a DES?, (ii) water solely can form a DES, then to what extent do the nonbonding interactions influence the melting points and to increase their thermal stabilities?, (iii) solvatochromic parameters and solvation behavior of a WDESs, (iv) how much do the solubilities of the studied metal halides in water get decreased when water forms DESs with the ChCl?, (v) to get initial idea about the solubility of the WDESs to the Co and Li ions from spent Li-ion battery as the WDESs are thermally more stable than water and some DESs have already showed good extractability to the metals, (vi) formulation of water-based DESs and their unique physical property measurements, (vii) structure elucidation using quantum chemical and radial distribution function calculations, (viii) optimization of the spectroscopic measurements to obtain the best responses of the water-based DESs to explain their extreme depression of freezing points, (ix) IR and Raman spectroscopy of the specific cluster structures of WDESs (1:3

and 1:4 ChCl:H_2O), (x) exploring the potential of the solvents to enhance the solubilities of some sparingly soluble active pharmaceutical ingredients (APIs), (xi) evaluate the toxicity of the solvents to the biological system, and (xii) evaluation of their efficacy as a drug-delivery vehicle.

1.2.2.2 Therapeutic deep eutectic solvents (THEDES)

Bioavailability of drugs is the key factor for successful drug delivery [63]. Studies showed that about 90% of the lead compounds and 40% of market drugs are poorly soluble in water [63]. Besides, over 40% of new drug candidates require formulation help to improve their solubility and dissolution [59]. Since a huge percentage of drugs have less bioavailability than required [64], a few methods (e.g., lyophilization, amorphous solid dispersion, particle size reduction, complexation, and salt formation) have been used to enhance the bioavailability of such problematic drug molecules [65,66]. Solubility enhancement and changing release kinetics are the two most promising ways to fix these problems [67]. Optimization of the bioavailability keeping pharmacokinetic variability at minimum levels must be taken under consideration during any new formulation approach [68].

Based on key factors, e.g. solubility, dissolution, and absorption, oral drugs are categorized into four groups. This classification is called ‘biopharmaceutical classification system (BCS)’, which has been considered as a standard classification system since 1995 [69]. It guides formulation scientists to determine the suitable dosage form and the bioequivalence tests [70]. **Table 1.2** shows BCS classification system with their major properties [71].

Except for some common drug molecules, most of the examples provided in the table have already been studied as eutectics (**Table 1.3** and **1.4**).

Table 1.2. Biopharmaceutical classification of drugs based on their bioavailability.

Class	**Properties**	**Examples**	**References**
BCS Class I	Behaves like oral solution, high solubility, high permeability, rapid bioavailability	Propranolol, paracetamol, salicylic acid, lidocaine, DL-methionine.	[71,72]
BCS Class II	Low solubility, high permeability, variable bioavailability, need to enhance dissolution rate, suitable for controlled release	Ibuprofen, itraconazole, coenzyme Q10, and Azithromycin	[72–74]
BCS Class III	High solubility, low permeability, low bioavailability, problematic for control release	Ranitidine, tetracycline, acyclovir, Aspirin, peptides, nicotinamide.	[71–73]

BCS Class IV		Low solubility, low permeability, poor and variable bioavailability, not suitable for oral drug delivery	DL-methionine, Ciprofloxacin, Neomycin	[72,73]

Drugs belonging to BCS Classes I-III are mainly studied in the form of THEDES to observe their efficiency to overcome the problems associated with them [75–77], but the drugs belonging to Class IV have not been explored as eutectics.

Therapeutic DESs require at least one active pharmaceutical ingredient (API) for their formulation. Similarly, for the formulation of AADES, at least one amino acid is needed. APIs and amino acids can act as either the HBAs or HBDs in a DES structure. THEDESs have been formulated to apply in the pharmaceutical or biological fields [21,23–25]. AADES are used for the enhancement of the solubility of drugs and proteins [63,81] and in several other fields, such as improvement of biosynthesis [82], radioactive I_2 capture [83], extraction of phytochemicals [84], oil separation from ore [85], and enzymatic hydrolysis of lignocellulose [86]. Although THEDESs and AADESs are becoming popular, a detailed review article is not available which could help researchers exploring updated information of these fields. Therefore, the aim of this review is to provide a

detailed information on the formulations, structural features, and the applications of the THEDESs and AADESs reported to date.

Studies proved that when an API is administered to a biological system in the form of a eutectic, the efficiency of membrane transport, intestinal absorption, solubility, and controlled release are significantly improved [76,87,88]. The most common HBAs of the THEDESs are choline chloride (ChCl) and menthol, which can combine with a large variety of APIs, such as acetylsalicylic acid, ibuprofen, and phenylacetic acid [76,79]. Eutectic mixtures have been used for the formulation of drugs, which could have melting points either below or above the ambient temperature (**Table 1.3** and **1.4**).

Formulation

THEDESs are typically prepared by the mixing of two components at a certain molar ratio employing thermal treatment methods. The mixture is heated at 40-80 °C in covered glassware under constant stirring (≤ 600 rpm) at atmospheric pressure until a homogeneous liquid form [87,89,90]. The temperature could be higher, depending on the melting points of the constituents used for the formulation of a THEDES. It takes 30 min to three hours to obtain the homogeneous liquid solution. After formulation, it should be preserved into a desiccator or stored at -20 °C, as the chemicals (e.g., ChCl and menthol) used for the formulations of THEDESs are highly hygroscopic. Different formulations of the THEDESs are listed in **Table 1.3** and **1.4**. It is observed that ChCl, menthol, urea, and glycerol are the most common constituents. Sometimes the same compound can act as HBA in one THEDES but may act as HBD in another THEDES. For instance, API could

act as HBA when their salt form is used for the formulation, but same API could act as HBD when their pure form is used.

Table 1.3. Therapeutic deep eutectic solvents which have eutectic points above ambient temperature.

HBA	**T_m (°C)**	**HBD**	**T_m (°C)**	**molar ratio**	**T_e or T_g* (°C)**	**References**
Coenzyme Q10	50-52	L-Menthol	39.0	6:4 (%w/w)	37.0	[91]
		Lauric Acid	43.8	7:3 (%w/w)	37.9	[92]
Ibuprofen	75-77			3:7	35.2	[93]
		Thymol	49.6	2:3 (%w/w)	32.0	[76]
Lidocaine	68.0	DL-Camphor	174-179	1:1	33.0	[94]
		Tetracaine	148[95]	1:1	30.0	
Paeonol	52.5	DL-Menthol	39.0	4:6	≤32.0	[96]
Lidocaine	68.0	Stearic Acid	69.3	1:1	43.0	[97]

Testosterone	151.0	DL-Menthol	39.0	1:4	39.9	[98]
Ibuprofen	75-77			1:3	-50.1*	[87]
ChCl	305.0	Salicylic Acid	159.0	1:1	68.0	[99]
		Thymol	49.6	1:2	67.0	
		Paracetamol	168.0	1:1	41.0	
Tetracycline	170-175	Glycerol	18.1	1:2	62.0	
Ticlopidine	189.0			1:2	67.0	
Borneol	202.0	DL-Menthol	39.0	2.5: 7.5	N/A	[88]
Myristic Acid		S-Limonene	-90.0	1:1	47.7	[100]
				1:2	47.5	
				2:1	51.6	
Ibuprofen	75-77			8:1	AT	
Sulfathiazole	202.5	Urea	133.0	5.2:4.8 (%w/w)	118.0	[101]

**NA= Not Available, T_m= melting point, T_e= eutectic point, T_g= glass transition temperature, AT= ambient temperature, and the T_m of the HBAs and HBDs are also listed from PubChem [102].

Table 1.4. Therapeutic deep eutectic solvents which have eutectic points below the ambient temperature.

HBA	**T_m (°C)**	**HBD**	**T_m (°C)**	**molar ratio**	**T_e or T_g*(°C)**	**References**
Propranolol	96.0	Decanoic Acid	31.9	3.5: 6.5 (% w/w)	15.4	[103]
		Lauric Acid	43.8	3:7 (% w/w)	15.9	
Ibuprofen	75-77	Methyl Nicotinate	38-43	1:1 (% w/w)	AT	[104]
		DL-Menthol	39.0	2.5: 7.5 (% w/w)	13.0	[76]
		L-Menthol	39.0	3:7 (% w/w)	19.0	
		1,8-cineole	1.5	2:3 (% w/w)	-13.0	
		Lidocaine	68.0	1:1	-27*	[105],[106]

Itraconazole	166.2	Phenol	40.9	2.4: 7.6	<0	[107]
				3.1: 6.9		
Lidocaine	68.0	Lauric acid	43.8	N/A	6.0	[108]
		Prilocaine	37.4	1:1	18.0	[109],[110]
ChCl	305.0	Resorcinol	109.8	1:1	6.0	[111]
		Aspirin	135.0	1:2	-67.0*	
Ranitidine	69-70	Glycerol	18.1	2:1	-87.0*	
Phenformin	176.5			2:1	-69.0*	
Ranitidine	69-70	Urea	132.7	2:1	-31.0*	
Adiphenine	113.5			2:1	-45.0*	
		Aspirin	135.0	2:1	-23.0*	
Ranitidine	69-70			2:1	-37.0*	
Lidocaine	68.0	Decanoic Acid	31.9	1:1	-61.0*	[112]
		Hexanoic Acid	-3.0	1:1	-56.0*	
		Linoleic Acid	-6.9	1:1	-71.0*	
		Oleic Acid	16.3	1:1	-47.0*	

		Phenyl salicylate	76.7	3:2	18.2	[113]
ChCl	305.0	Aspirin	135.0	1:1	AT	[79]
		Phenylacetic acid	76.7	1:1		
DL-Menthol	39.0	Aspirin	135.0	3:1		
		Phenylacetic acid	76.7	2:1		
				3:1		
		Decanoic Acid	31.9	1:4	17.0	[114]
Decanoic Acid	31.9	Limonene	-90.0	1:1	14.3	[115]
				1:2	7.8	
				2:1	20.9	
DL-Menthol	39.0			1:1	AT	
				1:2		
				2:1		
ChCl	305.0	Ascorbic Acid	190-192	2:1	AT	[116]

Acrylic acid	13	Lidocaine-HCl	80-82	3:1	-78.4*	[117]
Methacrylic acid	16				6.8	

**NA= Not Available, T_m= melting point, T_e= eutectic point, T_g= glass transition temperature, AT= ambient temperature, and the T_m of the HBAs and HBDs are also listed from PubChem [118].

Structural Insights/Features

Choline chloride (ChCl) and menthol are the two most common constituents to formulate THEDESs. Therefore, structural features of the ChCl and menthol-based THEDESs are discussed in this review. The first category is the ChCl-based THEDES. The nonbonding interactions among the ChCl and HBD molecules play a major role for the formation of THEDES. The types of nonbonding interactions include anion-pi, cation-pi, hydrogen bonds, halogen bonds, and alkyl-alkyl interactions [90]. Among all the interactions, hydrogen bonding between the chloride anion of ChCl and the hydrogen of hydroxyl or carbonyl of the HBDs are the main forces. The major interaction and the orientations of the components are shown in **Figure 1.2**, where 1:1 ChCl: phenylacetic acid (PAA) is the THEDES. Experimental and computational IR and Raman vibrational spectral analysis, as

well as the molecular dynamics simulation, radial distribution function, density functional theory calculations, and solvatochromism are reliable tools to demonstrate the interactions [90].

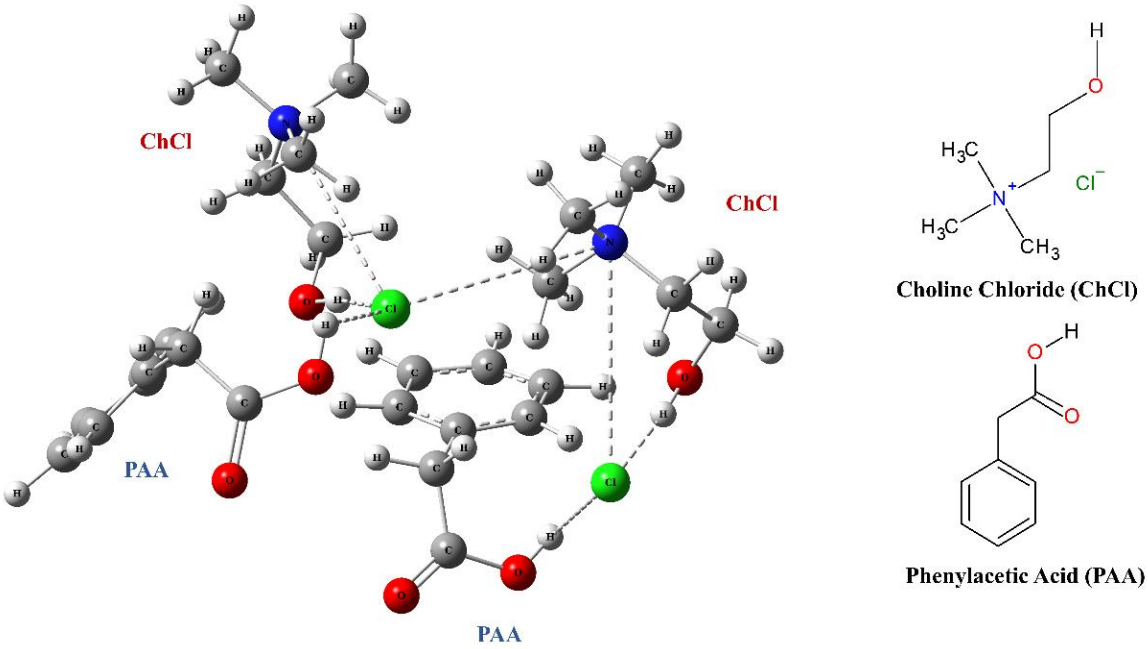

Figure 1.2. Nonbonding interactions among the components of choline chloride (ChCl):phenylacetic acid (PAA) (1:1) THEDES and the two-dimensional structures of its components are shown. Choline chloride is the structure with N atom (blue), Cl^- ion is shown as green, and the structure with aromatic ring is the phenylacetic acid. In the structures, oxygen is shown with red color.

It is crucial to understand the structural orientation of the constituents of a THEDES to get the reasoning behind its eutectic nature. Noncovalent interactions predominantly determine their thermal stability, molecular vibration, melting point, density, and viscosity. Choline chloride-based THEDESs exhibit a highly interconnected hydrogen-bonding network,

wherein the choline cation and -OH functionalities of HBA and the functionalities of the HBD molecules interact strongly with the Cl^- anion [90]. Besides, methyl protons on choline could interact via C-H…π interactions, depending on the HBDs used for the formulation. Chloride anion could also form anion-π interactions with the phenyl group of PAA, and choline cation could form cation-π interaction with the same aromatic-pi electrons of the PAA. One of our recent studies on 1:1 ChCl-Aspirin (ASA) THEDES showed that the nonbonding interactions (e.g., hydrogen bonds and electrostatic interactions) play a major role to form the eutectics and the distances of hydrogen bonds of the stable cluster conformers are ranges from 1.7 to 2.5 Å [90]. Charge delocalization and solvatochromism studies proved that Cl^- forms a charge transfer bridge between the choline cations and the HBD molecules [90].

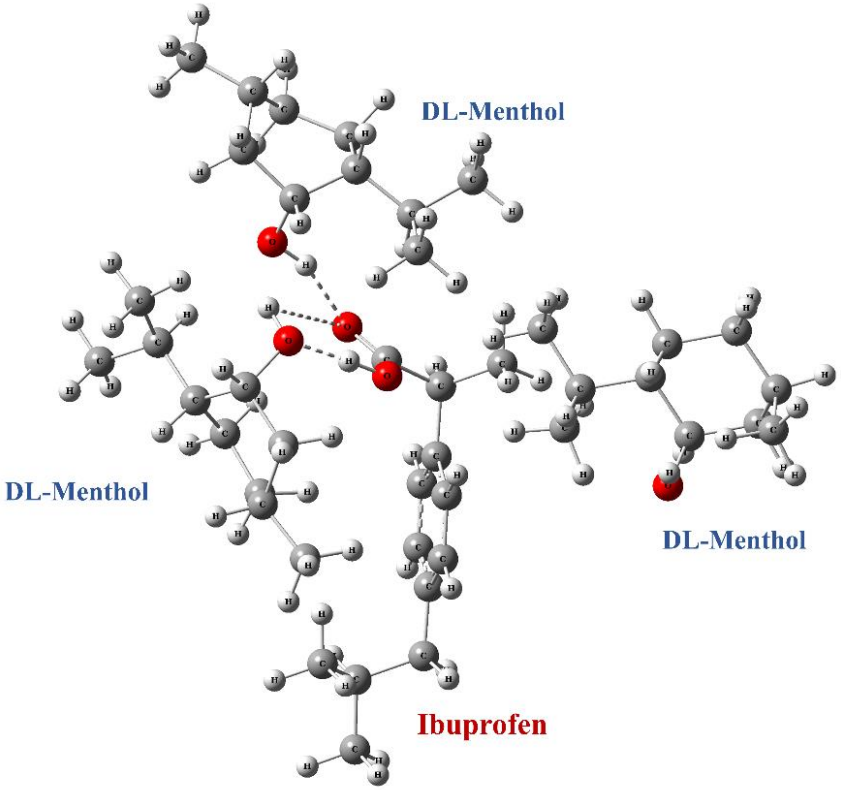

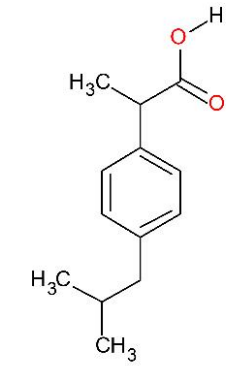

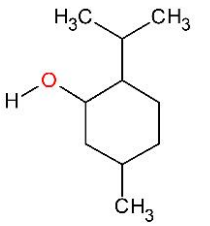

Figure 1.3. Major nonbonding interactions in D, L-Menthol:Ibuprofen (3:1) THEDES structure and the two-dimensional structures of its components, where atoms are shown as, hydrogen = off-white, carbon = grey, oxygen = red, and noncovalent interactions = dot lines.

Another major category of THEDES is menthol-based eutectics. Structural properties and nonbonding interactions of a menthol-based DES could be investigated with the same tools listed earlier. Structures of these THEDESs have not been studied as much, but a few studies suggested that the menthol interacts with the other constituents using its -OH group and the lipid alkyl tail [119,120]. For example, menthol interacts with the ibuprofen molecule by H and O atoms of its OH, where the contributing atoms of the ibuprofen are O of the C=O and H of OH of the -COOH (**Figure 1.3**) for 3:1 DL-menthol:ibuprofen THEDES. Interactions from the lipid alkyl tail could be alkyl-alkyl interaction and unconventional C-H hydrogen bond [121] FTIR studies on the THEDES formulations reported in Stott et al. (1998) article also proved that the ibuprofen forms THEDES with thymol (**Table 1.3** and **1.4**) by forming strong hydrogen bonds among their carbonyl and hydroxyl groups [76].

Applications of THEDES

Applications of THEDES have not been rigorously studied. These applications can be categorized in the following ways, (i) interactions of the THEDESs with the biological system, such as skin permeation and intestinal absorption, (ii) physicochemical changes, for example dissolution and solubility enhancement, (iii) controlled drug release, and (iv)

other applications, like improvement of anti-cancer drug delivery by the formulation of THEDESs.

(i) Permeation enhancement of transdermal drug delivery system

Transdermal drug delivery is one of the most popular administration routes for analgesics because it offers several advantages, such as the extension of the duration of activity, minimization of pain, reduction of side effects, and controlled drug release. Since it often faces problems related to permeation through the membrane, eutectic formulations have been used to overcome the problems. Some applications of the eutectics are the following:

Adela et al. studied the 1:1 lidocaine (L):prilocaine (P) eutectic mixture, where both the constituents are local anesthetics [122]. They investigated the efficiency of the release of L and P on oil-water dispersed phase and their solubilities through the membrane separately and in the form of eutectic. The enhancement of the distribution coefficient of the L and P were observed while applied in the form of THEDES. Besides, the drugs had higher escaping tendency in liquid phase when they are administered as 1:1 L:P. This mixture was further emulsified in water with a surfactant to overcome the limitations (lower permeability and drug release rate) of the conventional oil-water emulsions of the local anesthetics. The authors also found that the permeability and the rate of drug release of the mixture in aqueous solution increased with the increase of the concentration of the L-P mixture.

Lidocaine is an anesthetic that can either be injected into the body to act as a nerve blocker or applied topically on the surface of a tissue or mucus membrane to act as a local anesthetic [123]. Lidocaine is very soluble in both organic and polar solvents allowing movement

through the skin to the binding sites through the blood with no issue [124]. The major problem that belongs to the drug delivery of lidocaine is transdermal permeation because of its high melting point. Wang et al. (2014) improved the efficacy of lidocaine drug delivery as by formulating a eutectic mixture with ibuprofen [125]. They performed the study using a Franz cell and silicone membrane and concluded that the solubility of lidocaine and ibuprofen were enhanced when applied as the THEDES form. Even in solution, they can maintain strong intermolecular hydrogen bonding with each other, which allows them simultaneous transportation through membrane with much higher transport rates than their corresponding commercial crystalline salts. This should lead to a range of transdermal treatment options where two strongly interacting APIs can be combined to influence the membrane transport synergistically and provide simultaneous delivery to the blood stream.

Berton *et al.* (2017) studied the same eutectic mixture using an animal model. They topically applied the mixture to Sprague-Dawley rats by dissolving the mixture (e.g., 1:1 lidocaine: ibuprofen) in a vehicle cream [126] The concentrations of the APIs in blood plasma were monitored over the time as an indication of systemic absorption. Faster and higher systemic absorption was observed for the hydrogen bonded DES than the absorption of the salt forms e.g. lidocaine-Cl or lidocaine-docusate. Interestingly, a differential transdermal absorption was observed between lidocaine and ibuprofen when the THEDES form was applied. It indicated higher interactions among the tissue and the components of the cream, which could facilitate permeating through the skin as a neutral complex and enter systemic circulation.

Stott *et al.* investigated transdermal delivery of a model drug (e.g., ibuprofen) by forming its eutectic systems with terpenes to observe the enhancement of the drug permeation [76]. The molar ratios and the melting points of the mixtures are listed in **Table 1.3**. Ibuprofen permeated across the human epidermal membrane from the THEDESs manifold faster than the saturated aqueous solution. For instance, 2:3 (%w/w) ibuprofen:thymol produced a flux of 150 mg/cm^2/h, which was 5.9 times the flux produced from the saturated aqueous solution of thymol in the case of terpene pretreated skin. Moreover, it was 12.7 times higher than the flux from the saturated aqueous solution across non-pretreated skin. FTIR studies indicated that the terpene used to formulate the THEDES forms hydrogen bonds with the ibuprofen, which results in the depression of their melting point, and eventually facilitates the enhancement of the permeation.

Itraconazole, belongs to BCS class II and is an antifungal drug which has high logP value and molecular weight. Low aqueous solubility and high hydrophobicity of the itraconazole could cause irregular absorption and insufficient plasma concentration. To overcome these issues, Park et al. (2012) studied the permeability of the itraconazole by topical administration by forming their eutectic mixture with phenol [127]. They used hairless mouse skin to perform the experiment. The eutectic mixtures of 2.4: 7.6 and 3.1: 6.9 itraconazole:phenol were applied through the skin using a Franz diffusion cell. The amount of itraconazole permeated through the skin was determined using high-performance liquid (HPLC). They found that despite the high logP value and molecular weight, itraconazole can permeate through skin in the form of THEDES. In this way, itraconazole could be administered topically and could overcome the problems associated with the oral dosage form, such as inadequate plasma concentration and erratic absorption.

Kasting *et al.* [128] proposed a relationship between transdermal flux and melting point of the permeant based on ideal solution theory. They stated that the ideal solubility of a permeant in the skin lipid could be increased approximately exponentially by decreasing its melting point for any given molecular weight. Results indicated that a reduction in the melting point of a permeant will have a direct effect on its solubility in skin lipids and can increase the transdermal permeation.

Duarte *et al.* (2017) compared experimental permeability of the APIs including ibuprofen, benzoic acid, and phenylacetic acid and their permeability in the form of THEDES [129]. In brief, they measured the permeability using a glass Franz-type diffusion cell and a polyethersulphone (PES-U) membrane. The membrane was placed between the two compartments while the receptor compartment was filled with PBS solution, and the donor compartment was loaded with the same amount of API in the powder form or in the form of THEDES with a few mL of PBS. Time periods for the diffusion was taken for 5 min and hourly from 1 to 8 h at 37 °C. The amount of API diffused was determined using a microplate reader. Permeability of ibuprofen, benzoic acid, and phenylacetic acid increased about 3, 7.5, and 1.1 times, respectively, when applied as THEDES.

(ii) Intestinal absorption enhancement

Shen *et al.* used 3:1 menthol:borneol THEDES and its microemulsion for the study of daidzein absorption in the rat intestinal membrane using a diffusion chamber system [88]. The microemulsion was composed of ethyl oleate (oil), cremophor RH40 (surfactant), PEG400 (co-surfactant), and water. Both the eutectic mixture and its microemulsion enhanced the intestinal absorption of daidzein *in vitro*. Bioavailability of the daidzein

eutectic and the eutectic-microemulsion were increased by 1.5 and 3.7 times compared to the daidzein suspension. They found that when 3% of the eutectic mixture and microemulsion (containing 3% eutectic mixture) were added to the mucosal surface, the absorption of daidzein was significantly increased, although the mechanism of absorption enhancement is still unclear. Since daidzein has been used as a traditional medicine, the safety profile should be good [130]

(iii) Control release of drugs

Leija et al. transformed lidocaine hydrochloride into THEDESs by incorporating polymerizable counterparts (e.g., acrylic and methacrylic acid) [131]. These polymer-drug complexes were synthesized by free-radical frontal polymerization through forming hydrogen bonds among the lidocaine-salt and the polymers, where Cl^- works as a bridge. The properties of the eutectics allow frontal polymerization in bulk with full conversion, which was achieved in a one-pot synthesis. It yielded monoliths of polymers loaded with a high concentration of drug. *In vitro* experiments proved that the drug can be released in a controlled manner triggered by the pH, ionic strength, and solubility of the drug in the dissolution medium. The controlled release of the drug was maintained by swelling of polymers and the specific interactions among the drug molecules and the polymers. They concluded that the controlled drug release could be achieved not only by the monomers and THEDESs studied but also varying the monomers (as HBD) and crosslinkers. Similar polymer systems were also used for the DES to control drug delivery. Pradeep Kumar *et al.* [132] used an amphiphilic polymer with DES for tumor-targeting cancer therapy. In this case, DES (formulated using CABAL (3-(4-(4-(bis(2-

chloroethyl)amino)phenyl)butanoyloxy)-N,N,N-trimethylpropane-1-aminium chloride) and 1,4-butanediol (BD) in various ratios) influenced the formation of FA-g-β-alanine-co-PCL which eventually can act as a doxorubicin (DOX) carrier. They applied the system against MDA-MB-231 cancer cell line (*in vitro*) and breast cancer cell model (*in vivo*). The amide bond of the carrier (DES@FA-g-β-alanine-co-PCL) was degraded by the lysosome in cancer cells, which facilitates the control release of DOX and enhances the anticancer effect. In another study [133], they used proline-lactic acid-based DES to form similar micelle (DES-g-PGA (polyglutamic acid)-FA (folic acid)) to control release of the anticancer drug paclitaxel (PTX). Their study demonstrated that the DES-based drug carrier are efficient for anticancer drugs, which can minimize the adverse side effects to the normal cells.

In the previous studies, the DESs were used as the carrier of a drug molecule, but Aroso *et al.* (2015) [87] formed a THEDES (3:1 menthol:ibuprofen) to improve the efficiency of ibuprofen release at the target. The THEDES system was used to design an advanced drug release system employing supercritical fluid technology. To investigate this new approach, they performed a comparative dissolution study of the ibuprofen-powder and ibuprofen-THEDES. They found similar dissolution efficiency for the pure ibuprofen and the ibuprofen in the form of THEDES. The similar efficiency profile indicates that in the solution the nonbonding interactions among the menthol and ibuprofen molecules might be dissociated. Furthermore, they conducted the drug release study in the buffered saline by impregnating ibuprofen and ibuprofen-eutectic in a carrier (starch:poly-ε-caprolactone polymeric blend or SPCL). This highly porous carrier has melting point at 60 °C, which

facilitates the application in biological systems. They found a faster release profile of ibuprofen in the form of THEDES, which is mainly governed by diffusion.

Silva *et al.* performed a similar study [116] using the same carrier (SPCL) and they also got a faster rate of drug release. However, they did not apply the THEDES (2:1 ChCl:ascorbic acid) directly as a drug system, rather they used the THEDES as a solubilizing agent of dexamethasone (DEX). A controlled drug delivery system was developed by supercritical fluid sintering of a SPCL blend doped with THEDES-solubilized DEX. Aliquots were collected at different times and analyzed employing HPLC. This study suggested that the THEDES is not only used for the formulation of a drug but they could also be used as a solubilizing media.

Recently, they formulated some ternary THEDESs, e.g. citric acid:L-arginine: H_2O at molar ratios of 1:1:7, 1:1:6, 1:1:5, and 1:1:4 [134]. They used these THEDESs systems for tuberculosis therapy employing supercritical carbon dioxide technology. Besides the drug release study, cell viability study or *in vitro* cytotoxicity assay of the THEDES was evaluated against L929 cell line. This study proved that along with the advantages of the improvement of drug release and dissolution profiles, the THEDESs do not compromise the cell viability. Therefore, THEDESs seems safer to use.

(iv) Solubility and dissolution enhancement

Duarte *et al.* (2017) also studied solubility enhancement of the APIs (e.g., ibuprofen, benzoic acid, and phenylacetic acid) similar to their study on permeability [129]. The solubility measurements were performed with the pure APIs and their THEDES formations. Briefly, an excess of API and THEDES saturated solutions were prepared in

PBS (phosphate-buffered saline) solution at room temperature (20 °C) by stirring for 24 h. The determination of the solubilities of the APIs were performed by a microplate reader. They found that the solubilities of the APIs increased in 3:1 menthol:ibuprofen, 3:1 menthol:benzoic acid, and 2:1 menthol:phenylacetic acid about 12.8, 2.1, and 1.2 times, respectively. Therefore, THEDES can offer enhancement of permeability, dissolution, and solubility, although the mechanism of action is not fully understood.

Win *et al.* studied the dissolution rate of the sulfathiazole and urea eutectic mixture. This study showed that the dissolution rate of sulfathiazole in the form of THEDES is 700 times higher than its pure form [135]. The formation of the eutectic mixture of 5.2:4.8 (%w/w) sulfathiazole:urea (**Table 1.3**) enhanced the reduction of the crystal size of the API and made it highly soluble in water. Solid dispersion of the sulfathiazole increased the physiological availability of the drug and showed 12 times faster dissolution than its pure form.

(v) Improvement of anti-cancer drug delivery by the formulation of eutectics

Although limonene has chemotherapeutic properties against many cancers (e.g., breast, lung, prostate, and gastric), it is highly toxic even to the healthy cells [115]. Direct use of it to treat cancer cells is not feasible in terms of cell viability. Therefore, Pereira *et al.* (2019) studied the potential use of some limonene-based THEDES to treat cancer [115]. They formulated a total of 14 THEDES using limonene, among them only 1:4 ibuprofen:limonene showed successful inhibition of HT29 cell proliferation without compromising the cell viability. H29 cell line was incubated for 24 hours to perform the antiproliferation assay by treating the components and the THEDESs. Cytotoxicity assay

was assessed with the human Caco-2 cell line. After seven days of cell culture, the cell line was incubated with the THEDESs for 24 hours. EC_{50} values showed that the 1:4 ibuprofen:limonene can reduce the proliferation of HT29 cell line without compromising the cell viability. It proved that ibuprofen could have a synergistic effect to the limonene for the anticancer treatment. It also led to the enhancement of anti-inflammatory activities of ibuprofen, which could indirectly help the anticancer therapies.

1.2.2.3 Amino acid-based deep eutectic solvent (AADES)

Amino acid-based deep eutectic solvents (AADES) are another type of emerging and potentially green solvent, which is naturally benign, biodegradable, sustainable, and eco-friendly [136,137]. To formulate AADESs, at least one of the components should be an amino acid. AADESs have been used in various areas of research, such as cosmetics, food, drugs, animal feeds, and polymer production [138,139]. They have shown a lot of promise in several other fields, such as solubility enhancement of drugs and proteins [63,140], biosynthesis [141], radioactive I_2 capture [142], extraction of bioactive compounds [143], separation of oil-carbonate [144], and depolymerization of lignocellulose [145].

Formulation

Two methods have been primarily used to formulate AADESs, vacuum evaporation and heating. For the vacuum evaporation method, components are dissolved in water, mixed, and heated. Their dissolution could be enhanced by vortexing or applying ultrasound, and finally the water is evaporated [146]. In the heating method, components of the DESs are

mixed at a certain molar ratio and heated in covered glassware under constant stirring until a homogeneous liquid forms [147,148]. Studies showed that most of the AADESs have been prepared using heating. To formulate an AADES, selected components are mixed at a certain molar ratio (range of 10:1-1:10). Then the mixer is heated at 25-100 ºC with constant stirring at 400-1200 rpm for 0.5-24 h until a clear and homogeneous solution forms, depending on the nature of the components and their molar ratio [144,149,150]. Synthesized eutectics are dried at 45 ºC in a desiccator over P_2O_5 [151].

Table 1.5. Different combinations of amino acid-based deep eutectic solvents and their HBAs, HBDs, and molar ratios are also listed.

HBA	**T_m (°C)**	**HBD**	**T_m (°C)**	**Molar ratio**	**T_e or T_g* (°C)**	**References**
Bu_4NBr	103.0	Aspartic acid	270.0	1:9	25.2	[152,153]
				1:10	32.8	
				1:11	31.8	
		Glutamic acid	199.0	1:8	30.6	
				1:9	29.3	
				1:10	28.9	
		Arginine	260.0	1:6	25.1	

				1:7	26.4	
				1:8	26.2	
Betaine	293-301	Lysine	224.5	1:1	AT	[145]
		Arginine	260.0	1:1		
		Histidine	287.0	1:1		
Sucrose	186.0	DL-Proline	208.0	1:2, 3:1	<-50*	[154]
				1:4		
Lactic acid	16.8			1:1		
Citric acid	153.0			1:1, 1:2		
DL-Malic acid	131.0			1:1		
D-(+) Glucose	146.0			1:1, 3:5		
D-Sorbitol	95.0			1:1		
D-(+) Glucose	146.0	L-Proline	205.0	3:5		
		D-Proline	223.0	3:5		
DL-Malic acid	131.0	L-Serine	246.0	1:1, 2:3		
		β-Alanine	207.0	1:1, 2:3		

Citric acid	153.0			1:1		
L-Cysteine	240.0	Lactic acid	16.8	1:8, 1:12, 1:16	NA	[142,155]
L-Methionine	281.0					
L-Tryptophan	290.0					
Glycine	233.0					
Valine	298.0					
L-Leucine	293.0					
L-Proline	205.0	D-glucose	146.0	1:1	NA	[143]
		Sucrose	186.0	2:1		
		D-sorbitol	95.0	1:2		
		Glycerol	17.8	2:5		
		Citric acid	153.0	1:1		
		Laevulinic acid	33-35	1:2		
		Oxalic acid	189-191	1:1		
		Lactic acid	16.8			

		DL-malonic acid	131.0			
		Malonate	199.0			
		Urea	133.0			
		L-methyl urea	99.0			
		Acetamide	221.2			
Arginine		Oxalic Acid		1:1	AT	[156]
		Tartaric Acid			AT	
		Glutamic Acid			~30.0	
DL-Proline	208.0	Oxalic acid dihydrate	101-102	1:1	AT	[157]

**NA=Not Available, AT=Ambient Temperature, T_m=melting point, T_e=eutectic point, T_g=glass transition temperature, and the T_m of the HBAs and HBDs are also listed from PubChem [118].

Structural features

Formation of a DES depends on the strength of the noncovalent interactions among its constituents, which directly affects the physical and chemical properties, stability, and phase-transition temperature of the solvents [158]. Different techniques have been applied to explore the structure of AADES, such as ^{1}H-NMR, FTIR, and Raman spectroscopy [90,159]. Based on the noncovalent interactions, structures of the AADES can be classified into two types. The first is formed by the electrostatic interaction, e.g. quaternary ammonium salt-based AADES or betaine (trimethyl glycine or $(CH_3)_3N^+CH_2CO_2^-$)-based AADES. Since it does not have any halide anion, betaine and the amino acid molecules can directly interact with each other using electrostatic forces. Hydrogen bonds among the functional groups (e.g., -COOH and -NH) could also facilitate formation of the AADES [145,160]. For better understanding, those interactions are shown in the **Figure 1.4**.

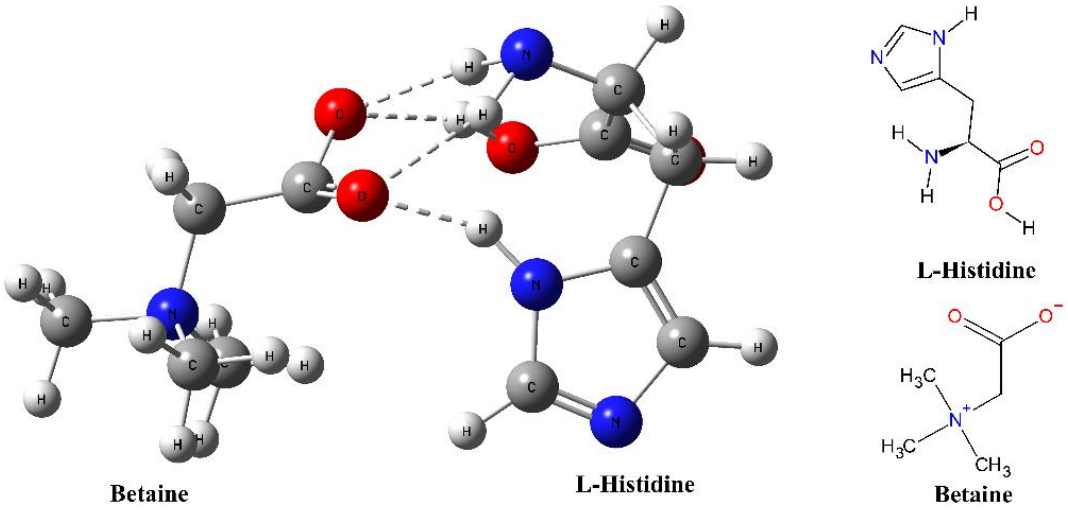

Figure 1.4. Major interactions are illustrated in the cluster structure of 1:1 betaine:L-histidine, where betaine is the hydrogen bond acceptor and L-histidine is the hydrogen bond donor molecule, where atoms are shown as, hydrogen = off-white, nitrogen= blue, carbon = grey, oxygen = red, and noncovalent interactions = dot lines.

The second major type of AADES is formulated by nonionic hydrogen bond acceptors and donors. In this class, proline-based AADES is the most common type. Dai et al. (2015) investigated the formation and the structure of 1:1 proline:malic acid using NOESY (^{1}H-^{1}H-nuclear overhauser enhancements) and FTIR spectroscopy [20]. They revealed that O=C-O-H---N is the major hydrogen bond in the DES system. That means -COOH of the malic acid is donating a hydrogen bond to the N of proline. Their study also demonstrated that when the molar ratio of proline-malic acid increases, the number of hydrogen bond increases. Besides, alcohol group containing HBDs are another major type of HBDs for the AADES formulation. To understand their structure, 2:5 L-proline:glycerol [143] is considered being shown in **Figure 1.5**. Glycerol is an efficient HBD for the formulation of many types of DESs because it offers long range diffusivity. Therefore, it can form a strong hydrogen bonding network in the DES system [161].

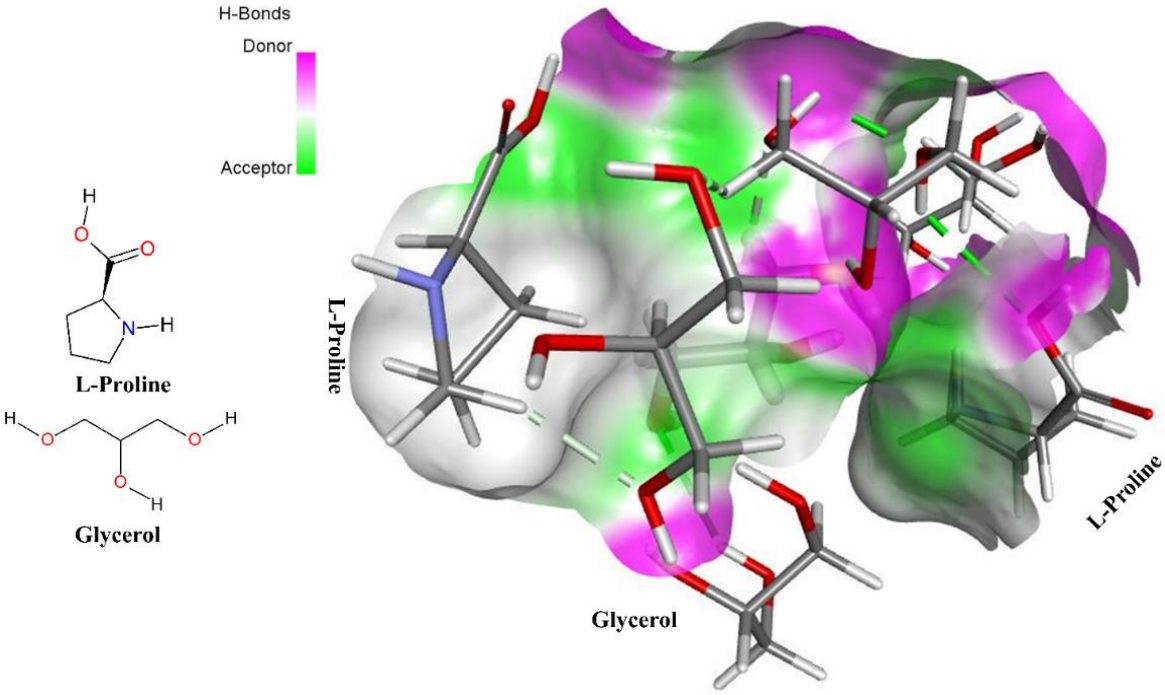

Figure 1.5. Glycerol is diffusing in the structure of 2:5 L-proline:glycerol AADES, where the L-proline is the hydrogen bond acceptor and glycerol is the hydrogen bond donor molecule, where atoms are shown as, hydrogen = off-white, nitrogen= blue, carbon = grey, oxygen = red, and noncovalent interactions = dot lines.

Applications of AADES

(i) Biological applications

Amino acid-based DESs show remarkable efficiency to improve bioavailability, synthesis, and conversion of drugs. L-glutamine and glycine (2:5) AADES media can increase the biosynthesis of ethyl (S)-4-chloro-3-hydroxybutanoate with the increase of the reductase activity by 1.67-fold compared to the water control media [141] He *et al.* formulated a novel AADES with the combination of one molar choline acetate (ChAc) and one molar lysine to improve the reaction efficiency for whole-cell-catalysis [162] In their study, asymmetric bioconversion of CFPO (2-chloro-1-(3,4-difluorophenyl)ethenone) to (S)-CFPL ((S)-2-Chloro-1-(3,4-difluorophenyl)ethanol) occurred in the AADES mediated by recombinant *E. coli* cells. It was used as a model reaction, where the AADES were assessed as an excellent media for their performance in bioreduction. It was observed that the AADES can improve the efficiency of coenzyme regeneration and permeability of cell membrane during the bioreduction process. It can also increase the substrate loading by 3.3-fold compared to the aqueous media.

Stability is a key factor in the protein chemistry to avoid unnecessary aggregation and denaturation. Proteins can be aggregated by storage conditions, incorrect folding during protein expression, perturbation during purification, formulation, freeze-thawing, drying,

ultrafiltration, and transportation [163]. Since aggregation of a protein is a big problem, different additives have been used to enhance the stability. L-Arginine is one of the widely used additives to enhance protein refolding by inhibiting aggregation [164,165]. Golovanov *et al.* showed that L-arginine and L-glutamic acid separately can enhance protein stability, but an equimolar mixture of both synergistically could enhance the solubilities of the proteins studied 4.1-8.7 times their solubilities in the buffer solution [140]. They also interact with the oppositely charged residues of the protein, water molecules, and different ions in the buffer. Thus, it forms an alternative to stabilize proteins. The equimolar mixture could effectively reduce protein-protein interactions. Shukla et al. (2011) modelled the synergistic effect of L-arginine and L-glutamic acid on protein stability by simulating the system using molecular dynamics [166]. Their study revealed that the stability of the protein is related to the increase of the number of L-arginine and L-glutamic acids around the protein. An equimolar mixture of L-arginine and L-glutamic acid could increase the presence of additional molecules on the surface of the protein, increasing its stability.

Arginine-based DES could play an important role as a drug solubilizing agent [156]. In pharmaceuticals, one of the major concerns is the poor solubility of the APIs [63]. Studies showed that a huge number of the lead compounds and market available drugs are poorly water soluble, and the cost of launching a novel drug is extremely high [63,167]. Therefore, it would be a better approach to improve the efficacy and bioavailability of the existing drugs in their formulation stage [168]. Similar to the THEDES, arginine-based DESs have been reported as good drug solubilizing vehicles [156]. In this study, solubilization of lidocaine was studied in the arginine-based DES including (e.g., 1:1 molar ratio of arginine

with glutamic acid, oxalic acid, or tartaric acid). Results showed that the interactions among the lidocaine and the constituents of the DESs are responsible for the enhancement of the lidocaine solubility. Molecular dynamics study also showed that the proper selection and tuning of the HBDs and HBAs of a DES could significantly impact on their efficiency to enhance the drug solubility [156].

(ii) Radioactive iodine capture

Nuclear energy is one of the most efficient and clean energies. However, it produces an enormous amount of radioactive nuclear waste, some of which could cause serious damage to the environment even by a small release and it could cause cancer [169,170]. Therefore, the radioactive I_2 requires efficient entrapment to prevent its fatal effect to the environment and human health [171]. Studies recommended that some DESs are efficient to capture the radioactive I_2. For instance, Chen *et al.* captured radioactive I_2 using AADESs, such as cysteine:lactic acid, methionine:lactic acid, tryptophan:lactic acid, glycine:lactic acid, valine:lactic acid, and leucine: lactic acid, which are formulated at different molar ratios [142]. Their study showed that AADES can efficiently capture the radioactive iodine. Among the AADESs studied, 1:8 cysteine:lactic acid performed best and 1:8 leucine:lactic acid least well as the 1:8 cysteine:lactic acid can form a higher number of halogen bonds with the iodine.

(ii) Oil separation

Different types of oil-solid separation techniques (e.g., solvent extraction, pyrolysis, and microbial enhanced oil recovery) have been using in the fields of unconventional petroleum exploitation, pipeline deoiling, paper deinking, oil-contaminated water, and food industries

[172–175]. AADES-based separation is now considered one of most promising green approaches to separate oil and solid materials. Zhang *et al.* synthesized a novel amino acid ionic liquid-based DES (e.g., $TrpBF_4$/U) for the extraction of oil-carbonate minerals from the Indonesian asphalt ores [144]. They reported that amino acid ionic liquid-based DES can increase oil-recovery about 11% compared to the oil-recovery technique based on traditional ionic liquid (e.g., $[Emim]BF_4$). This is because DES can reduce of the interactions between the oil and mineral surfaces.

(iv) Extraction of bioactive compounds

AADESs have been also used to extract various food supplements, herbal medicine, and bioactive drug compounds [143,176]. However, some of these show poor bioavailability and solubility in biological systems [177,178]. Duan *et al.* studied the efficiency of the extraction of some phytochemicals using L-proline-based DESs [143]. Their study indicated that a flavonoid (e.g., icariin) is highly extractable with the L-proline-based DESs compared to sugar or alcohol-based DESs and methanol. Specifically, 1:2 L-proline:levulinic acid, 1:1 L-proline:malonate, and 1:1 L-proline:L-methylurea displayed higher efficiency of icariin extraction. L-proline:levulinic acid AADES showed similar extraction efficiency for anthraquinone to methanol. On the other hand, L-proline:L-methylurea AADES was found as an excellent solvent to extract the saponins compared to the other amino acid, betaine, and choline chloride-based DESs.

(v) Pretreatment of the biomass

To enhance the enzymatic hydrolysis of biomass, AADES can play an essential role. Liang et al. (2020) reported the hydrolysis of corncob biomass using 1:1 betaine:amino acid (e.g.,

arginine, histidine, and lysine) DESs with the water content ranging from 65-93 % [145]. They pretreated two mg of biomass in a covered glass bottle with one g of DES by applying 60 °C heat and 350 rpm stirring. Results showed that lignin and xylan were highly soluble in betaine:lysine and betaine:arginine solvents and poorly soluble in betaine:histidine DES. Furthermore, betaine:lysine and betaine:arginine successfully removed about 50% of lignin and xylan after pretreating the biomass at 60 °C for five hrs. The removal of lignin and xylan significantly increased the subsequent efficiency of enzymatic hydrolysis. On the other hand, betaine:histidine removed less lignin and xylan which seems to be insufficient to enhance the enzymatic hydrolysis. In this pretreatment processes, the optimum ratio of solid (biomass) to liquid (DES-water) is another important factor.

(vi) Greener synthesis of bioactive compound

AADES has been used to synthesize biologically active compounds. Indole and its derivatives are present in both marine and terrestrial plants [179] 3,3-diaryloxindole is one of the indole derivatives, which can be synthesized by the coupling reaction of indole and carbonyl compounds in different solvent media, such as dodecylsulfonic acid [180], silica-sulfuric acids [181], and ionic liquids [182]. All these methods require long times, toxic materials, expensive catalysts, and produce unsatisfactory yields. Therefore, a novel eco-friendly media is needed to synthesize the indole derivative to replace the use of hazardous and toxic chemicals. Research showed that the proline:oxalic acid dihydrate-based DES was used as a greener alternative to synthesize 3,3-diaryloxindole and chromone-based bis(indolyl)alkanes [183]. Excellent yield of the product with high purity was achieved using 1:1 proline:oxalic acid-dihydrate at ambient temperature. They also found that the

production of the desired amount of product was reduced at high temperature and in strong acidic medium because indole could be polymerized at those severe conditions. Therefore, optimum reaction condition should be maintained.

Overall, therapeutic, amino acid, and water-based deep eutectic solvents have shown a lot of promise. However, there are a lack of proper understanding to explore a novel formulation of DES. Major gap areas are- lack of structural information, use of user-friendly tools to extract structural information, a very few uses of cheminformatics to understand the behavior of DES. To understand their potential, chromatographic and spectroscopic techniques as well as computational tools could help immensely. Therefore, the goal of our research is fill up such gaps and show the potential ways to the future researchers.

CHAPTER TWO

THERAPEUTIC DEEP EUTECTIC SOLVENTS (THEDES)

ABSTRACT

In this study, atomic level interactions of 1:1 choline chloride (ChCl): acetylsalicylic acid (ASA) therapeutic deep eutectic solvent (THEDES) has been investigated by combining the molecular dynamics (MD), density functional theory (DFT) and spectroscopic (Raman and IR) techniques. Atom-atom radial distribution functions (RDFs) based on MD simulation reveal that hydrogen bonds are formed between $Cl^-\ldots HO_{Ch+}$ and $Cl^-\ldots HO_{COOH}$ of the THEDES, where Cl^- works as a bridge between ASA and Ch^+. Cation-anion electrostatic attractions are disrupted by highly interconnected hydrogen bonds. Cluster conformers of the THEDES are isolated from MD simulation and optimized using ωB97XD/6-311++G (d,p) level of theory, in which the strongest H-bonds are found among $OH_{Ch+}\ldots Cl^-$ (2.37 Å) and $Cl^-\ldots HO_{COOH}$ (2.40 Å). Charge transfer calculations, using CHEPLG and NBO analysis, disclose that the charge of Cl^- is reduced in the cluster structures and transferred to Ch^+ and ASA. Further analyses are conducted using experimental and computed spectroscopic data. These confirm the formation of the THEDES as peaks for -COOH, -COOR, and -OH functional groups of ASA and ChCl are either get broadened or disappeared in the spectra of the cluster conformers. Moreover, principal component analysis (PCA) assists to understand the feature of the simulated data and confirms the formation of the THEDES. Solvent selectivity triangle (SST) of solvatochromic parameters also demonstrate that this THEDES have some important properties similar to ionic liquids and common deep eutectic solvent. In the second part of

this chapter, non-salt HBA-HBD THEDES (1:1 L-Menthol: acetic acid) had been studied. Structural properties and nonbonding interactions of a menthol-based deep eutectic solvent were investigated in detail employing experimental and computational methods. Mass spectrometry analysis confirms the formation of 1:1 L-menthol: acetic acid. Molecular dynamics simulation was used to figure out the energetically most favorable cluster conformers of the 1:1 L-menthol: acetic acid system. Density functional theory (DFT)-ωB97XD/6-311G (d,p) level of theory was employed to optimize the isolated structures and calculate their thermochemical properties. Both experimental and computed IR were analyzed for the samples. Additionally, vibrational circular dichroism (VCD) spectra were measured to prove the chirality transfer. Further, principal component analysis (PCA) was used to analyze spectral data to make the data interpretation more vivid. All the spectral data analysis and nanostructure elucidation proved the spontaneous formation of the DES through formation of strong hydrogen bonding, where acetic acid dominated by strongly donating hydrogen bond to the menthol. Experimental solvatochromism and computed HOMO-LUMO gaps validated the reasoning. Moreover, comparative VCD and IR spectral analyses clearly indicate chirality transfer from chiral menthol to achiral acetic acid. This study suggests that various techniques, such as mass spectrometry, IR, solvatochromism, computed IR-VCD could be outstanding tools to elucidate nanostructure and nonbonding interactions of a DES, where VCD could be used as an excellent complimentary technique for the chiral molecule-based DESs.

2.1. Introduction

Drug delivery faces substantial challenges as many newly developed drug molecules have low solubility, bioavailability, and stability [184]. Developing a new drug molecule is enormously expensive. Therefore, various techniques such as amorphous solid dispersion, lyophilization, particle size reduction, complexation, salt formation, and solvent formation are emerged to improve solubility and bioavailability of the existing active pharmaceutical ingredients (APIs) [185],[186]. It is easily understandable that improving the bioavailability of already existing drugs is way more profitable than launching a new drug [187].

Ionic liquids (ILs) have received great attention in recent years to develop a potential pathway, applying its features to overcome some of the problems of drug delivery mentioned above [186]. ILs have also been reported as drug delivery vehicles, such as formulation of microemulsions, improvement of dissolution, and enhancement of transdermal delivery of sparingly soluble drugs [188,189]. However, due to the expensive production, high toxicity, and poor biodegradability, drug delivery by ILs has become a less attractive option over time [190]. Deep eutectic solvent (DES) is considered as an analogue of ILs and a potential alternative solvent with wide range of applications with less drawbacks [191].

In DES, a hydrogen-bond acceptor (HBA) and a hydrogen-bond donor (HBD) are mixed together, where significant depression of freezing point is one of the most common phenomena [192]. Among different kinds of DESs, therapeutic deep eutectic solvent (THEDES) is a new type in which at least one of its components must be an API.

Researchers successfully developed some THEDES to enhance their solubility, membrane transport, drug delivery, and bioavailability [193,194]. Formation of THEDESs based on choline chloride and menthol, combined with three different APIs including acetylsalicylic acid, benzoic acid, and phenylacetic acid were reported by Aroso and co-workers [194]. A few works have been reported based on experimental studies and MD simulation of DES. Perkins and co-workers worked on choline chloride-urea eutectic solvent combining simulation and experimental approach [195]. Comparing MD simulations and infrared spectrum, they suggested that a strong interaction between the NH_2 of urea and the chloride anion occurs. They also studied three more choline chloride based eutectic solvents using same methods and observed hydrogen bonding among the anions and HBDs, which supported their previous claim [196]. Sun *et al.* studied 1:2 ChCl:Urea (reline) using classical MD simulation and concluded that the spontaneous intercalation of urea molecules in choline chloride crystal lattice disrupt the ordered structure [197]. The simulated structure of the DES is in agreement with reported neutron diffraction structure [198]. Liquid reline and its mixture with water has also been probed by Evgenii *et al.*[199], and Shah *et al.*[200] employing different force fields. Albeit several experimental studies are available on THEDES, little to no work has been reported on their structural, thermodynamics and intermolecular interactions of THEDES with computational and experimental insights.

Charge delocalization via hydrogen bonds is one of the major reasons behind the freezing point depression [201]. Choline chloride and menthol are the common compounds for the formulations of DESs [201]. Various studies suggested that heat mixing at around 40 °C or mixing at ambient temperature with constant stirring are the preferred methods for the

formulations of menthol based-DESs [16,115,201,202]. To prove DES formation, exploring the impact of temperature, to determine their structures and the chemical properties, mass spectrometry can be employed [203,204]. Electrospray ionization (ESI) coupled mass spectrometry is well suited to identify diverse class of substances including volatile, non-volatile, polar, non-polar small molecules to large biomolecules [204].

FTIR spectroscopy is one of the most popular tools to examine intermolecular interactions and the formation of hydrogen bonds in a DES [205,206]. Vibrational circular dichroism (VCD) could be an excellent alternative and complementary technique to IR spectroscopy, when a DES is formed by at least one chiral compound [207]. VCD signatures are calculated by the difference between left and right circularly polarized IR radiation [208]. Gobi and his co-workers used VCD spectra to prove that hydrogen bond plays a major role to form 2-chloropropinoic acid-$CHCl_3$ complex [209]. Kessler *et al.* stated that DFT is a reliable method to compute VCD spectra and it can help to illustrate long-range interactions of a protein structure [210]. Principal component analysis (PCA), a renowned multivariate dimension-reduction tool, could be used to visualize subtle differences of spectral data of a large number of similar chemical structures [211–213].

Solvatochromism technique could describe a number of microscopic intermolecular properties of a solvent [214]. A deep eutectic solvent system is difficult to explain only by the typical solvent properties (e.g., dielectric constant or dipole moment) because it possesses many interactions, such as doubly ionic effect, hydrogen bonding, halogen bonding, π-π interactions, and Van der Waals forces [43,44,215]. Most of the available methods can determine only one major type of the interactions or properties.

Solvatochromic techniques can determine at least four major properties, such as transition energy (E_T^N), hydrogen bond donor acidity (α), hydrogen bond acceptor basicity (β), and polarizability (π*) by measuring and comparing the change of the solvatochromic responses of the UV-Vis absorbance probes (e.g., Nile Red, 4-nitroaniline, and N,N-diethyl-4-nitroaniline) dissolved in any solvent [43,46–48].

In this work, molecular dynamics (MD) simulation and density functional theory (DFT) calculations are employed to unravel the atomic level interactions of choline chloride (ChCl) based THEDES. Combined MD and DFT studies can assist to explain arrangements, orientations, interactions, and vibrations in THEDES [216–219]. The aims of this study are to find answers of following questions: i) what are the orientations of ChCl and acetylsalicylic acid (ASA) while they are forming THEDES, ii) how is the melting point is being decreased after forming THEDES, and iii) what are the driving forces, (iv) how multivariate statistical analysis, such as principle component analysis (PCA) can explain the spectra of different cluster structures of a THEDES further [220] and (v) is there any charge transfer and chirality transfer occuring among the components of the DESs after the formulation of DESs.

2.2. Experimental Section

2.2.1 Computational Details

Molecular dynamics (MD) simulation using YASARA Dynamics [221] program was used to generate all possible cluster conformers of the THEDES. Here, Amber 14 [222] force field was considered and the parcel mesh Ewald (PME) method [223] was used for

calculating the long-range electrostatic interactions. Five, ten, and twenty pairs of ChCl and ASA were simulated in gas phase for 10 ns and atom-atom radial distribution for one non-boning interaction was calculated. In all cases, the peak was found at the same distance with different probability, which is obvious as the number of pairs are different. Among them, five pairs could not demonstrate the broad scenario of the solvent system and twenty pairs seemed too complex as in that case, the system contains big clusters for which other parameters are difficult to calculate. Additionally, MD simulations were performed for the 5 and 20 pairs of menthol-AA. Considering the less complex system, having all interactions and stability lead the 10 pairs of menthol and AA system to be considered as the representative ratio for further calculation for the simplified. **Figure 2.1-2.2** explain how 10:10 reaction is better to generate cluster structures of the DES. For short-range Van der Waals and coulomb interactions, a cut-off radius 8.0 Å was applied. The particle-mesh Ewald (PME) method was employed to compute the long-range interactions [224]. Periodic boundary condition (cell box 58.81Å×58.81Å×58.81Å) and the temperature of 298 K were considered using the NVT ensemble for the simulation. An example of how we have extracted a single conformer out of a large structure calculated by molecular dynamics simulation have been given below using 1:1 menthol: acetic acid DES structures.

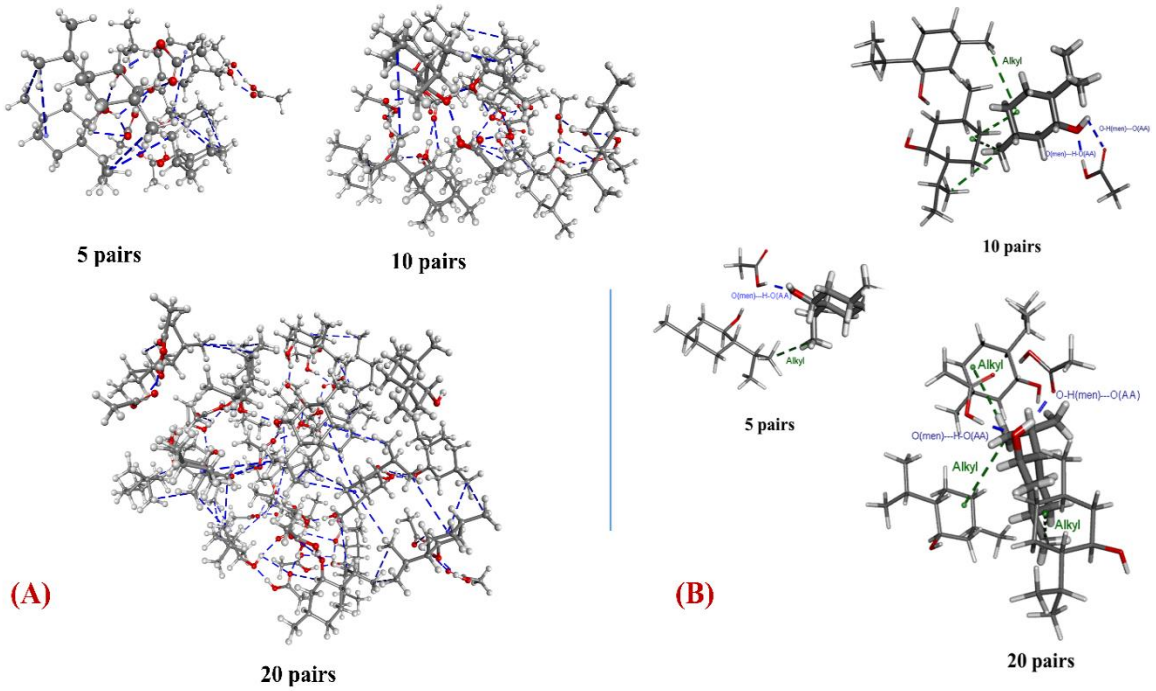

Figure 2.1. Images of the 5, 10, and 20 pairs of menthol-acetic acid MD simulations, **(B)** Nonbonding interactions of the 5, 10, and 20 pairs of menthol-acetic acid systems are also analyzed, where green lines represent alkyl…alkyl interactions and blue lines represent the major hydrogen bonds (e.g., O_{Men}---H-O_{AA} and O-H_{Men}---O_{AA}). Those are mainly responsible for the formation of the DES. 10:10 ratio represents almost all nonbonding interactions and comparable to 20:20 reaction.

Whether ten pairs-based simulation represented all types of interactions clearly (**Figure 2.2**). Therefore, ten pairs were selected as the representative sample of the DES system for further simulation.

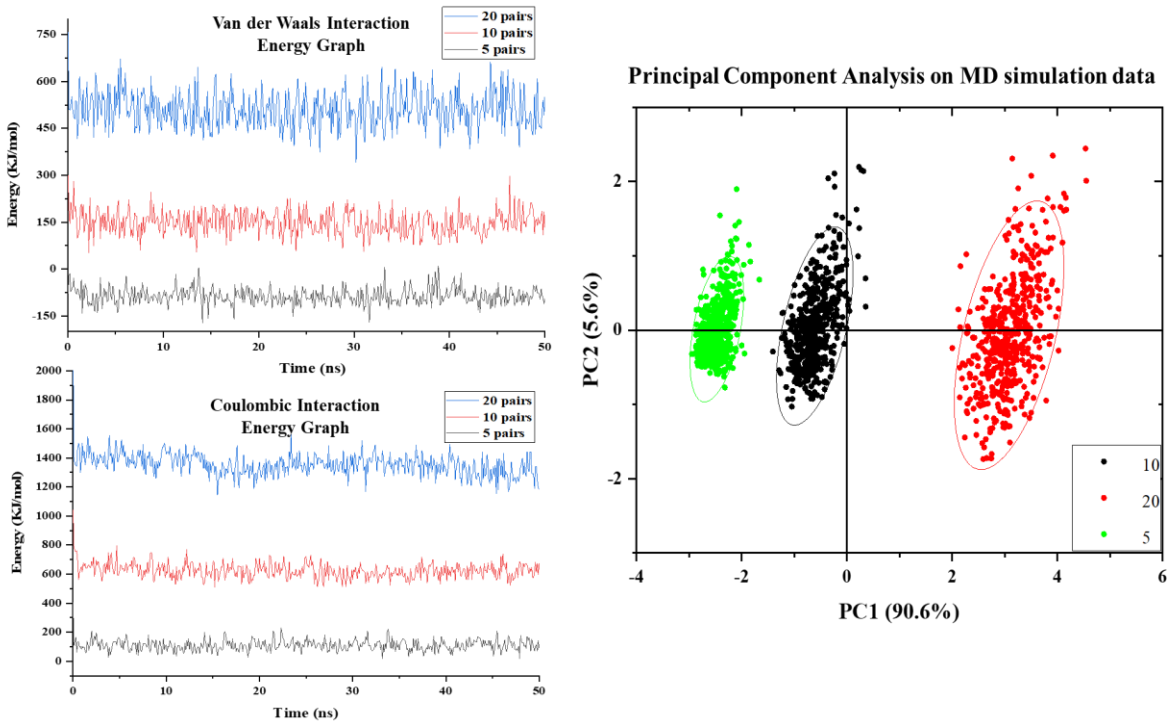

Figure 2.2. Van der Waals and coulombic energies are calculated of the 5, 10, and 20 pairs of menthol-acetic acid MD simulations. Furthermore, principal component analysis is conducted on the energy data to decide which pair should be best to isolate DES cluster structures further. Similar to the nonbonding interactions, energy data also shows that isolating of the energetically favorable DES cluster structures from 10:10 should best. Because Van der Waal and coulombic energy graphs, and PCA on the data show that 10:10 is energetically more stable and realistic. Energy pattern of 20:20 is fluctuating a lot, maybe because of they could have unrealistic bumps or energies during their simulation time.

The system was simulated for 50 ns to generate the atom-atom radial distribution function (RDF) of the system with high resolution and details. Periodic boundary condition (cell box of 36.75Å×36.75Å×36.75Å) and temperature of 298 K were considered using NVT ensemble for all simulations. The system was minimized and equilibrated with default

protocol of YASARA dynamics. Time step of 1.25 fs were used, and simulation snapshots were captured at every 100 ps. All simulations were done five times to observe reproducibility of the dynamics data by tracking the energy values and RDFs.

Quantum Mechanical (QM) Calculations and Kamlet-Taft Parameters. The isolated conformers were optimized at gas phase using DFT-ωB97XD/6-311G (d,p) level of theory for 1:1 men:AA and 6-311++G (d,p) level of theory for 1:1 ChCl:ASA. All quantum calculations were carried out using Gaussian 09 software package [225]. Out of the four best conformers, only the change of Gibbs free energy of the most spontaneous structure was further calculated in water phase using IEFPCM using the same level of theory to observe its spontaneity of the structure in a solvent having high dielectric constant. The electronic energy of this structure is also calculated with augmented double zeta basis set at DFT-ωB97XD/aug-cc-pVDZ level of theory. Structural and thermochemical properties were calculated from the optimized structures. HOMO-LUMO gaps were also investigated to understand orbital the electron delocalization among the components of the DES. HOMO-LUMO gap could provide insights of electron transfer or hydrogen bond transfer among the components. Besides, calculating ΔG, ΔE, ΔH, and ΔS values could add more chemical insights of the hydrogen bond formation and the spontaneity of the computed clusters. All the computational calculations helped to explain that how the cluster structures form or how spontaneous they are, but they could not provide any outcome of the extent the HBA and HBD molecules accept and donate hydrogen bonds. To get a more clear understanding of it, experimental solvatochromism was inevitable for this study. Four representative cluster systems were selected, and calculations were run for 1:1 molar ratio due to the limitations of DFT calculations. Population analysis was carried out using NBO

method [226], and the electrostatic potential derived charges were calculated employing the CHELPG scheme [227].

Computed IR, Raman, and VCD Spectra Analysis. IR, Raman and VCD spectra of all components and the cluster conformers were calculated in gas phase employing DFT-ωB97XD/6-311G (d,p) and 6-311++G (d,p) level of theory for 1:1 ChCl:ASA [215]. Although the exact NIST vibrational scaling factor was unavailable for this DFT method, all the spectra were multiplied by the scaling factor 0.957, which is closest to the method [228] Both IR and VCD spectral data were used to examine the most contributing atoms and functional groups to the formation of the studied DES system. This approach added deeper understanding to the experimental IR spectra and helps to observe the chirality transfer from menthol to acetic acid.

2.2.2. Materials

Nile red, 4-nitroaniline, N, N-diethyl-4-nitroaniline, dichloromethane (DCM) were purchased from Thermo-Fischer Scientific (Dubuque, IA) as the UV-Vis absorbance probes. Acetylsalicylic acid (ASA) and anhydrous choline chloride (ChCl) were purchased from Acros Organics, and analytical grade. L-Menthol were purchased from Acros Organics (NJ, USA). Acetic acid (glacial) was purchased from Fisher Chemicals (PA, USA). All the chemicals have purity ≥ 99.0 %.

2.2.3. Synthesis of THEDES

ChCl:ASA (1:1) was formulated by mixing anhydrous choline chloride and acetylsalicylic acid at 1:1 molar ratio at 80 °C for 3 hours in a covered beaker under constant stirring 600

rpm at atmospheric pressure until a homogenous liquid was obtained. After preparation, it was preserved into desiccator because the compounds are highly hygroscopic.

L-menthol:acetic acid (1:1) was formulated by mixing anhydrous L-menthol and glacial acetic acid at 1:1 molar ratio under ambient temperature and pressure for 1 h in a covered beaker with constant stirring ≤ 600 rpm until a clear liquid was obtained. Mass spectroscopy, ATR-IR, and solvatochromism experiments were conducted using freshly prepared DES as its components are highly hygroscopic. Prepared solvents can be kept in the -20 °C freezer for further use.

2.2.4. FT-IR and Raman Spectroscopic Methods

A spectrum two PerkinElmer FT-IR spectrometer coupled with $LiTaO_3$ (lithium tantalate) MIR detector was used to scan THEDES samples and their components. Spectra were recorded in transmission mode, averaging of 20 individual scans in the spectral region 400 to 4000 cm^{-1} with a resolution of 1 cm^{-1} at room temperature. Background collection was done before every sampling and data analysis was performed using Origin Pro software version 9.0. The experiment was performed to analyze the presence of non-bonding intermolecular interactions between HBA and HBD. For the analysis of pure HBA and HBD, Thermal Nicolet FT-IR 6700 was used with same spectral region and resolution.

To measure the sensitivity of the Raman spectra of ChCl, ASA, and 1:1 ChCl:ASA, a Horiba JobinYvon Raman (model-LabRAM 800HR) system was used, where spectral analysis carried out by Origin Pro 9.0 software. The laser source (Green laser-MPC 6000) was powered on, and the software linked to it was run in the computer. Samples were loaded in the sample holder and 10x magnifying lens was focused on the samples, where

the 530 nm wavelength laser (Green) was hitting over. Diffraction grating (300) and filter type were set via software to get the best scattered light for detection. In case of filter (D2), the lower the index was, the higher the intensity of scattered light would have been.

2.2.5. Principal Component Analysis (PCA) Method to Analyze Fingerprint Spectra

PCA is an exploratory statistical method that aims to reduce the dimensionality of the data to reduce the noise as well as highlights the variabilities present in multivariate spectra of different chemical compounds [229]. PCA decomposes the multivariate response arranged in an X matrix into a product of two new matrices as indicated by this equation: $X = T_k P_k^T + E$, where T_k is the matrix of scores which represent how sample relate to each other, P_k is the matrix of loadings which contain information about how variables relate to each other, k is the number of factors included in the model, and E is the matrix of residuals which contains the information not retained by the model. All calculations were performed with MATLAB 2015a (The Mathworks, Natick, MA, USA) equipped with the PLS Toolbox v. 6.2.1 (Eigenvector Research Inc., Wenatchee, WA, USA) [230]. It was also used to compare the efficiency of the VCD over IR technique in terms of distinguishing the subtle differences among the spectral data of the chiral molecule-based DES.

2.2.6. Solvatochromic Method

Solvatochromic measurements were accomplished using three widely used dyes including Nile red, 4-nitroaniline, and N, N-diethyl-4-nitroaniline. Individual dye solutions of 5×10^{-4} molar (M) were prepared in dichloromethane (DCM). The dye solutions were micropipetted and loaded to glass vials to mix them well with 1:1 ChCl:ASA and 1:1 L-men:AA. Control solution (methanol-dye) was similarly prepared. A 250-µL aliquot of

each sample was transferred into a 96-well plate in triplicate. A synergy H (Biotek) microplate reader was used to determine the wavelengths of maximum absorbances (λ_{max}) of the dyes at 25 °C. Absorbance readings were collected as triplicate by spectral scanning of the THEDES in Nile red (400-650 nm), N, N-diethyl-4-nitroaniline (300-450 nm), and 4-nitroaniline (300-450 nm) at 1 nm intervals. All solvatochromic properties of the DESs were calculated using the following equations.

$$E_T(NR)_{kcal.mol^{-1}} = \frac{28591.44}{\lambda_{max}(nm)} \quad \text{2.2.6 (i)}$$

$$\pi^* = 0.314\,(27.52 - \upsilon_{N,N-diethyl-4-nitroaniline}) \quad \text{2.2.6 (ii)}$$

$$\alpha = 0.0649\,E_T\,(NR) - 2.03 - 0.72\,\pi^* \quad \text{2.2.6 (iii)}$$

$$\beta = \frac{1.035\,\upsilon_{N,N-diethyl-4-nitroaniline} + 2.64 - \upsilon_{4-nitroaniline}}{2.80} \quad \text{2.2.6 (iv)}$$

$$E_T^N = \frac{E_T(solvent) - E_T(TMS)}{E_T(water) - E_T(TMS)} \quad \text{2.2.6 (v)}$$

Where, υ = wavenumber, α = hydrogen bond donor acidity, β = hydrogen bond acceptor basicity, π^* = polarizability, and E_T^N (unitless) and ET(NR) refer to transition energy. In this study, α and β values of the glacial acetic acid (HBD) and the DES have mainly been focused on.

2.3. Results and Discussion

2.3.1 Radial Distribution Function (RDF) Analysis by MD Simulation

To elicit the formation of eutectic solvents and their nonbonding interactions, the atom-atom radial distribution functions (RDFs) are calculated from MD simulations. RDF can be used to investigate the distances between two atoms in MD simulations, which gives the probability to find a particle at a certain distance from reference particle compared to the statistical distribution [198]. The atom-atom RDFs, which provided the atomic level insights into the overarching structure of the THEDES system, are represented in **Figure 2.3**. The complex nature of ChCl and ASA with multiple H-bonding or non-bonding sites produces broad peaks and poorly defined minima. **Figure 2.3(a)** illustrates the contact distances between the atoms of ChCl and ASA. The first peak is between chloride and the hydrogen (21) atom on -OH of ASA, which shows the contact distances between the hydroxyl hydrogen atom and chlorine anion. This tall and narrow peak demonstrates the presence of hydrogen bonding and the interaction is around 2.1 Å, which is consistent with the HBD interactions with chloride anion in previously studied other DES systems [195,196,231]. It is known that the hydrogen bond strength can be correlated to the distance between hydrogen bond donor (HBD) and hydrogen bond acceptor (HBA) [232]. **Figure 2.3(a)** also shows the RDF of the chloride and the HBD atom (O13) of the ASA as well as the RDF of Cl^- and O_{Ch+} atom of choline cation. According to the RDFs, the distances between $Cl^-\ldots O_{Ch+}$ and $Cl^-\ldots O_{ASA}$ are almost same, which signifies that Cl^- is working as a bridge between ASA and Ch^+.

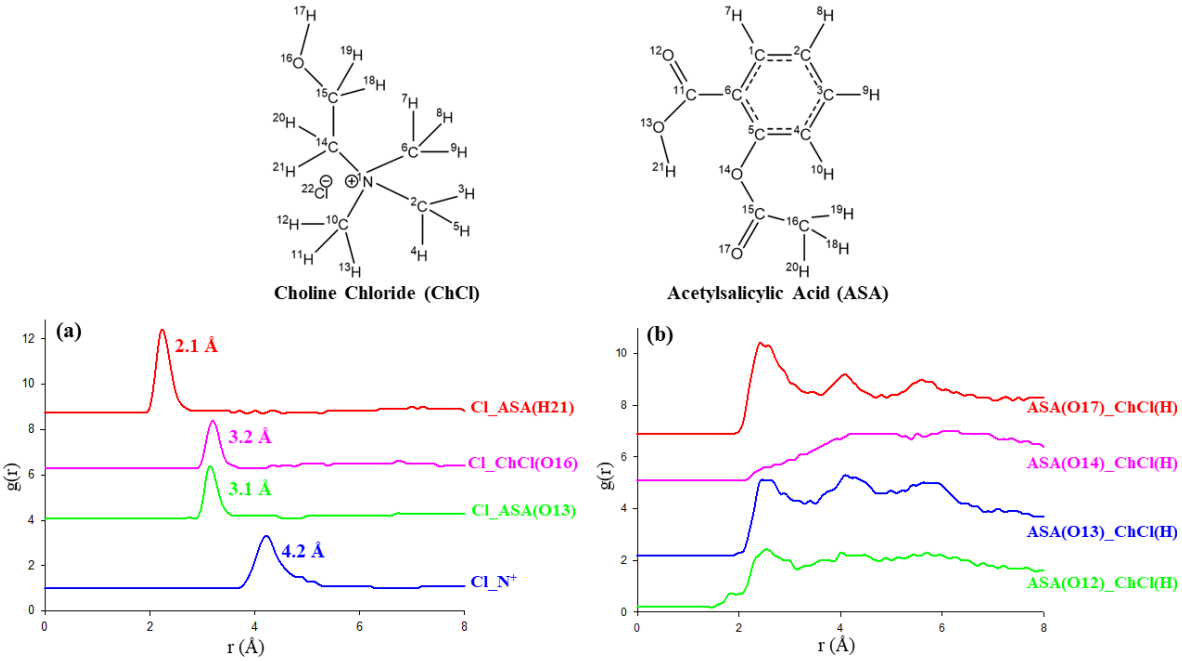

Figure 2.3. Atom-atom radial distribution functions (RDF) from MD simulations showing probability of (a) Cl^- around different moieties and (b) hydrogen atoms around different oxygen atoms.

These simulations suggest that the disruption to cation-anion electrostatic attractions of ChCl by ASA and forming highly interconnected hydrogen bonding in 1:1 ChCl: ASA, which could be one of the major rationales behind melting point depression. This disruption was estimated through the calculation of N^+-Cl^- radial distribution function, shown in **Figure 2.3(a)**. Two peaks are observed in this RDF, a strong peak at 4.2 Å and a weak interaction at 4.8 Å. A previous computational study on choline chloride–urea, choline chloride–ethylene glycol and choline chloride–glycerol found similar features, where a N^+-Cl^- radial distribution function was detected at ~ 4.10 Å [231]. The strong peak of the RDF appears at 4.2 Å can be attributed to the secondary interaction at 4.22 Å present in bulk choline chloride, which means that the primary interaction (4.02 Å) in bulk choline chloride

is displaced in the DES to 4.2 Å [233]. The weak interaction at 4.8 Å from the RDF signifies that the secondary interactions (4.22 Å, 4.28 Å) in bulk choline chloride are also displaced by ~0.6-0.7 Å in the DES. It can be inferred that the distance between N^+-Cl^- according to RDF analysis is small enough that ASA cannot reside between cation and anion. **Figure 2.3(b)** shows three strong non-boning intermolecular interactions among hydrogens (H) of ChCl and oxygen atoms from ASA including esteric oxygen (O17) of C=O group, carboxylic oxygen (O13) of -OH group, and carboxylic oxygen (O12) of C=O group. These peaks have distances less than 2.6 Å which are most likely form hydrogen bonding in it.

These results also indicate that the non-bonding interactions involved in ChCl and ASA play the major role for the formation of THEDES at ambient temperature. All types of non-bonding interactions are labeled in a three-dimensional structure (**Figure 2.4).**

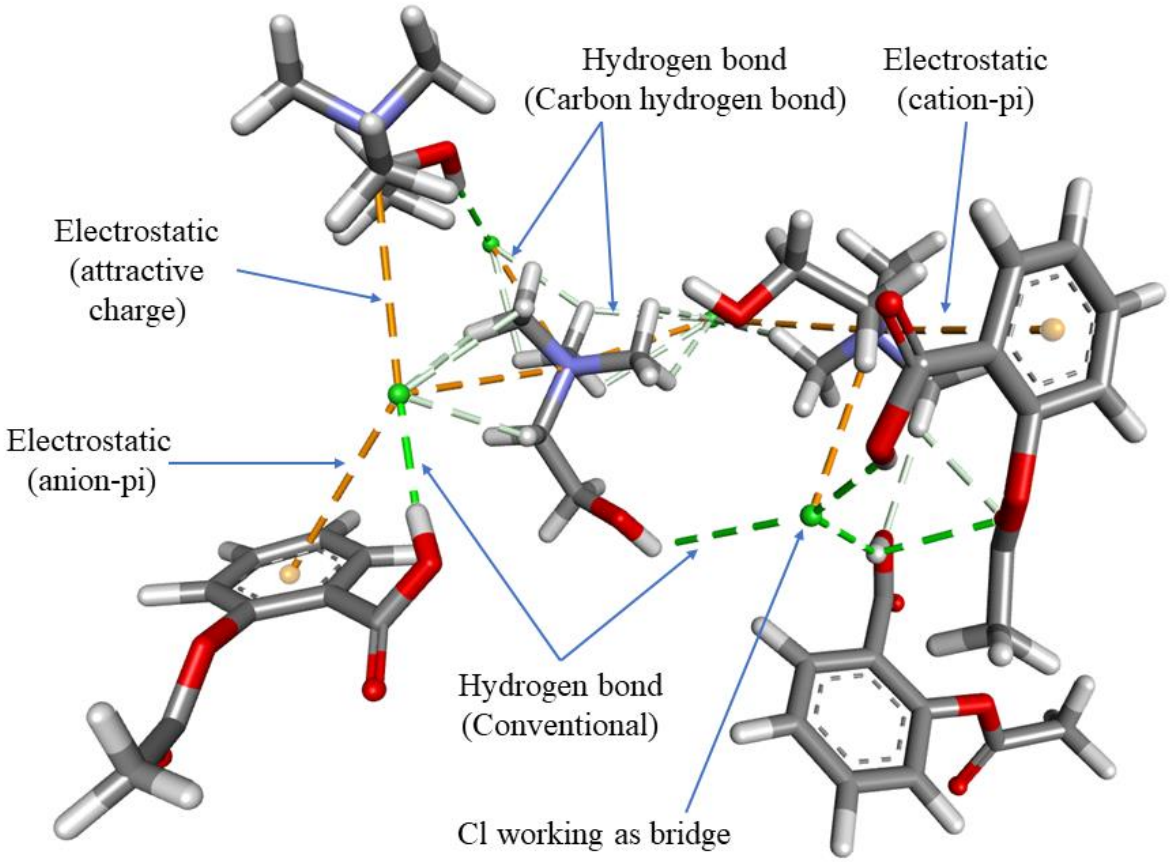

Figure 2.4. Simulation snapshots of THEDES environment showing all types of interactions present in the cluster systems. There are two types of hydrogen bonds, one is what we see typically, and another is carbon…hydrogen bond. This kind of classification is common in computational chemistry. However, in general term, carbon…hydrogen interaction is more accurate to describe them as dipole…dipole interactions. Hydrogen atoms are in white, carbon atoms are in ash, nitrogen atoms are in blue, and chloride ions are in green.

Among all of the interactions, hydrogen bonding between the chloride anion and the hydroxyl hydrogen (21) of ASA seems most important. Experimental IR data (given in the

vibrational analysis section) of ChCl, ASA, and 1:1 ChCl:ASA also supports the results obtained from RDF calculations.

2.3.2 Geometry and Hydrogen Bonding Analysis by DFT Calculation

The initial structures of 1:1 ChCl:ASA were isolated from MD simulation for the quantum calculation. Among those, the four most stable cluster conformers were considered for further optimization and calculation of their different quantum-chemical parameters. The pictorial illustrations of the four optimized conformers employing ωB97XD/6-311++G (d, p) level of theory are depicted in **Figure 2.5**.

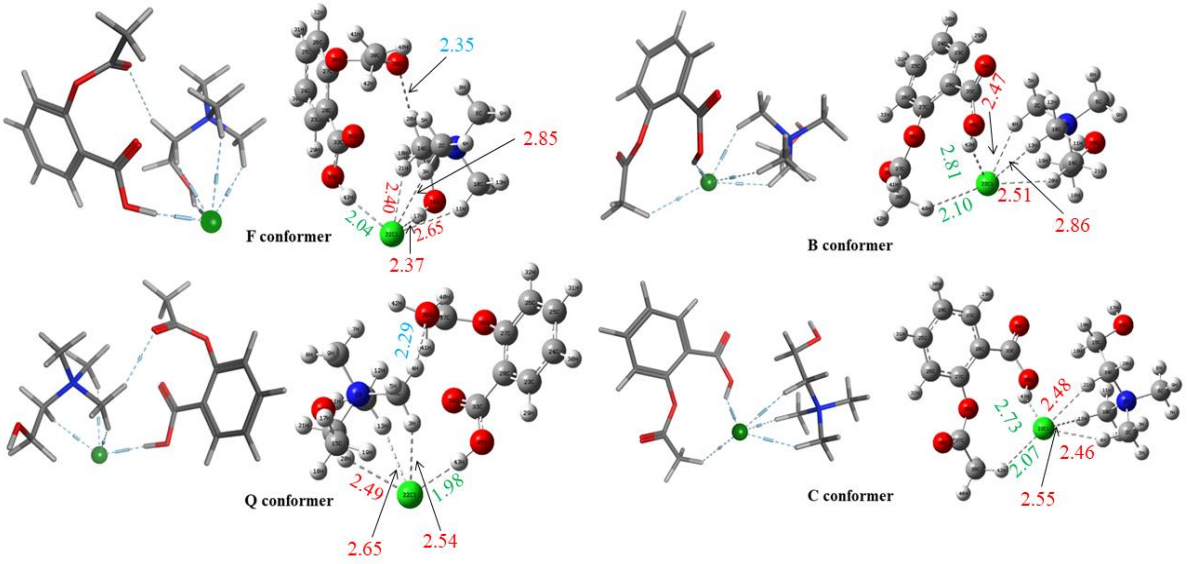

Figure 2.5. Optimized structures of four representative conformers (labeled as F, Q, B and C) of THEDES retrieved from MD simulation computed at ωB97XD/6-311++G(d,p) level of theory. Hydrogen atoms are in white, carbon atoms are in ash, nitrogen atoms are in blue, oxygen atoms are in red. The interatomic distances in red denote choline…Cl^-, in green denote ASA…Cl^-, in blue denote choline…ASA interactions.

Structural orientations of a DES are important to understand its eutectic nature because the way molecules interact determines its physical properties, such as melting point, thermal stability, and vibrational spectra. The THEDES system exhibits highly interconnected hydrogen-bonding network, wherein the ASA molecule interacts strongly with the Cl^- as well as the choline cation. Besides, the hydroxyl group of the carboxylic functionality on ASA interacts through H…Cl^- H-bond in all four conformers ranging from 1.98 Å to 2.10 Å. Analyzing F and Q conformers, it is found that the C=O end of the esteric functionality on ASA interacts with methyl protons on choline via C-H…π interactions with H…O distances 2.35 Å and 2.29 Å, respectively. Moreover, in all the four conformers, Cl^- is clearly acting as charge transfer bridge between choline cation and ASA, which is further confirmed via charge transfer analysis.

2.3.3 Charge Transfer Analysis

According to a recent review on DESs, charge delocalization between the anion and HBDs is occurring via hydrogen bonding interactions, which is actually responsible for the depression of freezing point of DESs [234]. Again, the strength of natural and ionic hydrogen bond correlates with the amount of charge transfer (NBO) from the HBA to the HBD [235].

The CHELPG partial charge analysis and NBO charge analysis were employed to investigate this proposed charge delocalization in our THEDES system. Four different representative conformers were analyzed. As can be seen in **Table 2.1**, the charge of chloride is significantly reduced (range between -0.723 to -0.780) in all investigated conformers along with the net increase in the negative charge on the ASAs ranging between

-0.042 to -0.075 according to CHELPG partial charge analysis. The same pattern of the results is observed in case of NBO charge analysis as well. Comparing the charge distribution in the THEDES system with its components reveals that the positive charge at the cationic core is increasing and negative charge at the hydroxyl group of choline is decreasing. These analyses give clear evidence that both of the functional groups are essential for the charge transfer occurring among the choline cation, chloride anion, and acetylsalicylic acid molecule through hydrogen bonding and electrostatic interactions.

Table 2.1. CHELPG and NBO charges on different components before and formation of THEDES mixture for four different conformers. Here, Ch^+: Choline, Cl^-: Chloride, ASA: Acetylsalicylic acid, Ch_N: N^+ of choline, Ch_O: Oxygen of choline.

	CHELPG					**NBO**		
	Ch^+	Ch_N	Ch_O	Cl^-	ASA	Ch^+	Cl^-	ASA
F conformer	0.786	0.263	-0.678	-0.744	-0.042	0.91	-0.842	-0.064
Q conformer	0.789	0.293	-0.715	-0.743	-0.046	0.933	-0.846	-0.087
B conformer	0.788	0.256	-0.711	-0.743	-0.045	0.946	-0.871	-0.075
C conformer	0.798	0.171	-0.722	-0.723	-0.075	0.939	-0.857	-0.082

Pure component	0.780	0.144	-0.729	-0.780	0	0.903	-0.903	0

2.3.4 Thermochemistry

In this study, the thermodynamic properties of ChCl, ASA, and the four cluster conformers of the studied THEDES were calculated and the results are summarized in **Table 2.2**. Thermochemical values for each THEDES conformers were obtained using the following equation: $\Delta X_{THEDES} = X_{THEDES} - X_{ChCl} - X_{ASA}$, where, X is either electronic energy (E), enthalpy (H), or Gibbs free energy (G). A moderate change of electronic energy, enthalpy, and Gibb's free energy are observed. The results indicate that after forming the solvent system, it becomes more stabilized compared to their pure components in gas phase. The corresponding electronic energy, enthalpy, Gibb's free energy changes for the most stable conformer (F) are, -98.61 kJ/mol, -101.11 kJ/mol, and -47.23 kJ/mol, respectively and for the second most stable conformer (Q) are -93.18 kJ/mol, -101.11 kJ/mol, and -44.53 kJ/mol, respectively. This happened due to the presence of higher number of non-bonding interactions in the F conformer (**Figure 2.5**). Analyses of all the studied THEDES conformers show that there are a number of stable positions possible for ASA around ChCl.

Table 2.2. The change in electronic energies, enthalpies and Gibb's free energies associated with formation of THEDES for four different conformers calculated at DFT-ωB97XD/6-311++G (d,p) level of theory.

Combinations	ΔElectronic energy (kJ/mol)	ΔEnthalpy (kJ/mol)	ΔGibb's free energy (kJ/mol)
B conformer	-75.38	-77.85	-28.75
C conformer	-70.76	-73.22	-13.94
F conformer	-98.61	-101.11	-47.23
Q conformer	-93.18	-95.65	-44.53

2.3.5 Experimental and Calculated Raman and FTIR Spectra Analysis

Acetylsalicylic acid is an acetyl derivative of salicylic acid. Therefore, this compound should have two peaks between 1650-1850 cm^{-1} on its IR spectra for its acid and ester groups [236]. In the 1:1 ChCl:ASA spectrum, two peaks in that range have been observed, where, 1673 cm^{-1} corresponds to the carboxylic acid group and 1751 cm^{-1} represents the ester group. However, both of the peaks are broadened and merged together due to the non-bonding intermolecular interactions between the ChCl and ASA. On the other hand, peak for -OH group of ChCl [195] was also broadened between 3135-3690 cm^{-1} in the spectrum of 1:1 ChCl: ASA, indicating strong H-bonds between -OH of ChCl and ASA (**Figure 2.6**). Besides, in the range of 900-980 cm^{-1}, quaternary ammonium group should show a characteristic peak [237]. Here, a peak at 961 cm^{-1} presents the quaternary ammonium group of ChCl and another peak at 1232 cm^{-1} represents the C-N stretching vibration [238]. Peak broadening also occurs this time due to strong doubly ionic effect [239]**.**

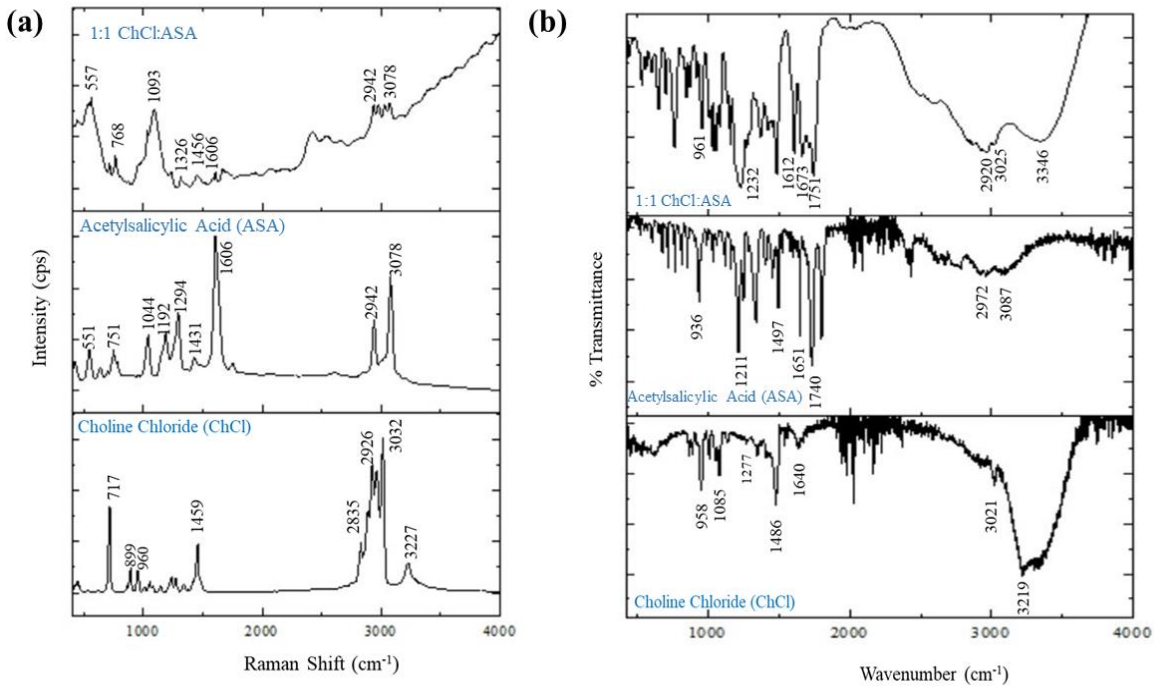

Figure 2.6. (a) Raman spectra and (b) FTIR spectra of ChCl (bottom), ASA (middle) and THEDES (top). These graphs are comparative representation of the spectral data of the components of DESs and the DES itself, which help to understand the changes of peak pattern in DES spectrum compared to the same peaks in their components.

When looking at the experimental Raman spectra in **Figure 2.6a**, the most recognizable peak of ASA spectrum was the C-C stretching vibration at 1606 cm^{-1}. While several other prominent peaks are also observed in the ASA spectrum below 1400 cm^{-1}, which are 1294 cm^{-1} and 1044 cm^{-1}. At around 3000 cm^{-1}, two CH-stretching vibrations, 3078 cm^{-1} and 2942 cm^{-1} on different carbons were observed for ASA [240]. On the other hand, two major CH-stretching vibrations, 2926 cm^{-1} and 3032 cm^{-1} were observed on ChCl spectrum. Symmetric νC-N peak at 717 cm^{-1} is intense in ChCl spectrum [241]. All of the peaks of the ChCl and ASA spectra seem to nearly disappear or merged together in the 1:1

ChCl:ASA spectrum and appear as broad peaks. The disappearance or merger of the peaks is another indication for the formation of the THEDES [242].

To compare the experimental and the computed Raman and IR spectra, a scaling factor of 0.957 was used as suggested in NIST database [243]. Calculated IR spectrum in **Figure 2.7b** shows that the peaks around 1700 cm^{-1}, specifically, 1611 cm^{-1} and 1777 cm^{-1} seem to indicate the presence of the carboxylic acid and ester functional groups of ASA, respectively. These are similar to the peaks observed in the experimental IR spectrum of ASA. Different conformers, however, seem to have slightly different wavenumbers for the same peaks. Conformer Q only appears to have one peak attributable to esters, at the 1716 cm^{-1}. Conformers F and B seem to have split peaks around this wavelength. Conformer F has peaks at 1721 cm^{-1} and 1799 cm^{-1}, while conformer B has peaks at 1725 cm^{-1} and 1794 cm^{-1}. Interestingly, the peaks for conformer B appear to be further shifted than the peaks for conformer F. ASA itself also seems to have a pair of peaks around 1700 cm^{-1}, however, they appear to be shifted toward larger wavenumbers, when the ASA is part of the THEDES. This is a significant change to note. Peaks around 2900 cm^{-1} would most likely be attributed to the C-H stretching vibrations, which typically produces peaks at 2800-3000 cm^{-1} range. These peaks are almost identical in their positioning in the spectra for conformer Q, conformer F, and conformer B. There are some of the peaks also seen in this range for the choline chloride. A majority of the calculated spectra also show a peak in the 3600-3800 cm^{-1} range, which is greatly separated from the rest of the peaks on the spectrum. This is highly likely due to the alcohol functional group of choline chloride. It is not confirmed that why a peak in this range is appeared for the acetylsalicylic acid. However, this is likely due to the -OH group on the carboxylic acid.

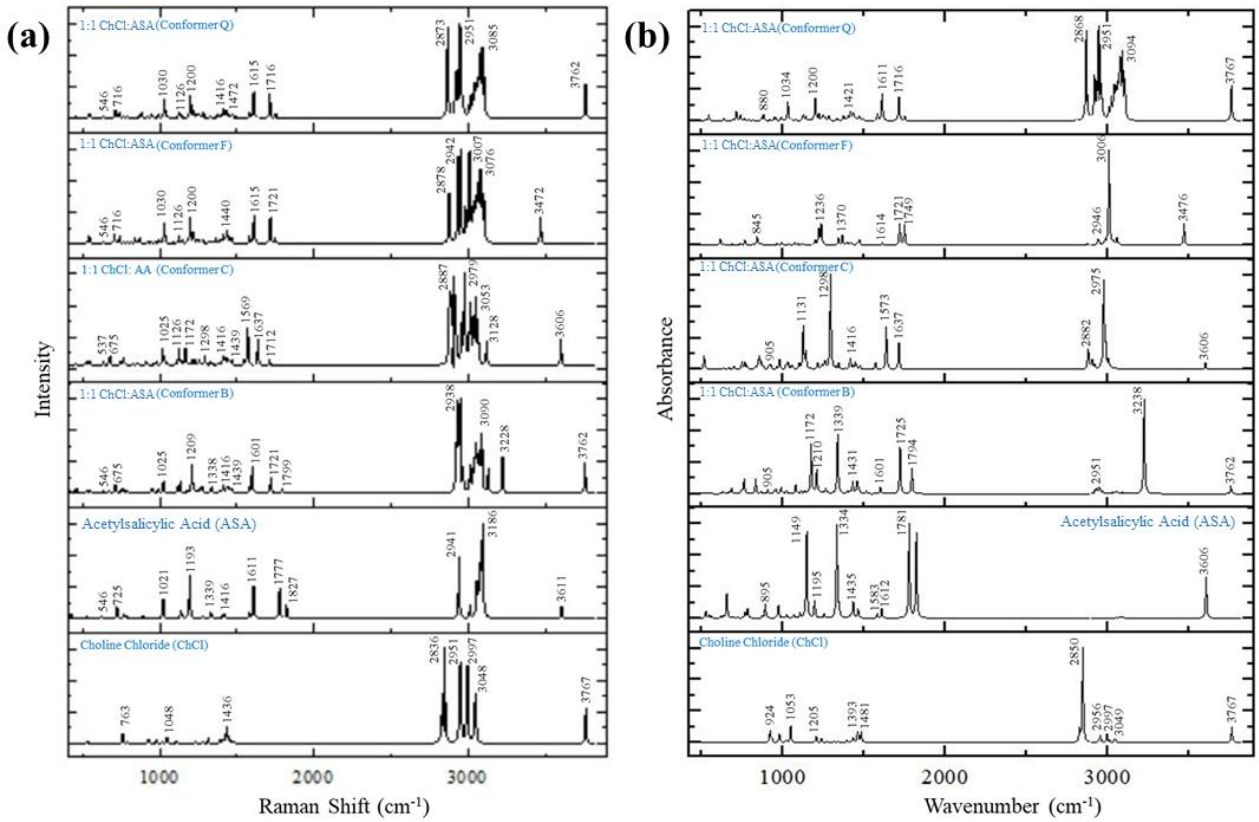

Figure 2.7. Calculated (a) Raman spectra and (b) infrared spectra of ChCl, ASA and four different conformers (labeled as F, Q, B and C).

Again, Computed Raman spectra in **Figure 2.7a** shows better baseline, which could help to better understand the comparison. There is a well-defined C-C stretching vibrations found between 1600-1640 cm^{-1} in the spectra of all four of the conformers and ASA. Similar to the experimental peaks of ASA, below 1400 cm^{-1}, two very definitive peaks 1021 cm^{-1} and 1193 cm^{-1} indicate the conformity of the calculated spectrum with the experimental spectrum. All of the spectra also show peaks around 2800-3100 cm^{-1}, which are the symmetric C-H vibrations similar to the experimental Raman peaks in the same region (**Figure 2.7a**). It has also been observed that peaks of ChCl and ASA in this range

merged together and emerge as higher number of peaks, which indicate the formation of THEDES.

It is difficult to distinguish the fingerprint region peaks of the spectra of four conformers. Therefore, in an attempt to identify the significant differences of four conformers in that region along with ChCl and ASA, simulated spectra were analyzed using a principal component analysis (PCA) algorithm. Spectral data are truncated to 400-2000 cm^{-1} for the convenience of the analysis as zero intensities are present in the longer wavelengths. Spectra are preprocessed using normalization and mean centering to highlight the separation of different groups. Data are cross-validated using the leave-one-out method while doing the analysis.

Figure 2.8 (a, b) illustrates the distribution of the pure components (ChCl and ASA) and four conformers in the PC1 and PC2 score axis. It is observed that the PC1 can successfully separate scores of ChCl and ASA for both Raman and IR data. It is rational as their spectral features are distinctive from each other. Scores of the four conformers are resided in between ChCl and ASA, which confirms the spectral features of these four conformers are the combination of ChCl and ASA. However, the score generated from IR spectrum of B conformer is located near to ASA in the PC1 score axis **(Figure 2.8b)**. This is probably due to the analogous location (around 1700 cm^{-1}) of the ester group of these two components, i.e., ASA and conformer B. On the contrary, scores of all four conformers, generated from Raman spectra, are resided near to ASA score **(Figure 2.8a)**. As Raman is sensitive towards C-C stretching vibration, peaks are appeared between 1600-1640 cm^{-1} in four conformers and ASA; which is probably positioned all the conformers near to the

ASA. Therefore, PCA analysis assists to visualize the similarity and dissimilarity of IR and Raman spectral data of ChCl, ASA and THEDES conformers.

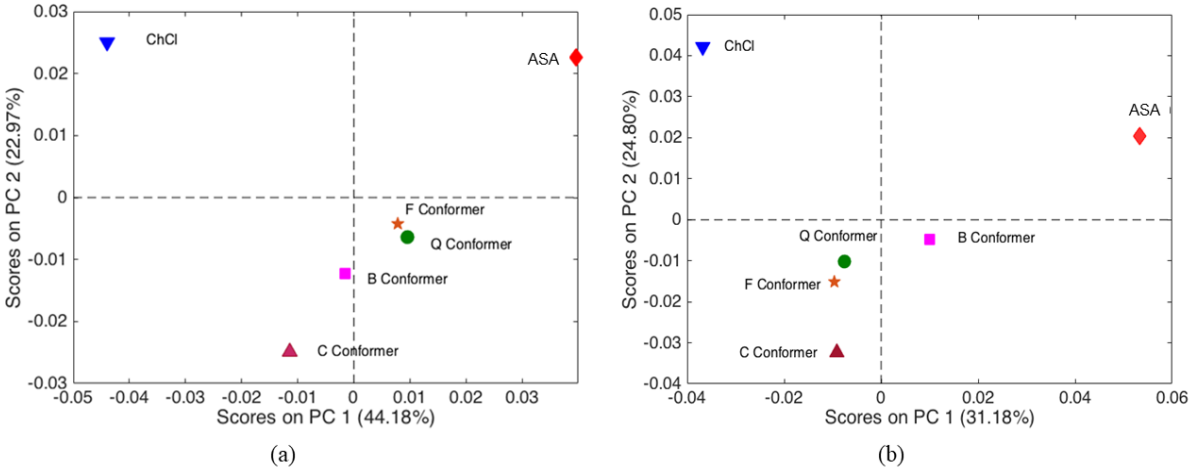

Figure 2.8. Score plots from principal components analysis of the (a) Raman and (b) IR simulated data (400-2000 cm^{-1}), specifically to compare complex fingerprint regions of the cluster conformers.

2.3.6 Solvatochromic Parameter Analysis

Although all of the solvatochromic parameters are obtained from 25-45 ± 0.2 ℃ at 5 °C interval, our focus is mostly on the parameters obtained at the ambient temperature as increasing temperature does not show any significant effect on the properties. At ambient temperature, transition energy, E_T(NR) and E_T^N (dimensionless) values are calculated from the solvatochromic responses of the UV-vis probs are found 47.49 and 0.518, respectively. Hydrogen bond donor (HBD) acidity (α) and hydrogen bond acceptor (HBA) basicity (β) show the measurement of the potential of HBD to donate a proton to HBA, and the potential of HBA to receive a proton from HBD, respectively. At 25 ℃, α value calculated for this

THEDES is found 0.259, and the β value is 0.553, which suggests that Cl^- is more prone to take a proton from the system. Solvent polarity measures the ability of the solvent to hold charge due to dielectric effect [244]. Solvent polarity (π*) should decrease with increasing temperature due to the thermal reorientation of dipoles which ultimately decreases the dielectric constant [245]. Polarity of the studied THEDES has followed this theoretical basis as at 25 ℃, π* value is 1.1023, however, at 45 ℃ it decreases to 1.0923.

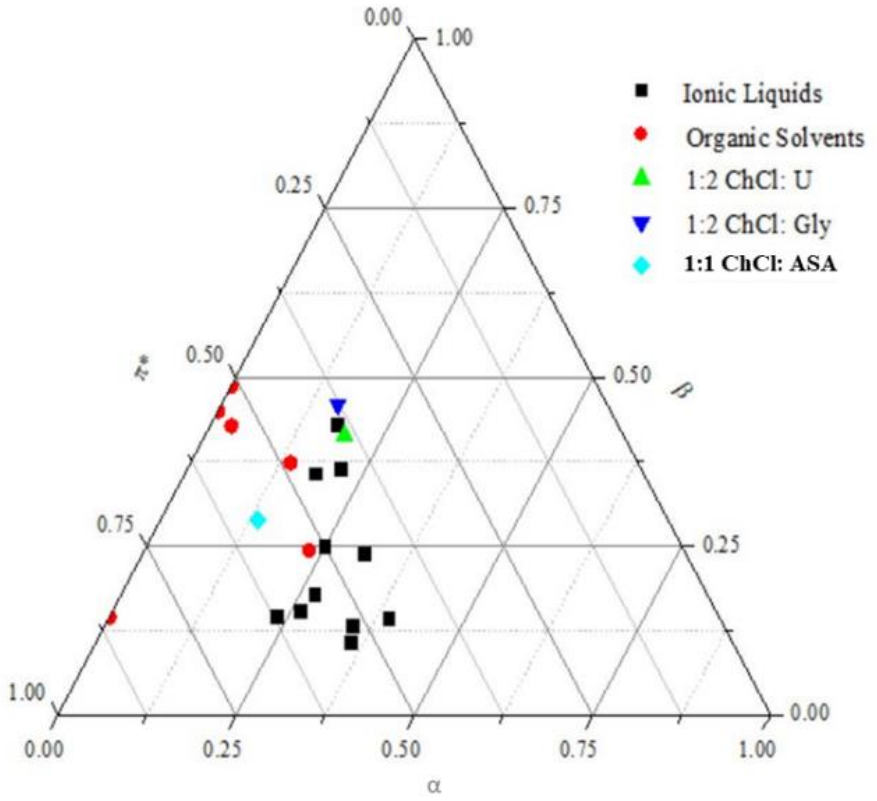

Figure 2.9. Kamlet-Taft parameters of 1:1 ChCl: ASA at 298K compared to selected organic solvents, ionic liquids and most common two of the DESs.

To get a comparative visualization of the Kamlet-Taft parameters (α, β, and π*) of the studied THEDES with some ILs, organic solvents, and DESs, a ternary plot **(Figure 2.9)**

is constructed by Origin Pro 9.0 software package using the data [246–252] tabulated in **Table 2.3**. Snyder introduced this type of solvent selectivity triangle (SST) to characterize the solvents and grouping them by plotting α, β, and π* of solvents [253].

Table 2.3. E_T^N, α, β and π* of selected ionic liquids, organic solvents, and most common DESs 1:2 ChCl: Urea and 1:2 ChCl: Glycerol collected from the literature along with 1:1 ChCl:ASA data used for ternary plot at 25 °C

Solvent	**E_T^N**	**α**	**β**	**π***
[Bmim][OAc] [46]	0.61	0.43	1.05	0.96
[Bmim][O_2CCH_2OH] [46]	0.61	0.44	0.87	1.12
[Bmpy][$N(Tf)_2$] [52]	0.544	0.427	0.252	0.954
[Bm_2im][$N(Tf)_2$] [52]	0.541	0.381	0.239	1.01
[Emim][PF_6] [52]	0.676	0.66	0.2	0.99
[Emim][NTf_2] [47]	0.657	0.76	0.28	0.9
[Emim]$N(CN)_2$ [52]	0.65	0.53	0.35	1.08
[HOEmim][AC] [47]	0.633	0.53	0.9	1.04
[Hmim][NTf2] [48]	0.65	0.65	0.25	0.98
[Hmim][OTf] [48]	0.67	0.67	0.52	0.98
[4-MBP][BF_4] [49]	0.636	0.53	0.533	1.066
Acetonitrile [52]	0.46	0.35	0.37	0.799
Acetone [52]	0.35	0.202	0.539	0.704
Dichloromethane [49]	0.309	0.04	0.578	0.733

Benzene [50]	0.111	0	0.1	0.59
Ethyl acetate [50]	0.228	0	0.45	0.55
Tetrahydrofuran [50]	0.207	0	0.55	0.58
1:2 ChCl: Urea [51]	0.58	0.41	0.87	0.82
1:2 ChCl: Glycerol [51]	0.53	0.32	0.90	0.74
1:1 ChCl: ASA	0.518	0.259	0.553	1.102

The ternary plot in **Figure 2.9** indicates that the Kamlet-Taft parameters of 1:1 ChCl:ASA are closer to the parameters of the ionic liquids than the organic solvents. Therefore, it is clearly a better alternative to ILs as it shares most of the excellent properties of ILs, but less toxic, easy to formulate, and less expensive.

To avoid the complexity, results and discussion of 1:1 menthol: acetic acid have been discussed below, separately

2.3.7 FTIR Spectroscopy. In this study, acetic acid (AA) and L-Menthol act as HBD and HBA, respectively. It was reported that L-menthol is an excellent HBA to form the DES with various HBDs even with big molecules like cholesterol [121]. Therefore, experimental ATR-FTIR analyses have been performed on L-menthol, acetic acid, and 1:1 L-men:AA to observe the contributions of the molecules or its functional groups to form the DES. **Figure 2.10** shows the FTIR spectra for L-menthol, acetic acid, and 1:1 L-Men:AA, and **Table 2.4** shows the relative shifts of the component's peaks in spectrum of the DES. It indicates that which component contributes more for the formation the hydrogen bonds.

FTIR spectrum of menthol shows a broad peak at around 3300 cm^{-1}, which corresponds to its hydroxyl group. Besides, the peaks in the range of 2870-2940 cm^{-1} correspond to sp^3 C-H bond. In the acetic acid spectrum, a sharp peak is observed at 1700 cm^{-1} for the -C=O of its carboxylic group and a band for O-H stretch of the same group is found at 3060 cm^{-1} [254]. Spectrum of 1:1 L-men: AA shows that the peak at 3300 cm^{-1} from the menthol gets broadened due to the H-bond formation with the AA molecules. This spectrum also shows that carbonyl peak for the eutectic gets sharper and shifts (shown in **Table 2.4**) to higher spectral region (~1710 cm^{-1}) compared to the same peak of the pure acetic acid (~1700 cm^{-1}). The higher percentage of peak shifting indicates AA as more contributing component to the formation of the classical hydrogen bonds.

Table 2.4 Relative wavenumber changes (%) in the spectrum of the DES.

Functional group		**Wavenumber (cm^{-1})**		**Relative changes (%)**
Acetic acid (AA)	**1:1 L-Menthol: AA**	**Acetic acid (AA)**	**1:1 L-Menthol: AA**	
C-O Stretching	C-O Stretching	1300	1290	-0.77
Carbonyl (C-O)	Carbonyl (C-O)	1700	1710	0.59
-OH	-OH	3060	3300	7.84
dl-menthol	**1:1 L-Menthol: AA**	**L-Menthol**	**1:1 L-Menthol: AA**	
Carbonyl (C-O)	Carbonyl (C-O)	-	1710	-

sp^3 C-H	sp^3 C-H	2870-2940	2870-2960	0.68
-OH	-OH	3290	3300	0.30

In the fingerprint region (1500 to 600 cm^{-1}) of the AA spectrum, a representative C-O stretching band appears at 1300 cm^{-1}. Similar band is found in the spectrum of the DES with lower intensity and is shifted to lower spectral region. In addition, peaks for C-H stretching at 1410 and 1460 cm^{-1} have been observed for AA and L-menthol, respectively. No significant new peak is appeared in that hydrocarbon region of the 1:1 L-men:AA spectrum. Overall, the spectral pattern of the DES correlates more with the AA spectral pattern and the higher percentage of peak shift of $-OH_{AA}$ suggest that AA strongly contributes for the formation of this DES.

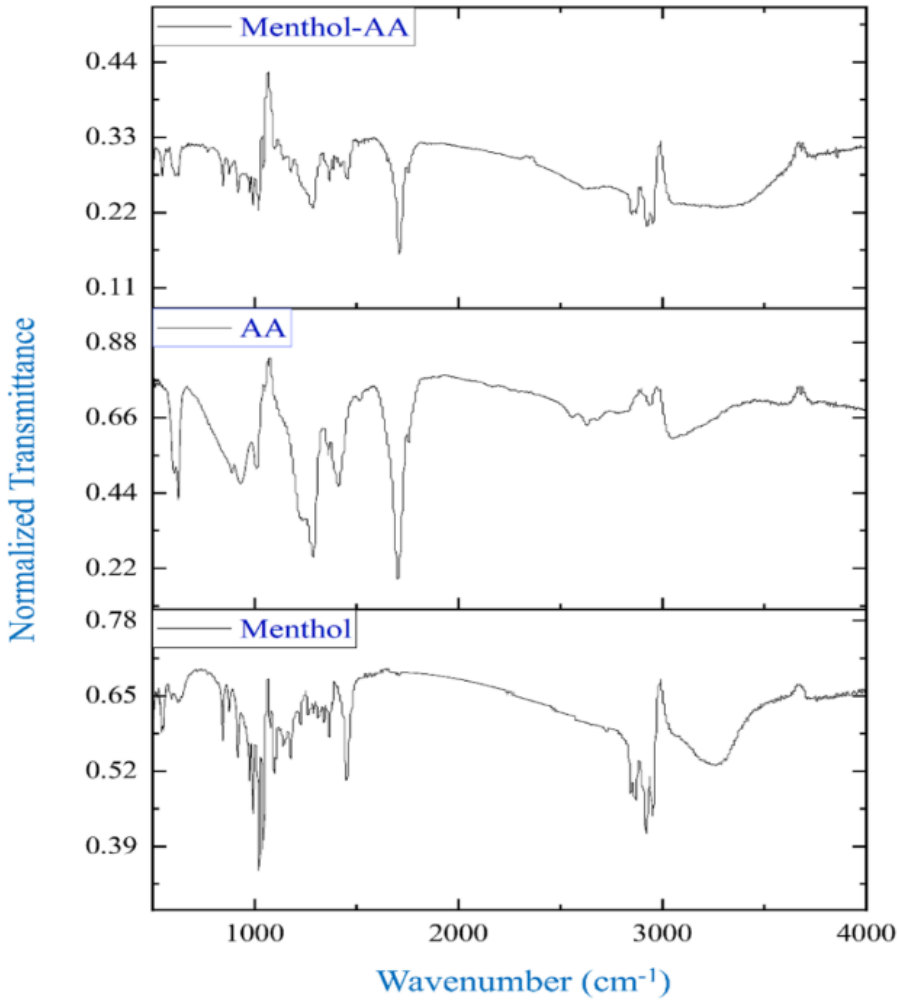

Figure 2.10 FTIR spectra of L-menthol (bottom), acetic acid or AA (middle), and 1:1 L-menthol: acetic acid (top)

The absorption bands for both L-Menthol and AA between the region 1500 to 600 cm^{-1} are difficult to interpret. Therefore, computed IR of the L-menthol, AA, and 1:1 L-men:AA are also analyzed. Since menthol is a chiral molecule, computed vibrational circular dichroism (VCD) spectra of them are studied to get understanding of the chirality transfer. Stronger contribution of acetic acid to form hydrogen bonds could be further analyzed in detail by the computed IR. Besides, chirality transfer from the menthol to acetic acid could

be proved using their computed VCD spectral data and principal component analysis (PCA).

2.3.8 Computed IR and VCD Spectra Analysis. The optimized clusters of the DES conformers show two major hydrogen bonds (**Figure 2.11)**, $O(20)_{Men}$---H(39)-$O(38)_{AA}$ and O(20)-$H(21)_{Men}$---$O(37)_{AA}$, which are mainly responsible for the formation of the DES. In all the cluster conformers, the $O(20)_{Men}$---H(39)-$O(38)_{AA}$ hydrogen bond distances ranges from 1.72 to 1.77 Å and the O(20)-$H(21)_{Men}$---$O(37)_{AA}$ distances range from 2.01 to 2.13 Å. Therefore, it can be inferred that $O(20)_{Men}$---H(39)-$O(38)_{AA}$ is the strongest hydrogen bond in all the structures. Due to the formation of the DES, some of the covalent bond distances and bond angles of menthol and acetic acid have changed in the cluster conformers (**Figure 2.11**). Values of ΔG (change in Gibbs free energy) and ΔH (change in enthalpy) for all conformers (**Table 2.5**) confirm that the formation of the DES clusters are spontaneous and the hydrogen bonds are strong enough to elongate the covalent bonds, such as O(7)-H(8) of acetic acid and O(1)-H(31) of menthol (**Table 2.5** and **Figure 2.11**).

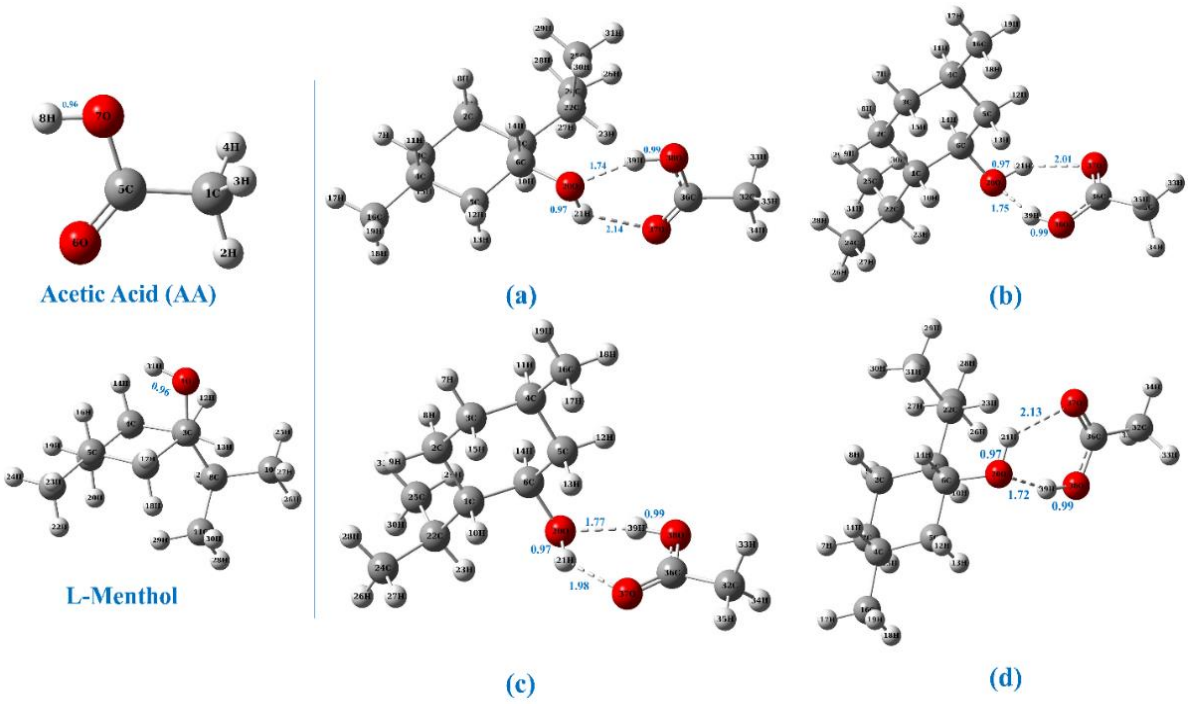

Figure 2.11. Energetically most favorable cluster conformers of 1:1 L-men: AA DES are (**a)** conformer A, (**b)** conformer B, (**c)** conformer C, (**d)** conformer D, which are optimized at DFT-ωB97XD/6-311G (d,p) level of theory and bond distances are in Å unit. Acetic acid and L-Menthol optimized structures are also given in this figure.

IR and VCD spectra can prove the hydrogen bonds and the elongations of the covalent bonds. Calculated IR and VCD spectra and the spectral data of L-menthol, acetic acid, and four cluster conformers of the DES in gas phase are presented in **Figure 2.12**. Menthol has an –OH functional group bonded with a chiral carbon and it shows C−O stretching vibration at a range of 1024-1056 cm^{-1}. In the computed menthol spectrum, the C(3)−O(1) stretching vibration has been shown at 1019 cm^{-1}. So, computed data shows close agreement to the experimental data. Between 1258 and 1455 cm^{-1} of the spectrum, C−H bending vibrations appear [255]. In the spectra of the cluster conformers, weak peaks for

C-H bending vibrations appear in the same region. That means, all the C-H peaks of menthol and AA in that region have been merged together and gotten smaller. It is an indication of DES formation.

Figure 2.12(a) shows that all the cluster conformers have C-H stretching vibrations at 1368-1406 cm^{-1} for menthol. Besides, conformer B and C show peaks at 657 cm^{-1} and 684 cm^{-1}, respectively for -O(38)-$H(39)_{AA}$ bending vibration. Morino *et al.* illustrated that methyl and methylene groups of menthol also have strong C−H vibrations in the 2848-2957 cm^{-1} range. Similar C-H peaks are observed in the calculated menthol spectrum between the range of 2800-3000 cm^{-1}. Moreno *et al.* reported that menthol shows a weak –OH stretching vibration at 3644 cm^{-1} [256]. In this study, weak –O(1)-$H(31)_{Men}$ stretching vibration appears at 3741 cm^{-1}.

In the AA spectrum, C(5)−O(7) stretching vibration is observed at 1183 cm^{-1} and C(5)=O(6) at 1800 cm^{-1}. C(36)=O(37) stretching vibrations in the spectra of the cluster conformers are found between 1745 and 1748 cm^{-1}. A weak peak for the –O(38)-H(39) functional group is detected at 3679 cm^{-1}, but the peak gets amplified and shifted to the lower wavenumber (3231-3263 cm^{-1}) in the spectra of the cluster conformers (**Figure 2.12a**). It has also been observed that the peaks appear for O(38)-H(39) of AA in the conformer's spectra are more intense than the peaks corresponding to the O(20)-H(21) of the pure menthol. It happens because -OH part of AA makes the stronger hydrogen bonding than -OH functional group of the menthol. To get better insight, it would be better to compare the bond distances of the O-H in menthol, acetic acid, and their DES clusters. When menthol and acetic acid are in their pure forms, bond distances of O(10)-$H(31)_{Men}$

and O(7)-H(8)$_{AA}$ are same (0.96 Å). But when menthol and acetic acid forms H-bonds between them, the O(38)-H(39)$_{AA}$ bond gets more elongated (0.99 Å) than O(20)-H(21)$_{Men}$ (0.97 Å) bond in all four cluster conformers **(Figure 2.11)**. It proves that stronger the H-bonding appears as more intense peak in the spectra. Therefore, peak for O(20)$_{Men}$…H(39)-O(38)$_{AA}$ appears stronger than the peak for O(20)-H(21)$_{Men}$…O(37)$_{AA}$.

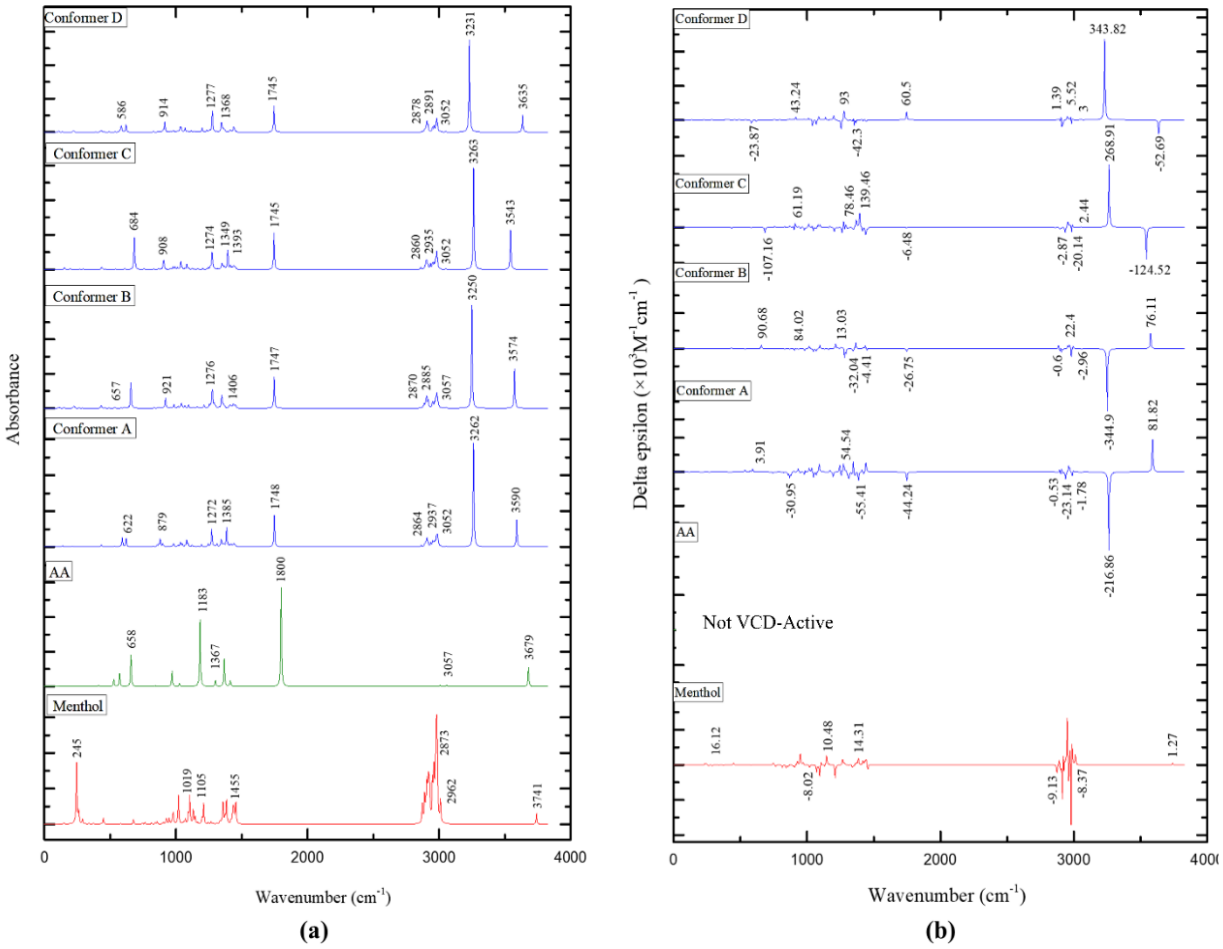

Figure 2.12. Calculated (a) IR spectra and (b) VCD spectra of L-menthol, acetic acid (AA), and the cluster conformers (labeled as A, B, C, and D) of 1:1 L-men:AA, where AA is not a VCD active compound.

Menthol is –OH group containing monoterpene. In **Figure 2.12(b)**, VCD spectrum of L-menthol has a peak for O(1)-H(31) bending vibration and the rotational strength is 16.12×10^{-44} esu^2cm^2. Negative rotational strength -8.02×10^{-44} esu^2cm^2 is obtained for C(3)−O(1) stretching vibration. Rotational strength values of $O(20)\text{-}H(21)_{Men}$ bending vibrations are 90.68×10^{-44} esu^2cm^2, -107.16×10^{-44} esu^2cm^2, and -23.87×10^{-44} esu^2cm^2 for conformer B, C, and D, respectively, where the value for conformer A is 3.91×10^{-44} esu^2cm^2. Besides O(1)-H(31) stretching vibration of menthol shows weak VCD rotational strength at 3741 cm^{-1}, which is 1.27×10^{-44} esu^2cm^2. In the VCD spectra of the conformers (**Figure 2.12b)**, the -OH peaks get intensified due to the strong hydrogen bonding [257] and their rotational strengths are 81.82×10^{-44} esu^2cm^2 (conformer A), 76.11×10^{-44} esu^2cm^2 (conformer B), -124.52×10^{-44} esu^2cm^2 (conformer C), and -52.69×10^{-44} esu^2cm^2 (conformer D).

Acetic acid (AA) is not a VCD active molecule, but in the spectra of the conformers a few strong peaks have been observed for AA. Values of the rotational strengths in conformer A, B, C, and D spectra are, 54.54×10^{-44}, 13.03×10^{-44}, 78.46×10^{-44}, and 93.00×10^{-44} esu^2cm^2, respectively for C(36)−O(38) stretching vibration, and 30.95×10^{-44}, 84.02×10^{-44}, 61.19×10^{-44}, and 43.24×10^{-44} esu^2cm^2, respectively for O(38)-H(39) bending vibration. These stronger positive and negative bands in the conformer's spectra than the menthol spectrum represent the formation of hydrogen bonding and chirality transfer. Due to the formation of $O(20)_{Men}\ldots H(39)\text{-}O(38)_{AA}$ and $O(20)\text{-}H(21)_{Men}\ldots O(37)_{AA}$ hydrogen bonds, O(38)-H(39) stretching vibrations of AA for the conformers show highly strong responses, -216.86×10^{-44}, -344.9×10^{-44}, 268.91×10^{-44}, and 343.82×10^{-44} esu^2cm^2, respectively.

In the L-menthol spectrum, one positive band having weak rotational strength has been observed over 3200 cm^{-1}. But in that region two strong peaks are emerged in all the spectra of the conformers. Stronger peak appears at lower wavenumber range (3200-3300 cm^{-1}) and the other one appears at higher wavenumber range (3500-3800 cm^{-1}). In all cases, one of them is a positive band and another one appears as a negative band. For example, in the spectrum of conformer D, VCD signal at the lower wavenumber range has positive rotational strength, which is -216.86×10^{-44} esu^2cm^2. At the higher wavenumber peak shows positive response and the value is 81.82×10^{-44} esu^2cm^2. These intensified rotational strengths clearly show the formations of $O(20)_{Men}\ldots H(39)\text{-}O(38)_{AA}$ and $O(20)\text{-}H(21)_{Men}\ldots O(37)_{AA}$ hydrogen bonds.

2.3.9 Principal Component Analysis (PCA). Principal component analysis was performed on the 400-2000 cm^{-1} spectral data of all IR and VCD spectra. The first principal component (PC1) explains the highest possible variability. In **Figure 2.13**, PC1 of IR and VCD spectra explains 53.1% and 65.9% of the spectral data, respectively. Then PC2 is accounted for the second largest variance of the spectral data, and it explains 25.0% and 13.2%, respectively. Therefore, PC1 and PC2 together illustrate the distribution of IR **(Figure 2.13a)** and VCD spectra **(Figure 2.13b)** of the pure components (L-menthol and acetic acid) and the four DES cluster conformers over 78% on the two PC score axes.

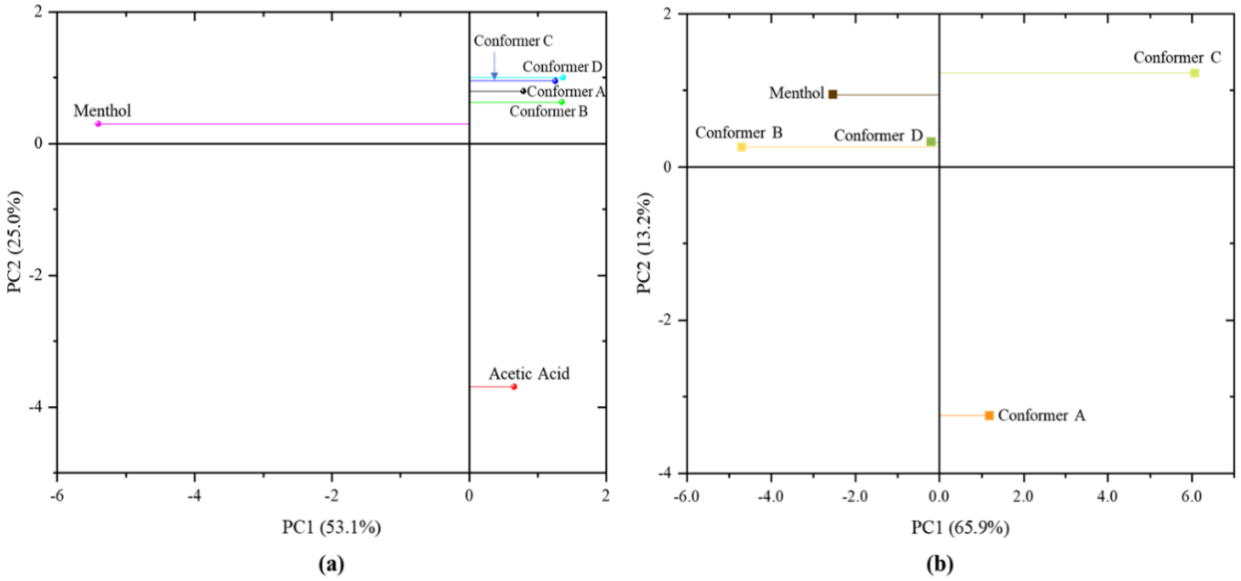

Figure 2.13. Score plots from principal components analysis of the (a) IR and (b) VCD simulated spectral data (400-2000 cm^{-1}), specifically to compare complex fingerprint regions of the DES cluster conformers.

It is observed that the PC1 can successfully separate scores of menthol and acetic acid for IR spectral data (**Figure 2.13a**). It is logical as their spectral features are distinctive from each other. Scores of the four conformers reside close to each other and away from menthol and acetic acid, which confirm that the spectral features of these four conformers are the combination of menthol and acetic acid. Although PCA of IR spectral data successfully separated menthol and acetic acid from their cluster conformers, it is unable to differentiate the PCA scores of the conformers (**Figure 2.13a**). PC1 can explain higher percentage of spectral data because it is driven by C-O, C=O, and C-H stretching vibrations of hydrocarbon region, where PC2 is driven by mainly C-O, C=O stretching vibrations.

However, the PCA scores generated from VCD spectral data can distinguish the conformers because VCD technique is selectively sensitive for chiral molecule menthol. Although AA is not a VCD-active compound, rotational strengths of the C-O stretching in the cluster conformer A, B, C, and D, are 54.54×10^{-44}, 13.03×10^{-44}, 78.46×10^{-44}, and 93.00×10^{-44} esu^2cm^2, respectively. Since the peaks correspond to the C-O stretching vibrations of AA, chirality has been transferred from the chiral menthol to achiral AA. Therefore, this clusters are well structured and show characteristic as a single complex chiral molecule. Therefore, PCA analysis helped to visualize the similarity and dissimilarity of IR and VCD spectral data of menthol, AA, and their DES conformers. It proves that VCD could be used as a complementary tool to the IR spectroscopy to investigate chiral molecule-based DES.

2.3.10 QM Calculation and Kamlet-Taft Parameters Analysis. Comparative HOMO-LUMO gap values of the components and the cluster conformers could help to get hints about how the charge delocalization has been occurred from one component through another component [258]. Lower HOMO-LUMO gap means higher chemical reactivity of a compound [259]. HOMO-LUMO gap values of menthol, AA, conformer A, B, C, and D, are 8.62, 7.12, 6.99, 6.90, 6.99, and 6.89 eV, respectively (**Table 2.6** and **Figure 2.14**). HOMO-LUMO gaps get decreased in the cluster conformers compared to the HOMO-LUMO gaps of its components, which indicate that the cluster structures are formed by the orbital overlapping or by charge delocalization from menthol to acetic acid and vice versa. It could also facilitate chirality transfer from the chiral menthol to the achiral acetic acid through their complex hydrogen bond network [260,261]. Change in Gibbs free energy (ΔG), electronic energy (ΔE), and entropy (ΔS) of the clusters have also been calculated in

the gas phase using DFT-ωB97xD/6-311G(d,p) level of theory (**Table 2.5**). ΔG values show that among the clusters, conformer D is the most spontaneous structure. Besides, ΔS values suggest that the cluster structures are spontaneous even at low temperature to high temperature.

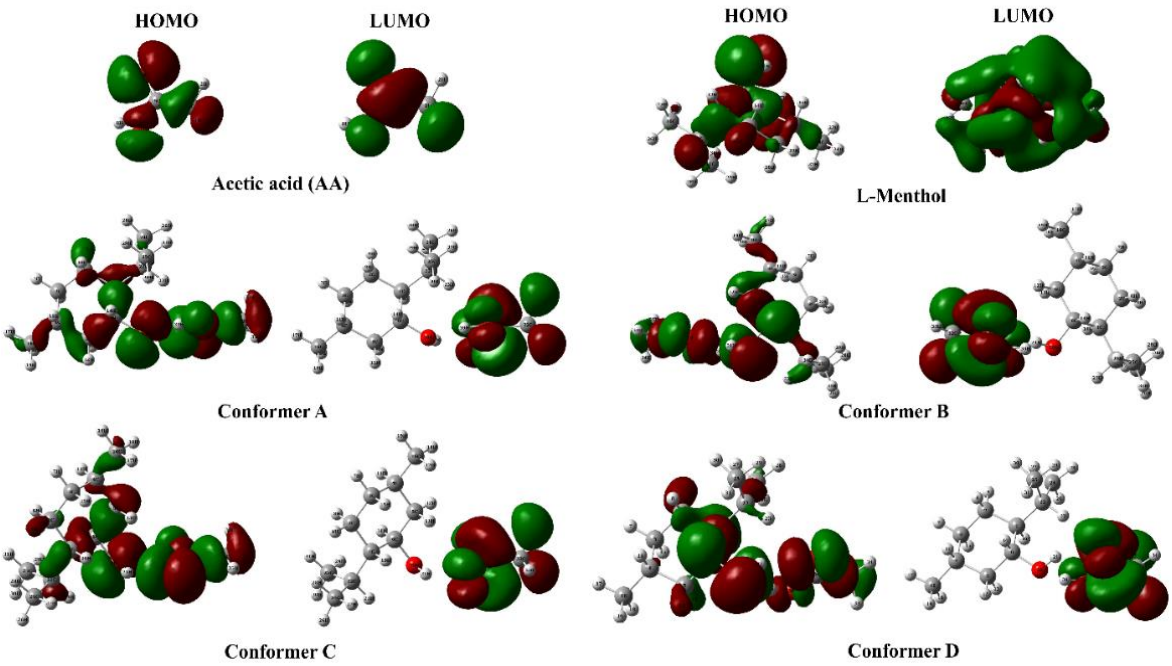

Figure 2.14. Selected frontier molecular orbital (HOMOs and LUMOs) of menthol, acetic acid, and conformers calculated at DFT-ωB97XD/6-311G (d,p) level of theory in the gas phase.

Since conformer D is the most spontaneous and it shares maximum characteristics of its components, ΔG value of this structure has also been calculated in high dielectric constant medium (water) using IEFPCM solvation model at the same level of theory. ΔG value is found as -7.94 KJ/mol at water phase. This is just for one orientation of 1:1 men: AA structure and this cannot show the overall scenario. It is well known that when water is

added at a certain extent to a hydrophobic DES then water molecules start to dominate the hydrogen bond formation [214]. However, a small amount of water could be added to this DES to get more intense and sharper spectroscopic peaks. Higher level basis set (aug-cc-pVDZ) is also used to calculate the electronic energy of conformer D to obtain more corrected electronic energy of the cluster. ΔE value is calculated as -55.25 KJ/mol using DFT-ωB97xD/aug-cc-pVDZ level of theory at gas phase. Since this basis set is computationally too expensive and the water phase calculation for DES cannot mimic experimental situations, all the calculations of this study have been conducted using DFT-ωB97xD/6-311G(d,p) level of theory in the gas phase.

Table 2.5. HOMO-LUMO energy gap (values in eV), ΔG, ΔE, ΔH (in KJ/mol), ΔS (in J/mol/K) of menthol, acetic acid, and the DES's conformers are calculated using DFT-ωB97xD/6-311G(d,p) level of theory at gas phase and standard condition.

Parameter	**Menthol**	**AA**	**Conformer A**	**Conformer B**	**Conformer C**	**Conformer D**
LUMO	-1.2	-2.83	-2.83	-2.82	-2.82	-2.84
HOMO	-9.82	-9.95	-9.82	-9.72	-9.81	-9.73
HOMO-LUMO gap (eV)	8.62	7.12	6.99	6.9	6.99	6.89
ΔG (KJ/mol)	-	-	-18.43	-16.87	-15.20	-22.24

ΔE (KJ/mol)	-	-	-56.12	-55.67	-54.27	-58.97
ΔH (KJ/mol)	-	-	-58.60	-58.14	-56.75	-61.44
ΔS (J/mol/K)	-	-	-134.77	-138.50	-139.43	-131.57

Hydrophobic deep eutectic solvent is a complex system and do not behave as typical solvent. It is difficult to picture the overall scenario of the solvent only by the quantum calculations. To make more sense of this system, experimental solvatochromism has been employed. Kamlet-Taft parameters including α, β, and π* can excellently explain a DES system [215]. Classical hydrogen bonds play the major role for the depression of the freezing point of the studied solvent. Measured solvatochromic parameters of methanol (control solvent) show high degree of agreement to the literature values, which proves the reliability of the experiment. The transition energy and polarizability of the methanol are found 54.98±1.07 kcal.mol^{-1} and 0.75 ± 0.01, where the literature values are 52.02 kcal. mol^{-1} [262] and 0.77 [263], respectively.

Kamlet-Taft parameters, such as α and β of AA and 1:1 L-men:AA are mainly investigated from this experiment. Both α and β values have been increased for the DES compared to glacial acetic acid (AA). The values are 1.14 and 0.43 for AA, and 1.61 and 0.61 for the DES, respectively. The values proved that both the hydrogen bond donation and reception have been increased at a great extent among the DES components compared to the pure

AA. These results indicate the formation of this DES is mainly driven by the classical hydrogen bonding, where AA dominates the formation. These values also suggest higher transition energy for the DES than the AA. The dimensionless E_T^N (transition energy) values of the DES is found 0.97, whereas for AA is 0.78. Higher transition energy represents lower polarizability of the DES. Polarizability values of the DES and AA are 0.55 and 0.65, respectively, which means electron cloud of among the components is well-distributed and localized compared to the glacial AA.

CHAPTER THREE

WATER-BASED DEEP EUTECTIC SOLVENT (WDES)

ABSTRACT

High viscosity of a deep eutectic solvent (DES) is one of the biggest challenges to use them commercially. In this study, two novel water-based low viscous DESs were formulated which could be easily applicable in many areas of research and industry, such as pharmaceuticals, waste management, and biorefining. To formulate the DESs, water was used as a sole hydrogen bond donor, where the hydrogen bond acceptor was choline chloride. Melting points of 1:3 and 1:4 choline chloride:H_2O were found to be significantly low, -79.21 and -79.25 °C, respectively. TGA proved that water could be relatively stable at a higher temperature when it forms the DESs. For example, in the TGA thermogram of 1:3 ChCl: H_2O, the crystalline water was found up to 148.64 °C and the onset point was 193.75 °C. Solvent selectivity triangle (SST) of Kamlet-Taft parameters proved that the DESs possess similar solvatochromic properties to ionic liquids. Therefore, solvatochromism helped to understand the solvation of the DESs. A simple analytical method was developed employing ion chromatography and atomic absorption spectroscopy to investigate the solubility of sodium halides, alkali chlorides, and cobalt chloride in the studied DESs. Solubility trends of the metal halides in both DESs were found same, NaCl > NaBr > NaI > NaF for sodium halides and LiCl > NaCl > KCl for alkali metal chlorides. Among all the studied metal halides, solubilities of the $CoCl_2$ and LiCl were found highest and the second highest, respectively. These findings indicated that the formulated DESs could be a good metal extraction media. Similar to the studies in the

previous chapters, experimental and computed IR, Raman, and quantum calculations helped to understand which molecules are contributing more to form the DESs and they proved that hydrogen bonds played major roles to form the water-based DESs. Solubilities of the studied drug molecules were found to be 1.3 to 6.7 times higher in the solvents than their solubilities in water. Cell viability assay of the WDES1 (1:3 ChCl:H_2O) compared to dimethyl sulfoxide (DMSO) against HEK293 cell line proved that the solvent is applicable to the biological system.

3.1. Introduction

Organic solvents, which are typically toxic to the environment, have been used for centuries. In the last few decades, some greener alternative solvents have been emerged and among them ionic liquids (ILs) show excellent qualities. Although ILs show a great promise, their toxic nature and expensive formulation make it difficult to use on a large scale [22–26]. To overcome the drawbacks, idea of deep eutectic solvents (DESs) has been emerged in the past two decades [27–31]. Deep eutectic solvents show a lot of promise in various fields, such as chemistry, material science, physics, and pharmaceutical science. It has the advantages of being nonflammable with negligible vapor pressure compared to molecular solvents and shares many beneficial qualities of ILs at the same time [32]. DESs are also cheaper to formulate, nontoxic, highly pure, easily recyclable, and biodegradable [33]. Although DESs are environmentally benign and considered as one of the most versatile alternative media nowadays, detailed knowledge of their miscibility, polarity, and

solvation behavior are yet to be explored. High viscosity and disruption of the eutectic environment by water ingestion cause major problems for their use on a large scale [34]. Recent studies reported that water has some unique effects on the physicochemical behavior and chemical structures of DES. If water is added to a DES system at higher mole fraction (e.g., >25%), both the HBA and HBD of the DES get hydrated and show higher diffusivity, and the water molecules dominate the hydrogen bond formation with the constituents of the DES, which eventually dampens the DES system [35]. Another study strengthened the claim that the water molecules make stronger interactions to the components of a DES than the interactions among themselves (e.g., water-water) or among the DES-DES clusters [36]. Viscosity of a DES typically decreases dramatically with the addition of a small amount of water. For instance, Savi *et al.* quantified that when approximately 10% of water is added to the 5:1 lactic acid:glucose DES, viscosity of the DES decreases by 85.9% [37]. Therefore, it is important to understand the role of water in field of DES.

To solve the problems, we came up with an idea to formulate a novel type of DES where water is used as the sole hydrogen bond donor. These DESs can be called as water-based DESs (WDESs). To date, only Marcus [38] claimed that some aqueous salt hydrates should be considered as DES. One of our research group members, Asare [39] did detail research and proved that water can be a sole hydrogen bond donor (HBD) to form DES with ChCl. In this study, we have focused only on the combinations of 1:3 (WDES1) and 1:4 ChCl:H_2O (WDES2).

Thermal behavior of a DES is crucial to know because it helps to estimate the range of its applicability [40]. To measure the eutectic point and thermal stability of the solvents, differential scanning calorimetry (DSC) and thermal gravimetric analysis (TGA) techniques have been widely used [41]. Solvatochromism technique could play an important role to select a proper alternative solvent for a specific application [42]. Similar to an organic solvent, a DES system is hard to describe only by dielectric constant or dipole moment because it possesses many interactions, such as doubly ionic effect, hydrogen bonding, halogen bonding, π-π interactions, and van der Waals forces [43–45]. Since most of the available methods allow examination of only one major type of interaction, a range of different probes are required to get a clear insight of the strength of solute-solvent interactions in a DES system. FT-IR and Raman spectroscopic methods are the two renowned, efficient, and available tools to observe the nonbonding interactions including H-bonding among the components, to prove the successful formation of DES, and to determine the water content in a DES [45,55]. Molecular dynamics simulation, being a highly effective toolbox in the world of molecular modeling, can track the motion of individual atoms as well as can explain their arrangements, orientations and movement of chemical structures with extreme details [56]. MD simulation act as a bridge between the atomic world to the macroscopic world of laboratory. The interactions amongst the molecules can be predicted and the insights behind bulk measurements can also be revealed [57]. Besides, DFT-based IR and Raman spectroscopy, quantum chemical calculation, and exploring nonbonding interactions of the optimized cluster structures of the DESs can add deeper understanding to the mechanism of formation [58].

As we discussed earlier in the THEDES chapter, solvatochromism helps to understand the solvation of the DESs, but solubility of ionic compounds in DESs has not been investigated a lot. Only a few works have been published based on metal oxide and sodium salt solubility in DESs using two methods, e.g. inductively coupled plasma-atomic emission spectroscopy (ICP-AES) [49,50] and the shake-flask method [51]. In this study, a simple solubility determination technique has been developed using ion chromatography (IC) and flame atomic absorption spectroscopy (FAAS) to determine the solubility of sodium halides, alkali chlorides, and $CoCl_2$ in the studied WDESs. Besides solvatochromism, solubility results could help to understand the extractability of the WDESs. Several studies on metal extraction, such as Li and Co extraction from Li-ion battery waste [5], extraction of Co and Fe from NdFeB magnets [52], dissolution and recovery of electrum, native Te, tellurobismuthite, galena, and chalcopyrite [53], and extraction of metal salts and oxides from incinerated sewage sludge and ash [54] using DESs have been reported. Therefore, it has already been established that certain types of DESs could be the excellent extraction media for the specific metal recycling process. Therefore, the aim of this study of the metal halides is to investigate the primary data of the Li and Co solubility of the WDESs.

Eutectic technology has already been proved as a promising way to improve drug delivery and solubility [61,264]. Other major advantages include that they can be prepared from low to nontoxic, cheaper, and readily available materials, and some of their eutectic points are remarkably low. In this study, WDESs are prepared by the cheapest possible materials, including choline chloride and water, which are typically nontoxic [62]. Besides, their extremely low eutectic points [62] and reasonably less viscosity compared to other DESs make them suitable for the pharmaceutical and biological applications. To prove their

applicability in the stated areas, solubility measurements of drugs and in-vitro experiments could be conducted using widely used HPLC-UV and MTT assay methods, respectively [265].

Poor drug solubility in the aqueous medium is one of the major challenges for formulation scientists [59]. Solubility could play a vital role to achieve optimum drug concentration at the target site and obtain the intended pharmacological responses [59]. Since a lot of oral drugs or drug candidates are poorly soluble in a biological system, scientists have been trying to overcome the problem by employing many techniques, such as chemical modifications of drug [59] solid dispersion, particle size reduction, crystal engineering, salt formation, use of surfactant, and complexation [60]. Formulation and delivery of the poorly soluble drugs using DES technology have shown excellent performance [61]. Although extensive studies should have been conducted, laboratory scale reports have already proved high potential of these approaches. Besides the qualities of the WDESs stated earlier, they also show high thermal stability and high polarizability [62]. Overall, the studied solvent showed a lot of promise for pharmaceutical and biological applications.

The overall objectives of this study are (i) To overcome the difficulties related to high viscosity of DES and answer the questions, such as why water disrupts or disturbs a eutectic environment or can water be a sole hydrogen bond donor (HBD) to form a DES?, (ii) If water solely can form a DES, then how much do the nonbonding interactions influence to decrease the melting points and to increase their thermal stabilities?, (iii) how much the solvatochromic parameters and solvation behavior of a WDES correlates to the selected ionic liquids?, (iv) explore their unique physical properties, (v) structure elucidation using

quantum chemical and radial distribution function calculations, (vi) optimization of the spectroscopic measurements to obtain the best responses of the unique water-based DESs, which could explain the major reasons behind their extreme depression of freezing points, (vii) computation of IR and Raman to focus only the specific cluster structures of WDESs (1:3 and 1:4 ChCl:H_2O), since experimental IR shows cumulative response of all possible interactions of the clusters exist in the systems and cannot differentiate the contributions of 3 and 4 portions of water, (viii) how much the solubilities of the studied metal halides in water decrease when water form DESs with the ChCl at certain molar ratios?, (ix) explore the potential of the solvents to enhance the solubilities of some sparingly soluble active pharmaceutical ingredients (APIs), (xi) evaluating the toxicity of the solvents to the biological system to explore its possibilities of safe application, and (xii) evaluation of their efficacy as a drug delivery vehicle.

3.2. Experimental Details

3.2.1 Materials

Nile Red, 4-nitroaniline, and dichloromethane (DCM) were purchased from Thermo-Fischer Scientific (Dubuque, IA). Choline chloride (ChCl), cobalt chloride ($CoCl_2$), sodium fluoride (NaF), sodium chloride (NaCl), sodium bromide (NaBr), sodium iodide (NaI), lithium chloride (LiCl), and methanol were purchased from Acros Organics. Potassium chloride (KCl) and N,N-diethyl-4-nitroaniline were purchased from Fisher Chemicals and Frinton Laboratories, respectively. All the chemicals have purity ≥ 98.0 %. Ultrapure water was used for the solubility test of the metal halides to get rid of any ion impurities.

All the active pharmaceutical ingredients (APIs) including salicylic acid, acetylsalicylic acid, paracetamol, 4-ethoxyacetanilide, acetanilide, and o-toluic acid were purchased from Acros Organics (USA), where all the chemicals had purity ≥ 99 %. Chemicals used for the in-vitro assay will be discussed in the cell line and cell culture subsection. Milli-Q water was used for the formulation of the WDESs and to conduct in-vitro assay.

3.2.2 Formulation of the WDESs

Water-based deep eutectic solvents (WDESs) were formulated by mixing anhydrous choline chloride and water at 1:3 and 1:4 molar ratios in a covered beaker with continuous stirring (600 rpm) for 30 minutes under atmospheric temperature and pressure until homogenous liquids were obtained. Solvents were monitored for 1 hour to confirm if there were any crystals left at the bottom of the beakers. After the preparation, solvents were stored in a desiccator.

WDES1 (ChCl:3H_2O) and WDES2 (ChCl:4H_2O) were formulated by mixing of anhydrous choline chloride with three and four molar ratios of water at ambient temperature for 30 minutes in a covered beaker with constant stirring (≤600 rpm) under atmospheric pressure until a homogenous liquid were obtained. The formulated solvents were monitored for an hour to confirm any crystal reformation, since homogeneous clear liquid is mandatory for the successful formulation of a DES. After the preparation, solvents were preserved in -20°C freezer. Although moisture absorption is not that much concern for the WDESs structure, all the experiments were conducted using freshly prepared solvents to avoid any unwanted effect of moisture. Their melting points, thermal stability, and solvatochromic properties were reported in our previously published study [214] and the work of Triolo *et*

al. [266]. Melting point of the DESs and water-DESs with different ratios are also provided in this study in the supporting information to validate the melting points of the previously claimed freezing points. In this study two different sets of results from two different experiments to obtain freezing points of 1:3 and 1:4 are demonstrated.

3.2.3 Differential Scanning Calorimetry and Thermogravimetric Analysis Method

Melting temperatures (T_m) of the WDESs were measured using a TA-Q2000 differential scanning calorimeter at a heating rate of 10 ℃ per min. About 10 mg of sample was weighed into an aluminum hermetic pan. An empty reference aluminum pan was kept under the same condition throughout the experiment. Both pans were covered with premium aluminum lids. DSC measurements for the WDESs were conducted within the temperature range of -80 ℃ to 100 ℃. The advanced Tzero^{TM} technology of the calorimeter controls temperature throughout the experiment because its thermocouple sensor ensures accurate heat flow into the samples by considering any asymmetries. Nitrogen gas was purged continuously at the rate of 20 mL per minute to avoid moisture contamination. Accuracy and reproducibility of the DSC measurements were ensured by the regular calibration of the instrument with an indium metal standard.

The heat tolerance of the DESs were analyzed using thermogravimetric analysis (TGA) method. TGA was conducted using Seiko 220 TG/DTA (Tokyo, Japan) instrument. A sample size of about 10 mg was placed in an aluminum hermetic pan. The samples (DESs) were heated from 30 to 300 °C at a temperature ramp of 10 °C per min under nitrogen atmosphere.

3.2.4 Solvatochromism

Solvatochromic measurements were carried out using three widely used dyes, such as Nile red, 4-nitroaniline, and N, N-diethyl-4-nitroaniline. Individual solutions of 10^{-3}, 10^{-4}, 10^{-5}, and 5×10^{-4} molar (M) of the three dyes were prepared in dichloromethane (DCM). Among the four concentrations, 5×10^{-4} M solution worked best for the WDESs. An appropriate amount of the dye stock solution was micropipetted and transferred to the clean and dry glass vials to mix with WDES1, WDES2, and methanol (control solvent). The glass vials were then capped, vortexed, and mixed well to get homogeneous solutions. A 200-μL aliquot of each sample was loaded into a 96-well plate. More details of solvatochromism procedure and mathematical equations could be found in the previous chapter.

3.2.5. Viscosity as a function of temperature, density, conductivity, and pH

The viscosity of all the WDESs were measured as a function of temperature. A Brookfield DV-III Ultra rheometer (Toronto, Canada) was used to determine the viscosities between -10 to 30°C at 10°C increments, but viscosity at standard temperature (25°C) was also measured. The temperature variation was obtained by employing an external water bath containing 50/50 polypropylene glycol and water with a TC Brookfield TC-502 circulator (Toronto, Canada). All the measurements were conducted with a CP40 spindle at a speed of 0.2 rpm.

Density is another important physical property of any DES, which affects the mass flow. Hence the suitability of the DESs for specific applications, such as separation or solubility

media could be determined. The densities of DESs were determined via the direct method at 22.1°C. A 1.00 mL sample of each DES was slowly pipetted using a calibrated micropipette into a pre-weighed vial. The masses were measured using Mettler Toledo analytical balance (Columbus, OH).

The conductivities of the WDESs were determined using Vernier Labquest 2 (Beaverton, OR) connected to a conductivity probe. In this measurement, 0.5M NaCl solution was used as the reference solvent for in-house calibration prior to the measurements. The measurements were conducted in triplicate at ambient temperature (22.1°C). The maximum conductivity range of the instrument was 20,000 µS/cm. The pH of the WDESs were determined using a Mettler Toledo FEP20 pH meter (Columbus, OH) at ambient temperature and pressure. The pH meter was calibrated using standard buffers of pH 4.0, 7.0, and 10.0.

3.2.6. Quantum chemical calculation

Gaussian 09 software package [267] was used to optimize the cluster structures of ChCl with $3H_2O$ and $4H_2O$ at gas phase which were generated and isolated after molecular dynamics simulation [215,268]. Vibrational frequencies were calculated with the density functional theory (DFT) employing ωB97xD correlation functional [269,270] and the calculations were conducted by 6-311++G(d,p) [271] basis set, which can produce reliable geometry and QC results for the long distant noncovalent interactions among the components of DESs. After computing change of electronic energies (ΔE), enthalpies (ΔH), and Gibbs free energies (ΔG) of one representative simple cluster structure of each DES (ChCl:$3H_2O$ and ChCl:$4H_2O$) were reported, which were selected based on the

highest negative ΔG value. MD simulations were conducted using YASARA molecular dynamics simulation platform. The detailed method of the MD simulations were described in the previous chapter. Furthermore, the computed Raman and IR spectra were also calculated from the optimized structures to get additional information for pure WDES structures, where a 0.957 scaling factor was used [45].

3.2.7. Raman spectroscopic measurements

Raman shift is used to observe rotational, vibrational, and low-frequency modes in a wide variety of chemical system [272]. It provides a fingerprint of a molecule by which that molecule could be distinctly identified. When a molecule changes its polarization by the exposure to an electromagnetic field, only then the Raman spectroscopic responses can be measured. Since polarizabilities of the formulated solvents were found, 1.162 and 1.001 for WDES1 and WDES2, respectively [62], they should give distinct Raman spectroscopic responses compared to their components. Measuring the responses could be difficult, as high heat could be produced due to the use of laser and magnification. Therefore, optimization of the Raman measurement was crucial.

In this study, a HORIBA JobinYvon Raman (model-LabRAM 800HR) spectroscopic system was used to analyzing the structural characteristics of the formulated WDESs relative to their constituents. At the beginning, a 10x magnifying lens was focused and the 530 nm laser (Green laser-MPC 6000) was hitting over the samples. The diffraction grating (300) and filter (D2) were set to get the better scattered light for the detection. The fiber optic light source was turned on and LabSpec6 software was used for spectral acquisition. Spectra were recorded from 400 to 4000 cm^{-1}, but only the region of 2500-3500 cm^{-1} was

focused for the comparative discussion. Except that region, extremely high noises were observed with no significant peak in the spectra. Computed Raman spectra were also added to explore the interactions of that specific region as the Raman spectral peaks of the WDESs were not as sharp and intense. Spectral data of the samples were obtained and the data analyses were conducted using Origin Pro 2021 software [273].

3.2.8. FT-IR spectroscopic measurement

A spectrum Two PerkinElmer FT-IR Spectrometer was used to scan ChCl, H_2O, WDES1, and WDES2. Spectra were recorded in transmission mode from 400 to 4000 cm^{-1} the spectral region with a resolution of 1 cm^{-1} at room temperature. Before each spectral collection, the background spectrum was collected. FT-IR spectroscopy was performed as a complimentary tool to Raman spectroscopy to explain the major driving forces or functional groups responsible for the formation of the WDESs. Computed IR spectra were also added to explore the interactions of only among the ChCl and $3H_2O$ or $4H_2O$. Experimental and computed IR spectra were also analyzed using Origin Pro 2021.

3.2.9. Ion Chromatography and Atomic Absorption Spectroscopic Method

To prepare saturated solutions of alkyl chlorides, sodium halides, and cobalt chloride ($CoCl_2$) in the WDESs, 100 mg of each metal halide was added to 5 mL of each WDES in a small covered beaker with continuous stirring at 600 rpm. If necessary, a small amount of WDESs was continuously added until a clear solution was obtained. This solvation process was monitored for about 48 hours to get an approximate solubility of the metal halides in the WDESs. Some of the metal halides got co-crystallized or supersaturated during the solvation period if the stirring and salt addition continued over 24 hours. Hence,

the preparation of the saturated solutions were performed for 24 hours in all cases. To get the true solubility of the metal halides, a simple method was developed using ion chromatography (IC) and flame atomic absorption spectroscopy (FAAS). From the initial study, we determined the approximate amount of metal halides required for the preparation of the saturated solutions. Therefore, to prepare samples for the analytical methods, we started with enough metal halides in 10 mL of WDESs and stirred continuously for 24 h. Saturated solutions were filtered using 0.2-µm filter and transferred to the glass vials. Exactly 0.1 mL of the saturated solution was micropipetted and dissolved in 1000 mL of ultrapure water and then two mL (except LiCl, one mL was taken for the second dilution) of that diluted solution was taken and dissolved in another 100-mL ultrapure water in a volumetric flask for the second dilution. Sample preparation for the AAS needed additional acid digestion step.

Prepared samples were analyzed using a Thermo Scientific Dionex ICS 1500 ion chromatography system. An IonPac CS12 (2×250 mm) column was used, and the eluent was 12 mM H_2SO_4. The flow rate was and 0.50 mL/min, respectively. Detection mode of the instrument is suppressed conductivity using a CERS 500 2-mm suppressor. PinAAcle™ 500 (Perkin Elmer) a corrosion-resistant flame atomic absorption spectrometer (FAAS) was used to analyze $CoCl_2$.

3.2.10. Solubility measurement method

To prepare saturated solutions of the studied APIs in the WDESs, 100 mg of each API was added to 5 mL of each WDES in a covered beaker with continuous stirring (≤600 rpm). If

necessary, a small amount of WDES was continuously added to the solution until the saturation point was reached. The solvation process was monitored up to 48h to confirm any occurrence of co-crystallization. After monitoring the initial steps, enough amount of API was added to each WDES to prepare the saturated solutions by continuous stirring for 24h. Samples were prepared for the HPLC analysis by filtering using a 0.2-µm filter, followed by dilution with Milli-Q water.

HPLC-UV was used to study the solubilities of the APIs in the WDESs, where a ZORBAX SB-C18 (4.6×75 mm i.d., particle 3.5-µm) column was used. Flow rate was maintained at 1.0 mL/min and the injection volume was set at 5 µL. A detection wavelength of 235 nm and mobile phase comprising 60:40% v/v water (0.1% formic acid):acetonitrile were used to analyze all the APIs except paracetamol. For the paracetamol, detection wavelength was set as 254 nm and the percentage ratio of the mobile phase composition was 90:10% v/v.

3.2.11. Cell culture and Cell viability assay

HEK293 cell lines were cultured in Dulbecco's modified Eagle's medium (DMEM) (GE Healthcare Life Sciences, Logan, UT) complemented with 10% v/v fetal bovine serum (FBS) (HycloneTM, GE Healthcare Life Sciences). Cell cultures were maintained at 37°C in a humidified incubator supplied with 5% CO_2. These conditions were utilized for succeeding cell culture techniques. Since both the WDESs behave similarly, following studies were conducted only with the WDES1. Besides, it was proved as better solvent for the less polar compounds than WDES2. Therefore, WDES1 was used as the drug delivery vehicle for aspirin.

The cytotoxic effect of WDES1 or DES was evaluated using MTT colorimetric assay. HEK293/pcDNA3.1 and HEK293/ABCC1 cells were plated into a 96-well plate (NEST®, Rahway, NJ) at a density of 5 x 10^4 cells/well in 100 µL culture medium. The next day, cells were treated with various concentrations (0.1%, 0.5%, 1%, 5% and 10% v/v) of the DES in 100 µL of DMEM media. Media only (untreated) was used as control. Post incubation for 72 h, 100 µL of culture medium was removed and cells were treated with 10 µL MTT dye (5 mg/ml in PBS) and incubated at 37°C for 4h. The MTT formazan product was dissolved in 100 µL 15% SDS containing 10 mM HCl. Cell viability was determined by measuring spectroscopic absorbance at 570 nm with a microplate reader (Hidex Sense Beta Plus., Turku, Finland). Results were expressed as a percentage of control values.

To show these DES as good drug vehicles, the therapeutic effect of aspirin on human embryonic kidney cell line, HEK293/ABCC1, which overexpresses multidrug resistance protein 1 (MRP1/ABCC1) and its control derivative, HEK293/pcDNA3.1, was evaluated. Initially, 10 mM aspirin stock solutions were prepared in pure DES and in DMSO. A dose-response curve was generated by treating HEK293/pcDNA3.1 and HEK293/ABCCI cells with various concentrations of aspirin. Cells were incubated for 72 h and MTT colorimetric assay was used to determine the cell viability.

3.3 Results and discussion

3.3.1 Thermal Behavior of the WDESs

Differential scanning calorimetry (DSC) measures heat flow and temperatures associated with the thermal transition in the WDES samples. The thermal phase of WDES1 and

WDES2 are analyzed using the TA Universal Analysis 2000 software. Melting points of the WDESs are obtained through the endothermic process and these were found at -79.21±0.28 ℃ for WDES1 and -79.25±0.32 ℃ for WDES2 (**Figure 3.1**). These results are cross-validated by keeping the WDESs in different freezers within the temperature range between -65.0 to -85.0 ℃. The depression of freezing point refers to the nature and extent of the intermolecular interactions among the molecules of HBA and HBD. Variety of interactions, such as electrostatic interaction, hydrogen bonds, halogen bonds, and van der Waals forces among the molecules cause that extreme depression of the melting points of the WDESs.

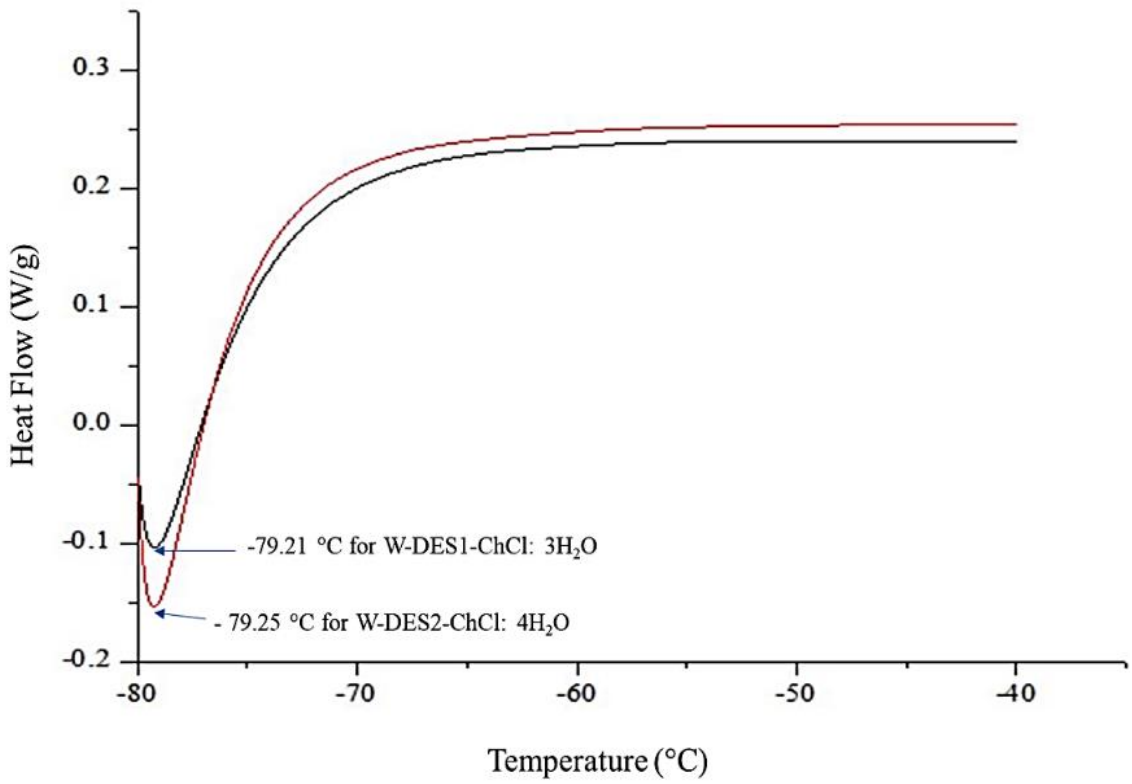

Figure 3.1. DSC curves of WDES1 and WDES2, where the downward peaks at around -79 °C show the melting points of the water-based DESs.

Stability of a solvent at high temperature refers to the strength of the interactive forces among the solvent molecules. Same intermolecular interactions stated in the DSC study make a solvent stable at high temperature. **Figures 3.2** represents the TGA thermogram of WDES1 and WDES2. The major physical transitions in the water molecules are observed at 193.75 and 197.73 °C, respectively. Crystalline water is found up to 148.64 °C for WDES1 and 116.13 °C for WDES2.

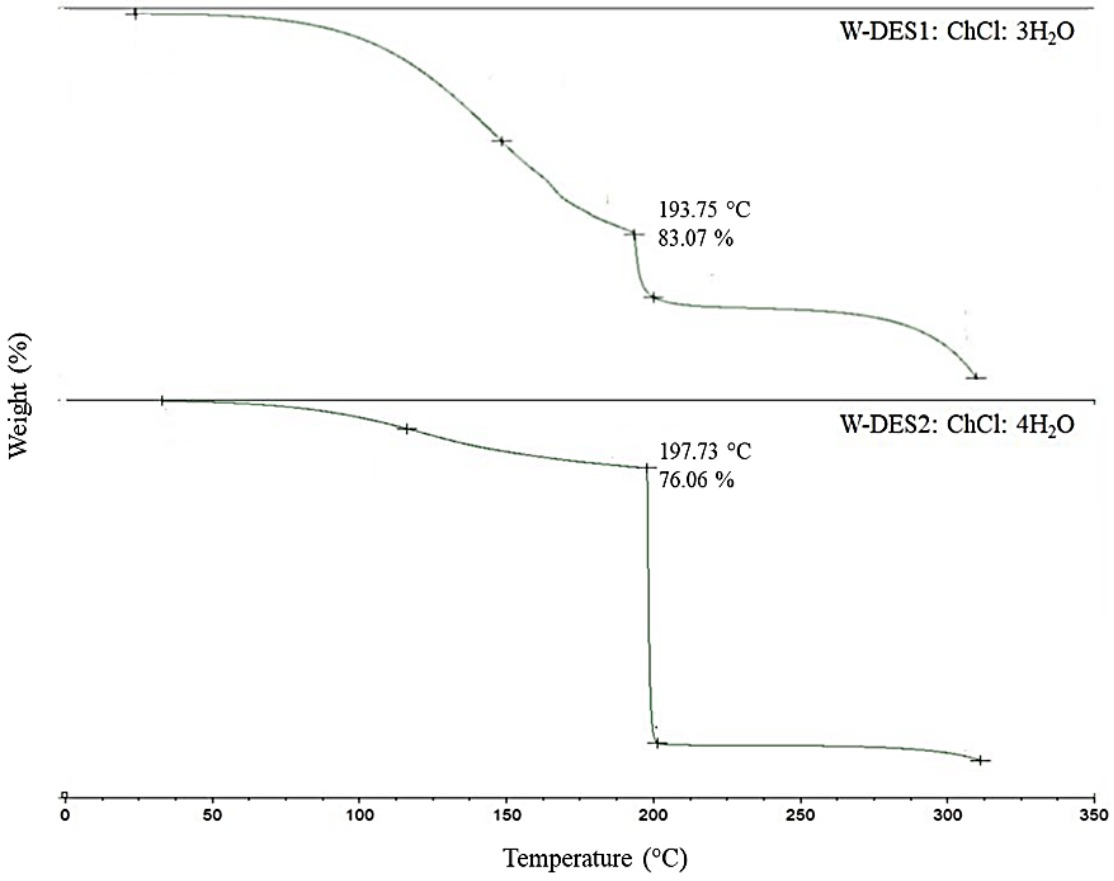

Figure 3.2. Thermogravimetric analysis of WDES1 and WDES2, where the downfall of the curve between 190-200 °C show the stability of the DESs.

High pressure in the capped aluminum pan and surrounding enclosure facilitate to determine the exact transition points at that high temperature. These results justify high thermal stability of the water molecules when they form WDESs with choline chloride.

3.3.2 Solvatochromic Parameter Analysis

Solvatochromic parameters including E_T(NR) or E_T^N, α, β, and π* of the WDESs indicate that their properties are analogous to ionic liquids [90]. This is due to the comparable intermolecular interactions which are involved among the WDESs and the dye molecules. Hydrogen bonds, electrostatic interactions or doubly ionic effect, halogen bonds, and van der Waal forces are the major interactions in the solutions. In this experiment, methanol is used as a control solvent. Measured solvatochromic parameters for methanol are close to the literature values, but slightly deviated. Reasons behind the deviation could be the dissolved gasses in the sample solutions and the moisture present in the dyes used for the solvatochromic measurements [274–277]. The transition energy and polarizability of methanol is found as 51.98 kcal.mol^{-1} and 0.79, where the literature values are 52.02 kcal. mol^{-1} [262] and 0.77 [263], respectively. The dimensionless E_T^N values of the WDES1 and WDES2 are found as 0.61 and 0.62, respectively at ambient temperature. Low transition energy values of the WDESs represent high polarity of the solvents. Polarity values are 1.1615 and 1.0014 for WDES1 and WDES2, respectively.

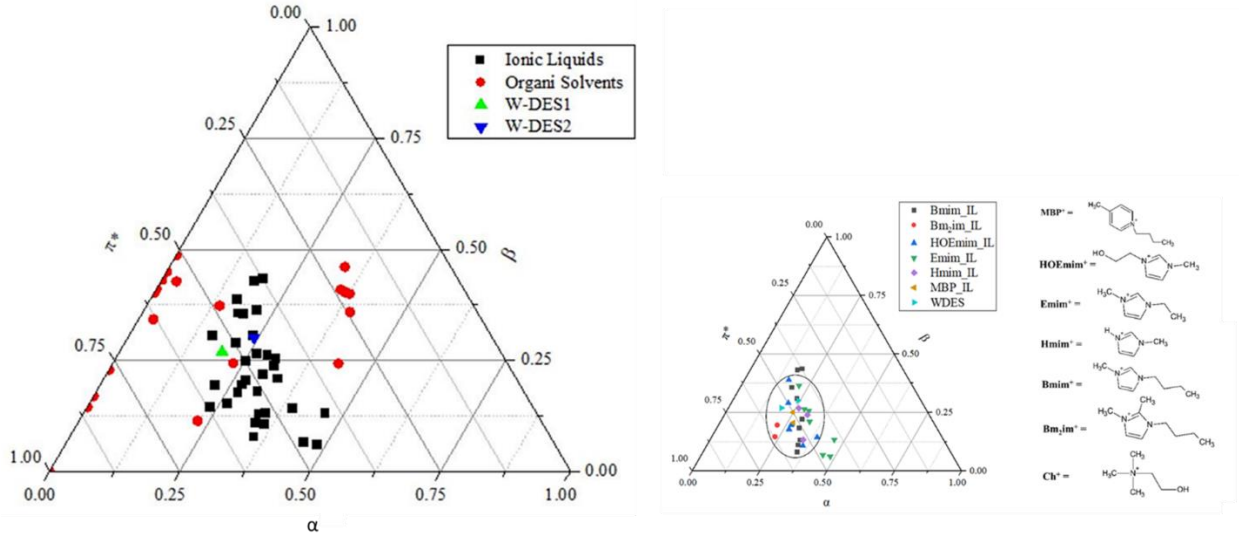

Figure 3.3 Ternary plot of Kamlet-Taft parameters (α, β, and π*), where the parameters of the WDESs were compared to some selected organic solvents and ionic liquids is depicted on the left side of this figure. Besides, ternary plot of Kamlet-Taft parameters (α, β, and π*) at the right side of selected ILs and WDESs, where the parameters of the choline cation-based WDESs are compared with the different groups of ILs based on their cations, such as Bmim, Bm2im, HOEmim, Emim, Hmim, and MBP.

To visualize the comparison, a ternary plot was constructed using Origin Pro 2020 software package [278] (presented in **Figure 3.3**). This ternary plot is called Snyder's solvent selectivity triangle (SST), which characterizes the solvents depending on their Kamlet-Taft parameters and makes clusters or groups of them by plotting α, β, and π* of the solvents in a triangle [279,280]. The triangle shows that the WDESs are closely related to ILs, but away from the organic solvents. That means the formulated DESs possess similar solvatochromic properties to IL, which indicates that they could be excellent extraction media for a variety of compounds. To get deeper insight of the analysis, another ternary

plot or SST (**Figure 3.3**) is plotted to compare the solvatochromic parameters of WDESs with only the ILs. Groups of the ILs are determined based on their cations to investigate if there is any correlation among the structural features of the WDESs and ILs. MBP-based ILs are located most close to the location of the WDESs, it could be because of both Ch^+ and MBP^+ have only one N atom (specifically one N^+) in their structures. Except these, all the other cations of the listed ILs have one N atom and one N^+ cation in their structures. HOEmim-based ILs also closely orients around the WDESs maybe because of both the Ch^+ and $HOEmim^+$ have N^+-CH_2-CH_2-OH group. Structures of the other cations are similar to the HOEmim except the -OH functional group and most of the selected ILs are clustered around the WDESs. Factors, such as types of anions, structural size, number of HBA and HBD atoms, number of rotatable, single, double, and hydrogen bonds could be the reasons behind the few anomalous results.

3.3.3 Viscosity, density, conductivity, and pH

DESs typically are highly viscous, which affects its mass flow. Intermolecular forces, such strong H-bonds, ionic interactions, and Van der Waals forces play important roles to reduce their mobility by reducing the void volume. The viscosities of the WDESs decrease with the increase of temperature (**Table 3.1**).

Table 3.1 Viscosities of the WDESs (ChCl:$3H_2O$ and ChCl:$4H_2O$) at different temperatures.

	Viscosity (mPa.s)	
Temperature (°C)	ChCl:$3H_2O$	ChCl:$4H_2O$

-10	943.67	1030.17
0	757.73	740.50
10	479.33	456.73
20	318.30	296.70
25	263.20	200.50
30	218.20	172.00

The viscosities of the WDES1 and WDES2 are 263.2 and 200.5 mPa.s at 25°C, respectively. Viscosity values of the two most common DESs- ChCl:Urea (1:2) and 1:2 ChCl:Glycerol (1:2) are 261 and 254 mPa.s at 25°C, respectively [281]. Therefore, the viscosities of the WDESs are quite similar to the viscosities of that well-studied systems.

Due to the intermolecular interactions, densities of the WDESs are found comparatively higher, 1.11 and 1.09 g/cm^3, than water. Conductivity and pH values are found 3350 μS/cm and 7.3 for 1:3 ChCl:H_2O and 3162 μS/cm and 7.3 for 1:4 ChCl:H_2O. The pH values of the 1:2 ChCl:Urea and 1:2 ChCl:Glycerol DESs are 9.4 and 7.8 at ambient temperature, respectively. They are high and moderately basic, while the WDESs are neutral. Except for the measurements of viscosity at various controlled temperatures, all the other measurements are conducted at ambient temperature (average 22.0°C). All the physical properties show the WDESs are a good fit for enhancing the solubility of organic molecules including active pharmaceutical ingredients (APIs) and could be used as safe drug delivery agent for initial assay. Before exploring that application, their structural properties are explored to explain why their viscosities and densities are high. It will help to understand

how the water molecules contribute to the formation of these water-based DESs. Besides, density and viscosity data of them and other molar ratios of water-based DES have been also described in the supporting information to clarify the outcome of 1:3 and 1:4 ChCl:H_2O more. Gutierrez *et al.* [282] studied the behavior of aqueous solution of similar DES and they suggested that freeze drying would be extremely helpful to explain their unique properties and behavior, such as structure, viscosity, density, polarity, and thermal behavior. Following the idea, freezing point of the studied DESs is analyzed using DSC as well as freeze-thaw method.

3.3.4. Structure optimization and quantum calculation

Structural features of simple computed cluster structures of the WDESs could help to understand the water-based DES in depth. However, one optimized cluster structure of each WDES is provided and their structural energies are calculated at gas phase.

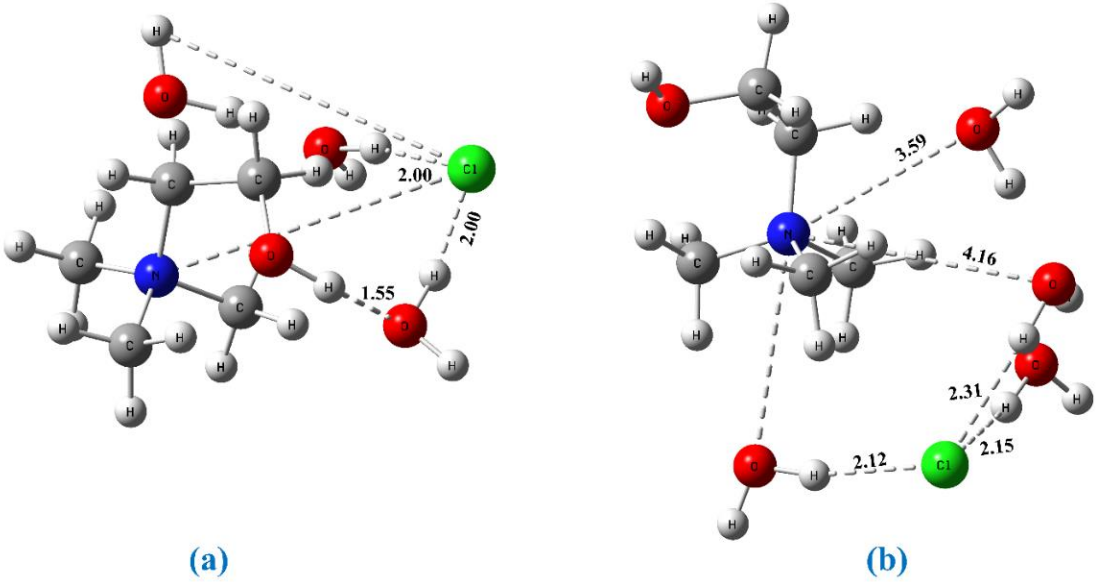

(a) (b)

Figure 3.4 Optimized structures of the ChCl:3H_2O (WDES1) and ChCl:4H_2O (WDES2), where the numbers represent the bond distances (nonbonding interactions) in Å unit, where the atoms are represented as follows oxygen = red, chloride = green, nitrogen = blue, carbon = grey, and hydrogen = off-white.

Figure 3.4 shows that water molecules are strongly interacting with the H atoms of choline (Ch^+) and taking the chloride ion away from the N^+. Besides, the water molecules are strongly interacting with the Cl^- ion. Thus, it helps to form strong clusters and behaves as a DESs. The strength of the nonbonding interactions is proved by the bond distances among the H atom of water and Cl^-, O atom of water to H-O of Ch^+, and O atom of water to N atom of Ch^+, which have been shown in **Figure 3.4**.

Table 3.2 Changes of electronic energy (ΔE), enthalpy (ΔH), and Gibbs free energy (ΔG) of the reported cluster structures of WDES1 and WDES2 are calculated at the ωB97XD/6-311++G(d,p) level of theory using density functional theory (DFT).

WDES	Energies (kJ/mol)		
	ΔElectronic Energy	ΔEnthalpy	ΔGibbs Free Energy
WDES1 (1:3 ChCl:H_2O)	-180.067	-187.500	-72.096
WDES2 (1:4 ChCl:H_2O)	-211.883	-221.797	-68.578

The electronic energy, enthalpy, and the Gibbs free energy of the WDES cluster structures are obtained using the following equation: $\Delta X_{WDES} = X_{WDES} - X_{ChCl} - X_{H2O}$ in the gas phase, where X is either electronic energy, enthalpy, or Gibbs free energy. The ΔG

values suggest that the clusters are spontaneous and highly stable. In one of our previous studies on ChCl:Aspirin (1:1) cluster structures using the same level of theory gave ΔG values ranges from -13.94 to -47.23 kJ/mol [45]. However, ΔG values are -72.10 and -68.58 kJ/mol for WDES1 and WDES2 structures, respectively (**Table 3.2**). Therefore, it shows that the WDESs are formed more spontaneously than the ChCl:Aspirin DES clusters. It maybe because of the higher number of nonbonding interactions exist in these structures, where water molecules help to make the complex interactions.

3.3.5. Raman spectra analysis

Raman spectroscopy provides a fingerprint of the molecules or samples by changing their polarization when exposed to an electromagnetic field. Therefore, the difference between the incident and absorbed light is detected by Raman, and unlike FTIR, Raman can detect homo-atomic molecules [283]. Peaks rarely appear in the same spot for different molecules as their chemical bonds are different [284]. Besides, peak position shows the kind of chemical bonding, peak shift illustrates the mechanical or thermal effects on lattice, peak width demonstrates about the degree of crystallinity [284]. Since water is a heat sensitive molecule, optimization of the measurement method is performed.

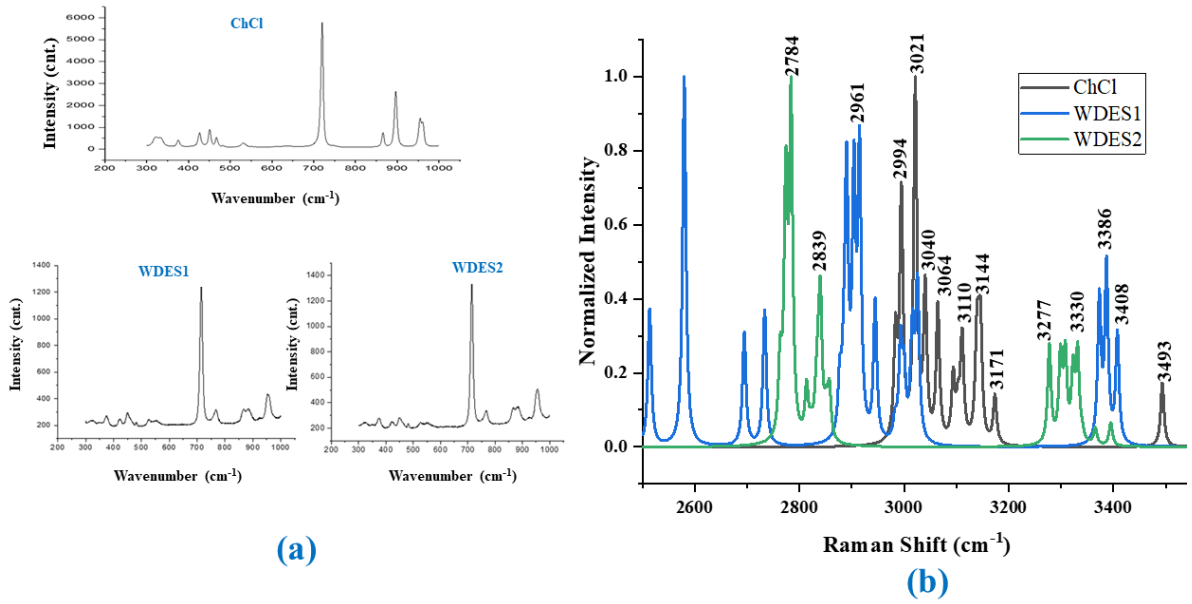

Figure 3.5 (a) Experimental Raman spectra of ChCl:3H_2O (WDES1), and ChCl:4H_2O (WDES2) compared with the spectra of their components Raman-active component ChCl (range between 200-1000 cm^{-1}), (b) computed Raman spectra of ChCl, WDES1, and WDES2 calculated from the optimized structures presented in **Figure 3.4** starting from 2500-3500 cm^{-1}.

Heat production is kept as low as possible during this experiment because WDESs are formulated using water. Therefore, the grating and the magnification are used 300 and 10x, respectively. The new peak position, size, width, and shift confirm the formation of nonbonding interactions, decrease in the degree of crystallinity of choline chloride, and thus successful formation of the WDESs. The hydrogen bond donor (water) dominates the overall formation process. Hydrogen bonding in Raman often observed as relatively small shifts at low frequency regions. The HBD, water, is not Raman active since it is nonpolarizable. The Raman spectroscopy analysis of the DESs are compared to the Raman

spectrum of the pure dried choline chloride (**Figure 3.5a**). The results indicate a significant peak shift to the left of the peak at 897 cm^{-1} of between 6-11 cm^{-1}. This shift is attributable to hydrogen bonding. Also, a large shift is observed in ChCl:H_2O (1:3). Again, a shift of 5 cm^{-1} observed at peak 720 cm^{-1} in all the DESs is attributable to hydrogen bonding. A new peak was observed at 771 cm^{-1}, which was nonexistent in the choline chloride spectrum. This peak may be because of stretching of the -OH group on the second carbon of the choline chloride, a consequence of weak hydrogen bonding.

Therefore, water is shown to be a stronger contributor or HBD for the formation of DES. Since the peaks are too small, computed Raman spectra of ChCl, WDES1, and WDES2 have also been calculated (**Figure 3.5b**). The peaks of ChCl at 2900-3200 cm^{-1} range also appeared in the computed Raman spectrum, where the peaks at 3144 cm^{-1} is for the -OH of the ChCl and the peaks between 2900-3100 cm^{-1} are due to C-H bonds. Due to the large number of interactions among the ChCl and water molecules, WDESs show a lot of characteristic interactions. In the spectrum of WDES1, the peak at 2580 cm^{-1} appears for C-H of choline, which represents interactions among Ch-OH…OH_2 and Cl^-…OH_2. The peak at 3021 cm^{-1} corresponds to another C-H vibration, which appears for an interaction between the C-H of choline and O-H of H_2O. In the spectrum of WDES2, the peaks at 3277 and 3330 cm^{-1} represent the interactions among H_2O…H_2O and H_2O…H-O of Ch, respectively. Both experimental and computed Raman spectra prove that there are many strong nonbonding interactions exist among the components of the WDESs, which leads to reduced crystallinity of ChCl and helps the successful formation of the WDESs.

3.3.6. FT-IR spectra analysis

Infrared spectral analysis is an excellent tool to investigate the reasons behind the successful formation of a DES [45]. It can help to determine the effect of water to the structure of DES [285]. Since the components of this study are only choline chloride (having -OH and C-O functional group) and water, these spectral data certainly help to make more sense about the formation of the WDESs and the contribution of water molecules. Even that peak in the spectra of WDES has appeared as more intensified and sharper compared to the same peak for ChCl. It indicates that water forms strong interactions with the $O_{C\text{-}O}$ atom of the ChCl.

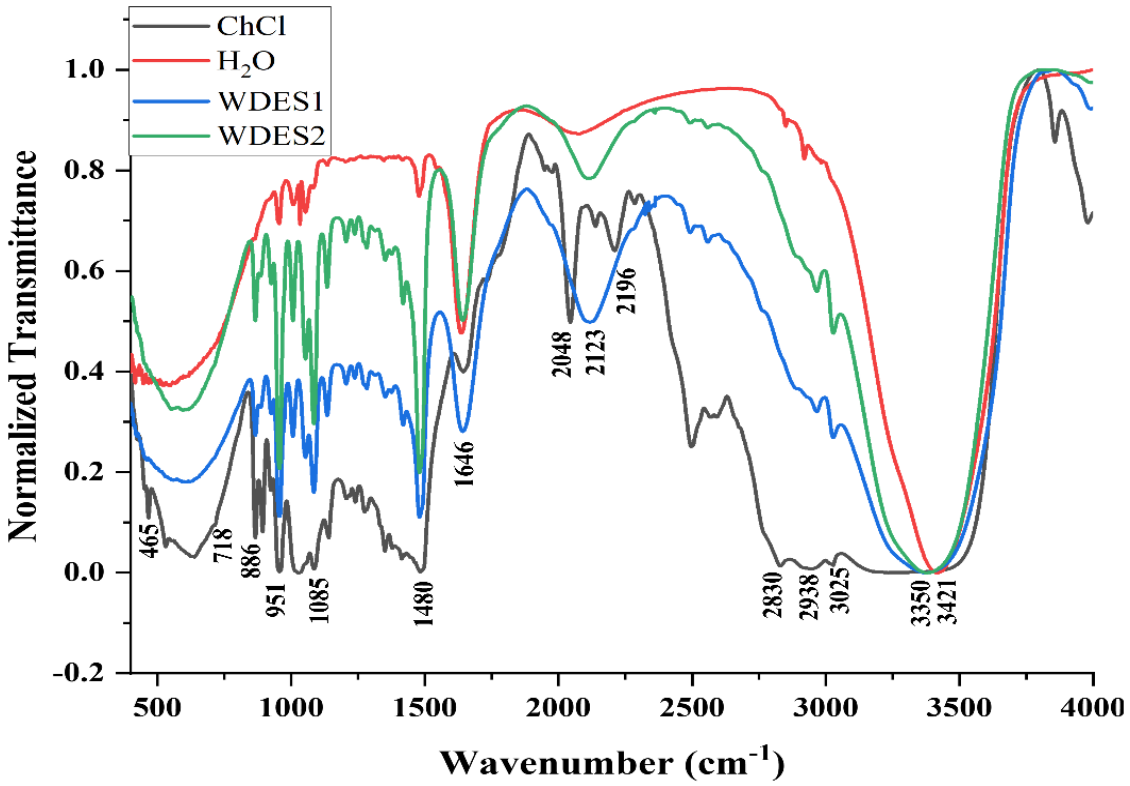

Figure 3.6 FT-IR spectra of ChCl:3H_2O (WDES1) and ChCl:4H_2O (WDES2) presented with the spectra of their components ChCl and H_2O.

The strong intermolecular interactions among the O-H of the water molecules generate a broad peak in the 3250-3750 cm^{-1} spectral region [285]. No clear peak is observed for the -OH group of ChCl in that region. However that broad peak gets more intensified and sharper for each of the WDES spectra. It confirms the formation of the strong intermolecular hydrogen bonds among the constituents. C-H stretching and bending vibrations at around 3033 and 1486 cm^{-1}, respectively, in the spectra of the WDESs are also intensified. It shows that nonclassical hydrogen bonds [286] are another major contributor to the formation of the WDESs. A nonclassical hydrogen bond is synonymous with induced dipole-dipole interactions between, for example, a –CH group and an electronegative atom, usually N, O, or F, on an adjacent molecule. The appearance of new peak, and peak shift, broadening, and intensification by influence of the classical and nonclassical hydrogen bonds prove that they are the major factors behind the extreme depression of freezing point and lattice energy of the constituents. Therefore, it is understandable that water plays a pivotal role for the formation of the DESs.

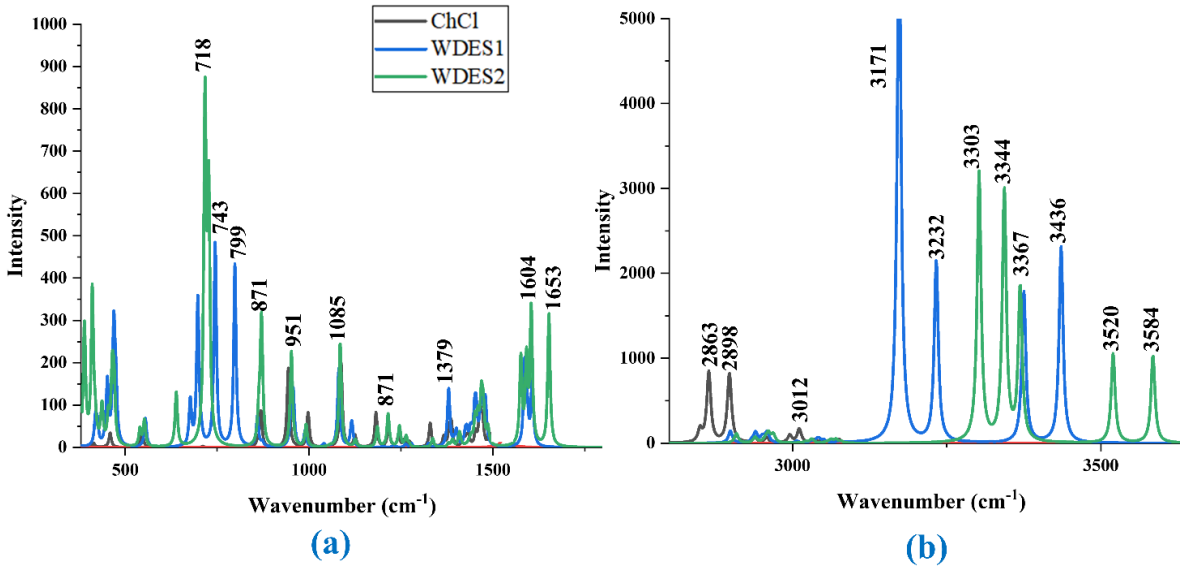

Figure 3.7 Computed IR spectra of ChCl, WDES1, and WDES2, where (a) represents the lower frequency range (400-1700 cm^{-1}) and (b) represents the higher frequency range (2800-3700 cm^{-1}).

The computed spectra of the ChCl and the WDESs help to understand the major interactions occurring in the pure form of WDES structures. WDES1 is formulated by the interaction with three water molecules. **Figure 3.7a** shows that at the lower frequency region of the WDES1 spectrum, 687 cm^{-1} appears for the interaction between Ch-OH…OH_2 and 1604 cm^{-1} appears for C-H_{Ch} vibration, which is interacting with the oxygen of a water molecule. Besides, 743 and 799 cm^{-1} peaks represent C-N vibration because of the interactions with the water molecules. A large peak emerges for O-H_{Ch} vibration at 3232 cm^{-1} (**Figure 3.7b**), which results from a long-range interaction among Ch-OH…OH_2 and Cl^-…OH_2. Further, a peak at 3436 cm^{-1} represents O-H vibration, is the result of Ch-OH…OH_2 interaction.

The WDES2 spectrum of its simple structure is a bit different. It also has similar peaks and mainly represents the Ch-OH interactions to Cl^- or water. However, a peak at 718 cm^{-1} has appeared for O-H vibration of water molecules because of the interaction with Cl^- and a water molecule (**Figure 3.7a**). C-O_{Ch} and C-H_{Ch} vibrations are represented by the peaks at 1085 and 1379 cm^{-1}, respectively, which are vibrated due to the interactions with Cl^- and water molecules (**Figure 3.7a**). In the higher frequency range (**Figure 3.7b**), 3303-3344 cm^{-1} peaks correspond to O-H of the water molecule and the vibrations occurring because of the interaction with another water molecule. The peaks above 3500 cm^{-1} correspond to the O-H vibrations of Ch^+ of WDES2 (**Figure 3.7b**).

3.3.7. Metal Halide Solubility in WDESs

Since DES is a complex and viscous solvent, it is difficult to measure the solubility of different compounds in it. In this study, a simple method is developed to determine the solubility of the metal halides in the WDESs under ambient temperature and pressure. Solubility of the sodium halides and alkali chlorides in the WDESs are determined using ion chromatography, and only $CoCl_2$ is analyzed by FAAS. **Table 3.3** shows the solubility of the studied metal halides in the water-based deep eutectic solvents.

Table 3.3. Solubility of the listed metal halides in water and the WDESs at ambient temperature.

	Solubility in Water and WDESs (g/100 mL)		
Metal Halides	**Water**	**WDES1**	**WDES2**
Sodium Halides Solubility (g/100 mL ±SE)			
NaF	4.3 [287]	1.616 ± 0.006	1.260 ± 0.015
NaCl	36.0 [288]	6.993 ± 0.068	5.861 ± 0.076
NaBr	94.6 [289]	4.971 ± 0.055	3.407 ± 0.041
NaI	184.0 [290]	3.634 ± 0.021	2.829 ± 0.032
Alkali Chlorides Solubility (g/100 mL ±SE)			
LiCl	84.5 [291]	8.388 ± 0.122	15.203 ± 0.238
NaCl	36.0 [292]	6.993 ± 0.051	5.861 ± 0.031
KCl	35.5 [293]	0.244 ± 0.014	0.257 ± 0.014
Cobalt Chlorides Solubility (g/100 mL ±SE)			

$CoCl_2$	53.0 [294]	20.981 ± 0.174	23.895 ± 0.301

*SE means standard error

It is observed that solubilities of the studied metal halides decrease considerably in the WDESs compared to their solubilities in water. The major reason behind the phenomena could be ion pair repulsion between choline chloride and the metal halides. Solubility trends of sodium halides and alkali chlorides in water are NaI > NaBr > NaCl > NaF and LiCl >> NaCl > KCl, respectively. But in the WDESs, solubility trends are NaCl > NaBr > NaI > NaF for sodium halides and LiCl > NaCl > KCl for alkali metal chlorides.

It is also found that LiCl and $CoCl_2$ are the two most soluble metal halides in the WDESs. It happens because the atomic size of both cations are so small that they can easily diffuse through the gaps the solvent systems. DES (e.g., ChCl:ethylene glycol) is an efficient extraction solvent for the two major metals (Li and Co [5]) of the spent Li-ion battery. Not only Li and Co metals, DESs are proved media to recycle other crucial metals (e.g., Fe and Te) and metal compounds [52,53,295]. Since our developed WDESs are least costly, nonflammable, stable at both higher and lower temperature compared to water, and efficient to solubilize Li and Co salts, they could be explored further to find out if they are also good extraction solvent for Li and Co metals from the waste of Li-ion battery.

3.3.8. Enhancement of drug solubility

Poor drug solubility in aqueous media or in biological system is one of the major challenges for the pharmaceutical industry. Since achieving necessary drug concentration at the target site is crucial to obtain intended pharmacological responses, scientists have been trying to

solve the problem in many ways [61]. Formulation of APIs as DES has become a popular technology nowadays [61].

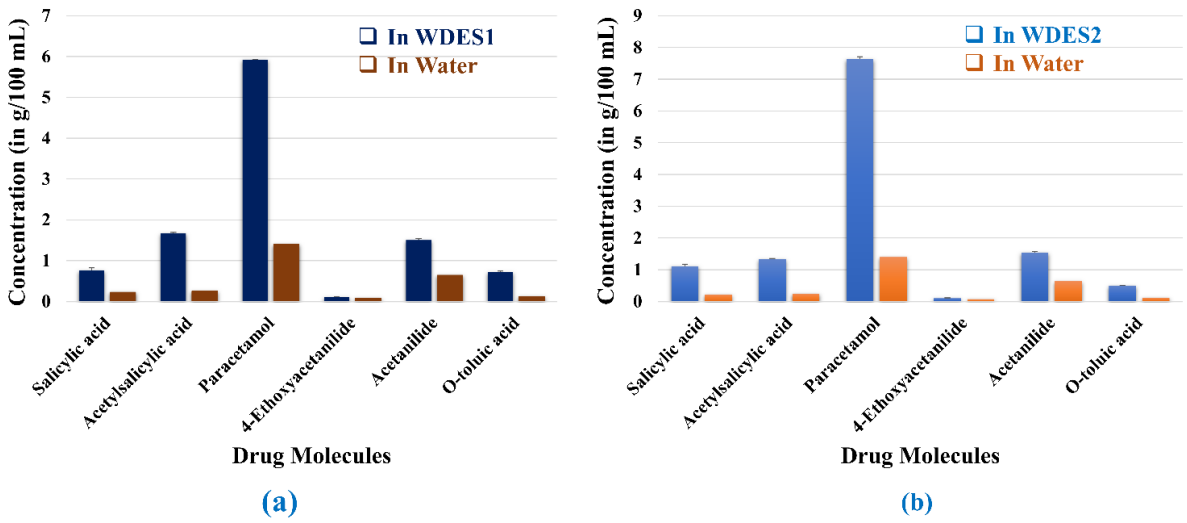

Figure 3.8 (a) Drug solubilities in WDES1 and (b) in WDES2 (blue), which are compared with their solubilities in water (either dark orange or light orange). All the measurements are reported in g/100 mL and determined at ambient temperature and pressure.

Except paracetamol, all the other APIs used in this study are sparingly soluble in water. Therefore, to observe the efficacy of the WDESs as solvent, saturated solutions of drug-DES are prepared in each WDES. HPLC-UV method is used to measure the concentrations of the APIs in each WDESs.

Table 3.4 Solubilities of the studied APIs in WDES1 and WDES2.

Drug molecules or APIs	In WDES1 (g/100 mL)	In WDES2 (g/100 mL)	In water (g/100 mL)

Salicylic acid (SA)	0.7560± 0.0664	1.1122± 0.0650	0.224 [296]
Acetylsalicylic acid (ASA)	1.6750± 0.0213	1.3325± 0.0219	0.250 [297]
Paracetamol (Par)	5.9258± 0.0789	7.634±0.109	1.400 [298]
4-Ethoxyacetanilide (EA)	0.1083± 0.0120	0.1030± 0.0121	0.077 [299]
Acetanilide (Ace)	1.5056± 0.0409	1.5412± 0.0390	0.639 [300]
O-toluic acid (o-Tol)	0.7210± 0.0241	0.49990± 0.00792	0.118 [301]

Table 3.4 and **Figure 3.8** show that the solubilities of the studied APIs have been increased about 1.3 to 6.7 times in WDESs compared to their solubilities in water. The solubility trend in WDES1 is: ASA (6.7)> o-Tol (6.11)> Par (4.23)> SA (3.38)> Ace (2.36)> EA (1.41) and in WDES2 is: Par (5.45)> ASA (5.33)> SA (4.97)> o-Tol (4.24)> Ace (2.41)> EA (1.34). The numbers in the parentheses represent the degree of enhancements of the drug solubilities in WDESs. Relatively polar APIs including paracetamol and salicylic acid are more soluble in WDES2, whereas less polar APIs, such as acetylsalicylic acid and o-toluic acid are more soluble in WDES1 (**Table 3**). The major factors behind the variations in the solubility trends of WDES1 and WDES2 could be the polarity, hydrogen bond formation ability, and molecular weight of the APIs.

3.3.9. Effect of WDES on the cell viability and their potential as drug vehicle

Solubility outcomes show a lot of promise, but the applicability of the formulated DES in a biological system should be explored. Therefore, a cell viability test of WDES1 and its potentiality as drug delivery vehicle has been evaluated via in-vitro (MTT) assay. Since

both WDESs behave similarly and WDES1 can increase the solubility of the aspirin more than the WDES2, WDES1 is used in these experiments.

The effect of different concentrations of WDES1 on the viability of HEK293 cells is examined. Using the same conditions, similar dose-response experiments (MTT Assay) are conducted with dimethyl sulfoxide (DMSO) and WDES1. DMSO is a widely known solvent for drug delivery and its effect on cellular functions have been studied in a wide number of cell types [302,303]. Thus, DMSO is used to as the control solvent in this study. Cell viability of the WDES1 has been examined by increasing the concentrations of it from 0.1 to 10% v/v. As shown in **Figure 3.9a**, treatment with 0.1% and 0.5% (v/v) WDES1 do not significantly affect the viability of HEK293/pcDNA3.1 cells. Furthermore, 1% and 5% v/v treatments for both WDES1 groups significantly lower the cell viability to 50-60%. The highest concentration (10% v/v) shows significant cell mortality. Overall, results show that low concentration (0.1 and 0.5% v/v) of WDES1 has no to little effect on cell viability, and thus might be considered a suitable solvent for drug delivery.

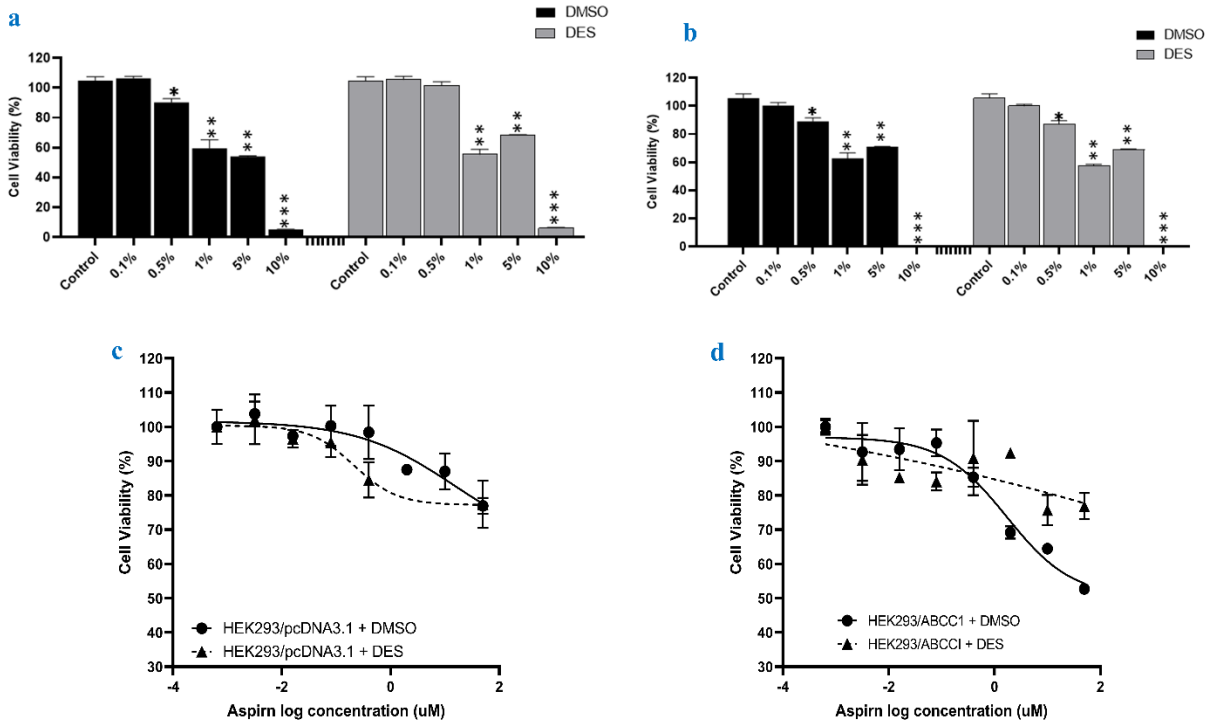

Figure 3.9 Cell viability and therapeutic effect of DES or WDES1. Dose dependent cytotoxic effect of DES and DMSO on **(a)** HEK293/pcDNA3.1 and **(b)** HEK293/MRP1 cell lines. Cells are treated with or without 0.1, 0.5, 1.0, 5.0, and 10.0% DMSO or DES and have been incubated for 72 h. MTT colorimetric assay is used to evaluate cell viability. Data are combined from two independent experiments done in triplicates and expressed as mean ± SEM * $p < 0.05$, ** $p < 0.01$, and *** $p < 0.001$ compared with the control. The therapeutic effect of aspirin with WDES1 as diluent is evaluated on **(c)** HEK293/pcDNA3.1 and **(d)** HEK293/MRP1 cell lines. Cells have been incubated for 72 h post treatment with increasing concentrations of aspirin reconstituted with pure DES or DMSO. Cell viability is determined using MTT colorimetric assay.

To test its ability as a pharmacological delivery vehicle, WDES1 is used as the chemical solvent to dissolve aspirin before evaluating the therapeutic activity of aspirin on HEK293 cells overexpressing multidrug resistance protein 1 (MRP1/ABCC1), which is a widely studied drug efflux protein prominent in many types of cancers, such as pancreatic and renal carcinomas [304–306]. In the presence of the WDES1, aspirin shows excellent inhibitory concentration (**Figure 3.9**). It indicates that the DES does not interfere with the therapeutic potential of aspirin. Comparing the results with DMSO, WDES1 shows excellent outcomes in terms of the enhancement of solubility, safe drug delivery, and maintaining therapeutic potential of a drug (**Figure 3.9**). Its safety features and extremely low melting point are added advantages to use them in the biological system. It could be assumed that by tuning the molar ratios of water depending on the polarity of the drugs and using highly pure ChCl could enhance the efficacies of the applications manifolds. The assumptions are feasible because we have already explored the possibilities of the successful formation of WDESs using higher and lower molar ratio of water [307].

CHAPTER FOUR

AMINO ACID-BASED DEEP EUTECTIC SOLVENT (AADES)

Abstract

Amino acid-based deep eutectic solvents (AADESs) are an emerging type of DESs with a wide range of applications. In this study, two novel AADESs were formulated using basic, L-(+) arginine (Arg), and acidic, L-glutamic acid (Glu), amino acids and glycerol (Gly) as the hydrogen bond donor (HBD) at a 1:3 molar ratio. The eutectic points of the formulated AADESs were -0.14°C for Glu-Gly and -1.36°C for Arg-Gly. The successful interactions among the constituents were investigated using FT-IR, ^{1}H-NMR spectroscopy, and mass spectrometry. These studies found that Glu-Gly may form ester impurities. However, mass spectrometry showed that the impurities are negligible. TGA revealed that both DESs could be applied up to 150-160°C without losing weight, while Glu-Gly could be used up to 200°C. Formation of Arg-Gly was strongly dominated by glycerol, while Glu-Gly DES was formed by an equal contribution of both components. Principal component analysis (PCA) also helped to visualize the spectroscopic outcomes. Since AADESs are excellent pretreatment media for biomass, lignin was treated as a model biomass in this study with the formulated AADESs to determine their reaction products. It was found that Arg-Gly can isolate only one monomeric compound (4-methyl benzaldehyde), while Glu-Gly can isolate three monomeric compounds. Oxidative depolymerization of the lignin residues

validated the outcomes obtained from the AADES-lignin reactions. Glu-Gly was more efficient for the lignin depolymerization because of its less viscosity, higher stability, acidic environment, and stronger hydrogen bond formation between lignin and glycerol.

4.1. Introduction

Solvents are ubiquitous chemicals for almost all industrial production including recycling, pharmaceuticals, cleaning, adhesives, paints, and synthesis. Most conventional solvents are organic and are typically toxic, volatile, flammable, and may be highly persistent in nature. Greener solvents, such as supercritical water, ionic liquids, and deep eutectic solvents (DESs) show promise to overcome such issues while maintaining high efficacy for similar applications. Among them, DES is the most recent and versatile alternative with advantages such as depolymerization and pretreatment of biomass without using sophisticated instruments, extraction of target compounds with higher efficiency, enhancing the bioavailability of drugs, and recycling of waste. DESs are typically formulated by mixing hydrogen-bond acceptor (HBA) and hydrogen-bond donor (HBD) molecules. Many noncovalent interactions, such as hydrogen bond, halogen bond, alkyl-alkyl, pi-pi, cation-pi, and anion-pi interactions help depress of their melting point and without forming new compounds [16] However, some cases trace amount of impurities can be formed. For example, if -OH and -COOH functionalities are available in the components and the mixing is conducted at higher temperature, ester impurities could form [203] Amino acid-based DES is comparatively a newer type of DES. Previously, Smith *et al.* (2014) proposed a general formula: Cat^+X^-zY, [17] where Cat^+, X^-, Y, and z refer to

cations of organic salts, halide anions, HBD molecules, and the number of HBDs, respectively for DES. We have proposed an extended classification in our recent review article and suggested that AADES should be an independent type because of their versatile applications [4].

AADESs are naturally benign, biodegradable, sustainable, eco-friendly, and are formulated by at least one amino acid [5,6]. Heating and vacuum evaporation have been primarily used to formulate AADES [7,8]. Their potential has been reported in various areas, such as food, drugs, animal feeds, cosmetics, and polymer production [9,10]. They showed a lot of promise in enhancing the solubilities of drugs and proteins [63,140] biosynthesis [82] in extracting radioactive I_2, and bioactive compounds [142,143] and depolymerization of lignocellulose [16]. It is crucial to study of their eutectic point, thermal stability, and physical and chemical properties before going for any application [17]. Evaluation of eutectic point and thermal stability of the solvents is performed with differential scanning calorimetry (DSC) and thermal gravimetric analysis (TGA) [18,19]. Viscosity and pH are important for the efficiency of newly developed methods, such as biomass pretreatment, solubility enhancement, and extraction [20,21].

Spectroscopic techniques, such as ^{1}H-NMR, FT-IR, and Raman spectroscopy have been used to elucidate the structural features and nonbonding interactions of DESs [90,159,268] Depending on the noncovalent interactions, two types of AADESs are the most common, ionic based and nonionic hydrogen bond acceptor/donor based. In both types of AADESs, hydrogen bonds are mainly formed using the functional groups including -COOH and -NH_2 [16,25]. However, it is also crucial to investigate other contributing forces behind their

successful formulations. Alcohol containing HBDs (e.g., glycerol) are popular HBD for AADESs because of long range diffusivity [26]. Recently, mass spectrometry has been used to determine all stable clusters of a DES [268,311].

Pretreatment of biomass using DES could enhance the efficacy of further enzymatic hydrolysis [312] Liang *et al.* reported that arginine and lysine-based AADES can efficiently hydrolyze corncob, where lignin and xylan were found highly soluble in the DES [145]. The pretreatment can significantly enhance the efficacy of the subsequent enzymatic hydrolysis step. To understand the contribution of a DES at the pretreatment step, determining the compounds isolated in the DES layer is crucial. Their residues could be further analyzed using a standard depolymerization method for further validation. For lignin depolymerization, cupric oxide and nitrobenzene can selectively break the ether linkages in lignin and isolate its phenolic monomers, keeping aromatic ring intact [28,29]. Gas chromatography-mass spectrometry (GC-MS) is an excellent technique to determine and quantify the monomers [315].

The overall objectives of this study are- formulation of acidic L-glutamic acid and basic L-(+)-arginine amino acid-based AADES, spectroscopic characterization of formations, exploring their major physical properties to explain the noncovalent interactions, and principal component analysis (PCA) of the IR data to understand the contribution of the components behind the AADESs formulations,, use of mass spectrometry to identify the major clusters and to show that the formation of any ester impurity is negligible,, determine whether the acid and basic AADES behave differently during the depolymerization of

lignin, perform CuO oxidation to validate the outcomes of AADESs treatments in terms of their effects on lignin structure.

4.2 Materials and Methods

4.2.1 Materials

L-(+)-arginine, L-glutamic acid, and glycerol were purchased from Fisher Scientific (Fairlawn, NJ). For DSC and TGA, Tzero aluminum pans were obtained from TA instruments (New Castle, DE). Alkali lignin was purchased from Sigma-Aldrich (St. Louis, MO). After the AADES treatment, lignin residues were used as the samples for the cupric oxide (CuO) depolymerization reaction. The CuO was purchased from Acros Organics (insert city, NJ). Methylene dichloride (DCM), sodium hydroxide (NaOH), and deuterium oxide (D_2O) were purchased from Fisher Scientific (Fairlawn, New Jersey). Since the purities of all the chemicals were over 98%, they were used without any further purification.

4.2.2 Formulation of the AADES

Amino acid-based deep eutectic solvents (AADESs) were formulated by mixing anhydrous L-(+)-arginine and L-glutamic acid with glycerol at 1:3 molar ratios in a tightly covered beaker with continuous stirring (≤600 rpm) for 4-5 hours at 80°C under atmospheric pressure until homogenous liquids were obtained. Formulated solvents were monitored further for a few hours to reassure no reformation of crystals. All measurements were conducted with freshly prepared solvents.

4.2.3 DSC, TGA, viscosity, and pH

Differential Scanning Calorimetry (DSC)

Melting points (T_m) or the eutectic points of the AADESs were measured using a TA-Q2000 differential scanning calorimeter (DSC). The heating rate was set 10 ℃/min and approximately 10 mg of AADES samples was weighed in the aluminum hermetic pans. An empty aluminum pan was used as the reference and kept under the same condition and the pans were covered with premium aluminum lids. The measurements were started from -60 to 40 ℃. The advanced Tzero^{TM} technology and its thermocouple sensor control the temperature throughout the experiment and ensure accurate heat flow into the samples by assessing any asymmetries. To avoid moisture contamination, nitrogen gas was purged continuously at 20 mL/minute. Accuracy and reproducibility of the instrument and measurements were ensured by the regular calibration with an indium metal standard. In our previously published article, the percent errors of the similar measurements using this instrument were obtained <1% [19], which showed the reliability and reproducibility of the measurements.

Thermogravimetric Analysis (TGA)

Thermogravimetric analyses of AADES samples were carried out using TG/DTA 220 from Seiko Instruments, Japan. Approximately, 10 mg of samples were taken in the TGA aluminum pan for the analyses. The oven temperature was raised from ambient to 560°C at a constant heating rate of 10 °C/min. Similar to DSC, nitrogen was used at a flow of 20 mL/min to maintain an inert atmosphere and to avoid sample contact with air. The nitrogen helps sweep the pyrolysis gases, such as H_2, CO_2, CO, CH_4, C_2H_2, and water vapor, from the system since they could interact with samples [316].

Viscosity and pH

The viscosities of the formulated AADESs were measured at ambient temperature (20.5 ºC) using a Brookfield DV-III Ultra Programmable Rheometer (Toronto, Canada). Certified Brookfield viscosity standards were used to conduct the calibration and the standard error was 1%. For each sample, 0.5 mL of AADES was taken on the CPE-40 cone spindle. All the measurements were conducted in triplicate.

Due to their highly viscosity, typical pH probes were unable to quantify the pH values. Therefore, Fisherbrand™ paper pH strips were used to measure the pH of the formulated solvents.

4.2.4 Fourier-Transform Infrared Spectroscopy. A Thermo-Fisher Scientific Nicolet 380 FTIR spectrometer with attenuated total reflectance mode was used for the sample analysis of the individual components and AADESs. The spectra of the HBA, HBD, and the DESs were recorded between 400-4000 cm^{-1} at ambient temperature. All signals were recorded with a resolution of 4 cm^{-1}. The spectral baseline was corrected, denoised, smoothed, and normalized employing Origin Pro 2021 software package [273].

Principal Component Analysis (PCA)

PCA reduces the dimensionality of the large spectral data to a smaller set of data by identifying their principal source of variation. It reduces the noise and highlights the variabilities present in the spectra of the studied compounds [317]. Therefore, it can help to visualize the correlation, differences, and contribution of the components for the formulation of DES [215,268] The equation: $X = T_k P_k^T + E$ can explain PCA, where T_k

shows how the selected samples are related to each other, P_k represents how the variables are related to each other, k is the number of factors, and E is the matrix of residuals included in this model. All calculations were performed with Origin Pro (2021) equipped with the Principal Component Analysis for Spectroscopy Application v.1.30. [278]

4.2.5 Nuclear Magnetic Resonance Spectroscopy. The ^{1}H-NMR spectra of the glycerol, L-(+)-arginine, L-glutamic acid, 1:3 L-(+)-arginine:glycerol, and 1:3 L-glutamic acid:glycerol were recorded employing a Bruker AVANCE III HD 600 MHz NMR spectrometer (Bellerica, MA), where D_2O was used as the solvent. A total of 16 scans of each sample was performed at ambient temperature. Samples of the AADESs and their pure components were prepared in 5-mm NMR glass tubes, where approximately 10 mg of the samples were dissolved in 0.5 mL of deuterium oxide (D_2O). The homogeneity of the solutions was assured by vortex mixing. After acquiring the signals, they were analyzed using Advanced NMR Processing & Interpretation Software.

4.2.6. Depolymerizing Behavior of AADES to Lignin

Depolymerization of alkali lignin was conducted by treating the lignin samples with AADESs followed by CuO oxidation depolymerization on each of lignin residues to validate the outcomes of first step.

Depolymerization of alkali lignin using AADES

About 500 mg of alkali lignin and 5 g of 1:3 L-glutamic acid:glyecerol were taken in a closed beaker. The depolymerization was conducted for three hours at 150°C and 500 rpm. After completing the reaction, the solution was cooled to ambient temperature. The

reaction mixture was diluted with water and transferred to a 50-mL centrifuge tube. To get a clear precipitate, two drops of concentrated HCl were added. When the pH of the solution reached pH 2.0, the solutions was centrifuged for 20 mins at 3000 rpm. The liquid was decanted to another beaker and the precipitate was transferred to a preweighted aluminum tray. The liquid was further extracted three times using dichloromethane (DCM) to isolate the monomeric compounds depolymerized from the lignin sample. The extracted DCM layer was evaporated using nitrogen. GC-MS was used to analyze the sample aliquots (**Figure 4.1**). The same procedure was followed for the treatment of lignin using 1:3 L-arginine:glycerol DES. The residues of the treated lignin samples were further treated using CuO oxidation or hydrothermal treatment to validate the monomers obtained by the AADES treatments.

Oxidative depolymerization of the lignin residue

Residues of the lignin samples were further washed with 1:9 ethanol:H_2O. The residues were then transferred to preweighted aluminum trays. They were dried overnight, washed with acetone, and dried for a few hours. The prepared samples were used for the CuO oxidation depolymerization reaction. The Pearl method was used after slight modification [318,319]. Approximately 100 mg of the Glu-Gly and Arg-Gly treated residues and one gram of CuO were mixed well in a 100-mL round bottom flask with water-cooling.

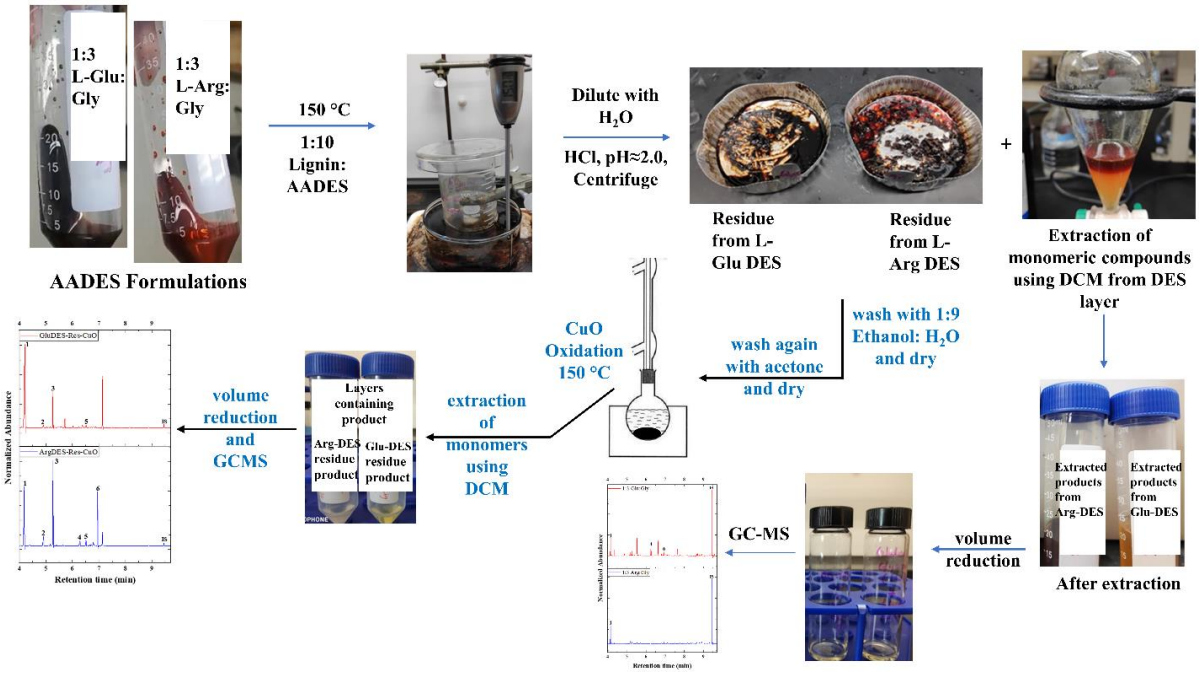

Figure 4.1. Schematic diagram of the alkali lignin depolymerization method using AADESs followed by CuO oxidation.

Nitrogen was used to degas the flask and to maintain the inert atmosphere of the reaction chamber. At ambient temperature, 15 mL of 2M NaOH was added to the reaction mixture and stirred. After solubilization, the reactions were carried out at 150°C for 2 hours with continuous stirring. Following the reaction, the flask was cooled down to room temperature. The reaction mixtures were acidified with concentrated HCl to maintain a pH at 2.0-3.0 and filtered. The acidified mixtures were extracted using DCM and the volume of DCM layer was further reduced to 5 mL. **Figure 4.1** illustrates the multiple steps of the procedure.

4.2.7. Gas Chromatography-Mass Spectrometry. Analysis of the final solutions were performed using Agilent 7890A gas chromatograph (Wilmington, DE) coupled with a

triple-axis mass spectrometric detector with electron-impact ionization (Agilent 5977B). An Agilent DB5 column (30 m×250 µm×0.25 µm) and ultrapure hydrogen carrier gas were used. Flow rate of the gas was set 1.2 mL/min and the temperature of the GC oven was initiated from 50°C. Heating rate of the method was set 20 °C/min and the temperature increased linearly upto 200°C. Afterward the temperature was held at 200°C for 1 min, then elevated to 300°C at the rate of 40 °C/min. That temperature held constant for 2 mins before returning to initial temperature. The MS analysis was performed using full-scan mode with a range of m/z 50-600. The Agilent ChemStation software was used to autotune the mass detector beforehand. The NIST database was used to identify the monomers extracted from the lignin and its residue samples [320]. It is understandable that pH would play the major role. However, a small model lignin structure and the components of DESs (amino acids and glycerol) were optimized using density functional theory (DFT) calculation at B3LYP/6-31G(d) level of theory [321]. Molecular dynamics simulations using YASARA program were conducted among the lignin and DES's components to understand the contribution of the HBA and HBD molecules towards the depolymerization of lignin [321,322]. The detail methodology of the quantum calculation and molecular dynamics study have been provided in the information.

4.3. Results and Discussion

4.3.1 Eutectic points and thermal stability of the AADESs

Differential scanning calorimetry (DSC) measures heat flow and temperatures relate to the thermal phase transition in the AADES samples. The thermal phases of Glu-DES and Arg-

DES are analyzed using the TA Universal Analysis 2000 software. Eutectic points of the AADESs are -0.14℃ for Glu-DES and -1.36℃ for Arg-DES (**Figure 4.2**). Melting points of the pure constituents (L-glutamic acid, L-(+)-arginine, and glycerol) are 224.0, 244.0, and 18.2℃, respectively [118].

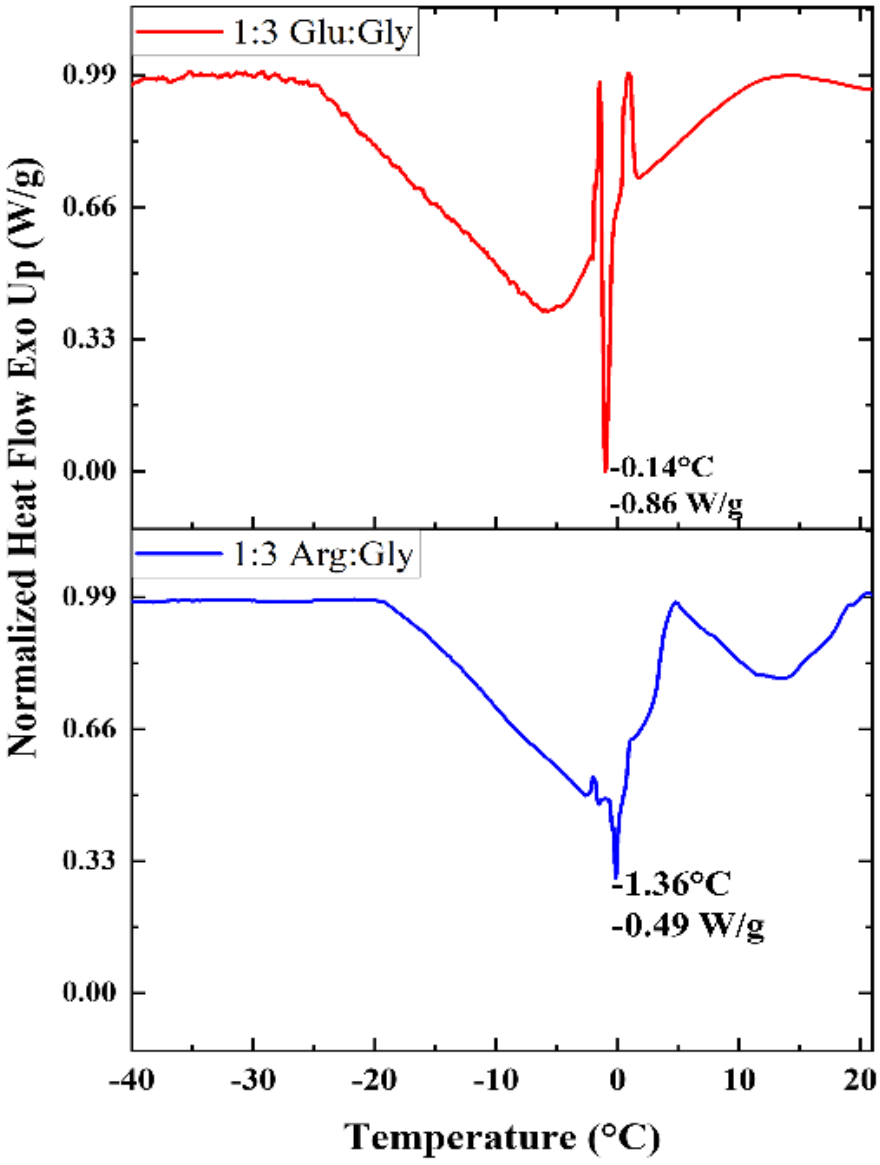

Figure 4.2. DSC curves of 1:3 L-glutamic acid:glyecerol (top) and 1:3 L-(+)-arginine:glycerol (bottom).

The extreme depression of the melting points of the DESs compared to their pure components indicate a significantly high extent of nonbonding interactions among the HBA and HBD molecules. Interactions, such as ionic, hydrogen bonds, and van der Waals forces could be the major players behind the high depression of the melting points.

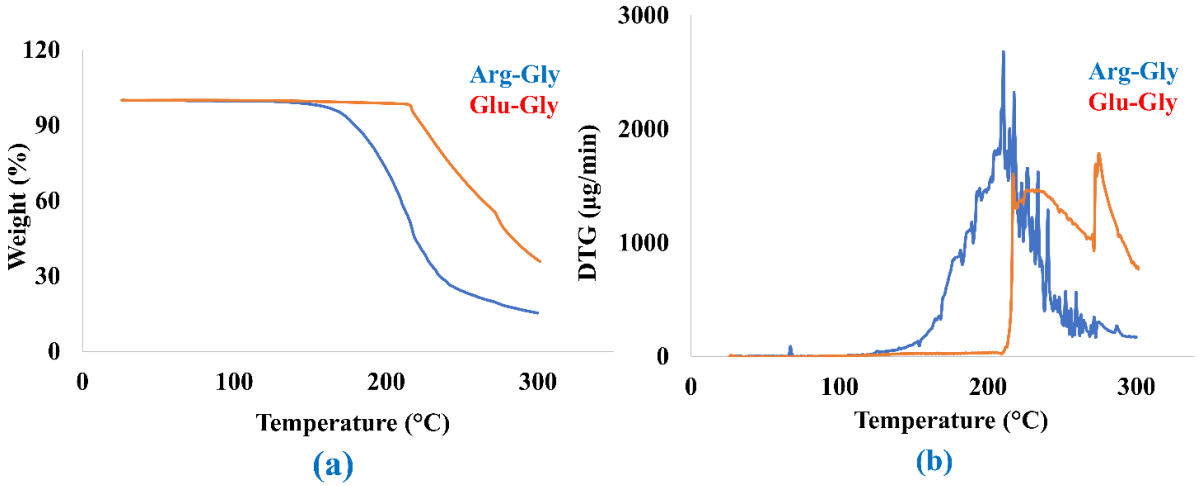

Figure 4.3. (a) percent weight loss (TG) curve and (b) rate of weight loss (DTG) curve of the 1:3 L-glutamic acid:glyecerol and 1:3 L-(+)-arginine:glycerol DESs.

In this study, thermal properties of AADESs have been investigated using thermogravimetric analysis. TGA of a material typically gives two different weight loss curves, percent weight loss (TG) and rate of weight loss (DTG). The TG and DTG curves of Arg-Gly and Glu-Gly are shown in **Figure 4.3** and their thermal changes, such as degradation stages, weight loss, remaining weight, rate of weight loss with respect to the temperatures are shown in **Table 4.1**. Thermal studies of the Arg-Gly and Glu-Gly show quite different decomposition behaviors. The initial weight loss of Arg-Gly occurs at the region of 65-100 °C, which could be because of the volatilization of water from the DES [323]. However, no weight loss is observed at this region for Glu-DES. Major weight loss

of Arg-DES has occurred at a single step starting at 100°C and continuing to 300°C. During this time, the maximum rate of weight loss is observed at 210°C. **Table 4.1** shows 84.36% weight is observed between 100 to 300°C, only 15.28% remains above that temperature. It indicates that most of the bonds among arginine and glycerol have already been broken down below that temperature.

Table 4.1. Major data are tabulated out of percent weight loss (TG) and rate of weight loss (DTG) curves of Arg-DES and Glu-DES.

Sample type	Degradation stage	Temperature range (°C)	Weight loss (%)	Residual weight (%)	DTG max
Arg-DES	1	65.5-70	0.1		
	2	100-300	84.36		210
	3	Above 300	-	15.28	
Glu-DES	1	210-271	40.47		
	2	271-300	21.71		275
	3	Above 300	-	35.78	

On the other hand, major thermal degradation of the Glu-DES occurred at higher temperature in two steps [324] It shows that Glu-DES is more stable at higher temperature. PCA of the FTIR study has also showed that Glu-DES is formed by almost equal contributions of the glutamic acid and glycerol (**Figure 4.5**). The first major degradation starts in the region of 210-271°C with a weight loss of 40.47%, which is mainly because of the thermal decomposition of glycerol and partial decomposition of glutamic acid [325].

Additionally, second major thermal decomposition occurs in the region of 271-300 °C, which is due to the continuous degradation of both components and mostly the glutamic acid [323]. It is also understandable from the DTG curve, which shows that the maximum rate of weight loss is occurred at 275°C. Higher degradation temperature and the remaining weight percent after 300°C shows that Glu-DES is thermally more stable than Arg-DES. The higher stability of Glu-DES could be because of the stronger interactions among the glutamic acid and glycerol molecules and the equal contributions of components. The following studies of FT-IR, NMR spectroscopy, and mass spectrometry will elaborate the reasoning behind these formations.

The Arg-DES and Glu-DES have viscosities of 1868±33.50 and 1241±38.31 cP, respectively. The results are presented as an average reading of triplicate samples with their standard errors. The presence of the excess interactions among the hydroxyl groups of glycerol molecules may account for its higher viscosity. Since both solvents are extremely viscous at ambient temperature, a typical pH probe was not successful to measure their proton concentrations. Therefore, pH papers were used to know their approximate pH values, which are 12.0 and 4.0 for Arg-DES and Glu-DES, respectively. Thermal stability, viscosity, and pH favors Glu-DES to treat the biomass or lignin at higher temperature. Before going further, we need to know the pattern of major nonbonding interactions and whether any impurities are formed during the formulations or not.

4.3.2. FT-IR Spectroscopic Insights

Relative changes of FTIR peak positions and shape of the AADESs compared to the peaks of their pure components could help to explain which functional groups form the major

nonbonding interactions (**Figure 4.4**). In this manner, contributions of each component behind the formation of DES could be revealed. The FT-IR spectrum of glycerol shows a broad peak around 3301 cm^{-1}, which corresponds to its hydroxyl group (**Figure 4.4**). The peak at 2931 cm^{-1} corresponds to the sp^3 C-H asymmetric stretching band. Moreover, peaks at 1034 cm^{-1} represents C-O stretching and at 1403 cm^{-1} shows either C-H bending or C-OH in-plane bending [326,327]. In the L-arginine spectrum, two sharp peaks are observed at 1551 and 1612 cm^{-1} for the C-N/N-H bending and C=O stretching vibrations of its carboxylic group, respectively. A broad peak for N-H stretching is noticed at 3020-3400 cm^{-1}, where O-H stretching of -COOH group could be hidden behind[328]. Similar peaks of C-H asymmetric stretching and C-O stretching band are detected in both glycerol and Arg:Gly spectra. Therefore, the formulation of Arg:Gly is dominated by the glycerol. In the spectra of L-Arg, N-H wagging, O-H out-of-plane, C-N stretching, and C-O stretching bands are observed at 771, 972, 1134, and 1327 cm^{-1}, respectively. [329,330] These peaks are not found as prominently in the Arg:Gly spectrum, which also confirms that glycerol dominates the formulation. In this formation, the major force is the hydrogen bonding, which is indicated by the peak broadening. The peaks at 1403 and 3301 cm^{-1} correspond to C-OH in-plane bending and O-H stretching, respectively. The peaks at 1551 and 1612 cm^{-1} correspond to C-N-H bending and C=O stretching vibrations, which are broadened in the Arg:Gly spectrum. This suggests that most of the O-H of glycerol forms hydrogen bonds with the N-H and C=O of the L-arginine (**Figure 4.4**).

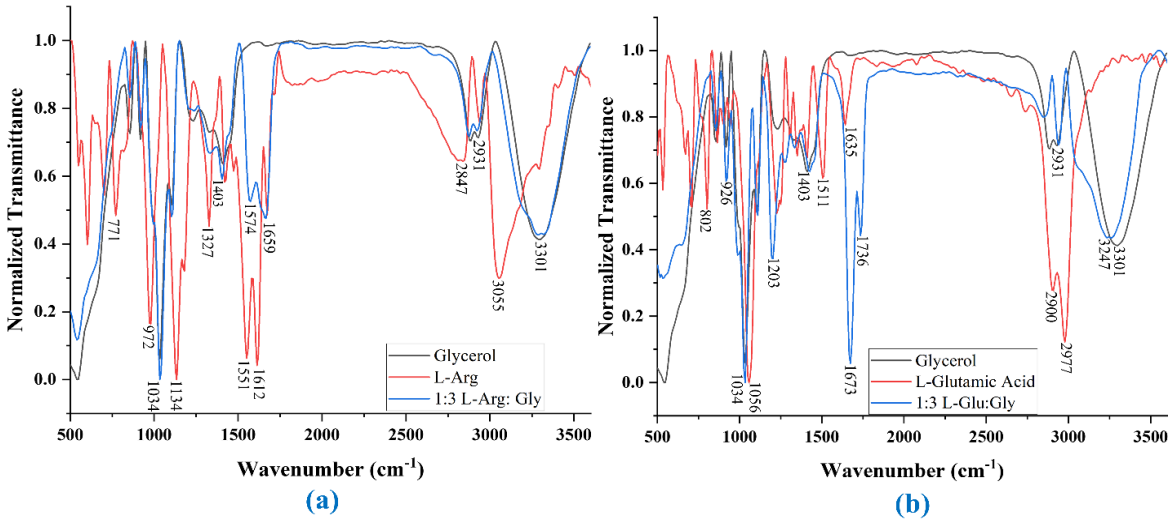

Figure 4.4. FT-IR Spectra of the AADES and their constituents (a) L-(+)-Arginine, glycerol, and 1:3 L-(+)-Arginine: Glycerol, (b) L-Glutamic acid, glycerol, and 1:3 L-Glutamic acid: Glycerol.

Similar situations are observed for the Glu:Gly spectrum, but glycerol is not highly dominating in this case. The spectrum of L-glutamic acid shows that the peak at 2950-3100 cm^{-1} appears for the O-H of -COOH. The peak for O-H in the Glu:Gly spectrum is broadened compared to the same peak in the Arg:Gly spectrum. Similar to the peaks of arginine, glutamic acid shows peaks at 1511 and 1635 cm^{-1} corresponding to C-N/N-H and C=O functionalities, respectively. The peaks are shifted to the higher wavenumbers 1673 and 1736 cm^{-1} in the spectrum of Glu:Gly, maybe because of the formation of ester impurities. This suggests glutamic acid has a stronger contribution to the formation of the AADES compared to arginine. The peak for N-H wagging at 802 cm^{-1} of glutamic acid was seen in the spectrum of Glu:Gly. It suggests that formation of the Glu:Gly is more dependent on the O-H…H-O and O-H…O=C interactions. Peaks at around 1215 cm^{-1}

correspond to C-O stretching vibration of glutamic acid and glycerol, which appears at 1203 cm^{-1} in the Glu-Gly spectrum. It appears as sharper, larger, and shifted to lower wavenumber.

PCA is performed on the 400-4000 cm^{-1} spectral data of all the IR spectra. The first principal component (PC1) explains the highest possible variability. In **Figure 4.5**, PC1 and PC2 explain 49.1 and 37.6 % of the spectral data, respectively. Therefore, both axes together can illustrate the distribution of IR spectral data of the pure components and the AADESs over 86% on the two PC score axes. Loading plot of the right side of the **Figure 4.5** shows the major functionalities responsible for the formulations of the AADESs and the contribution of glycerol to it.

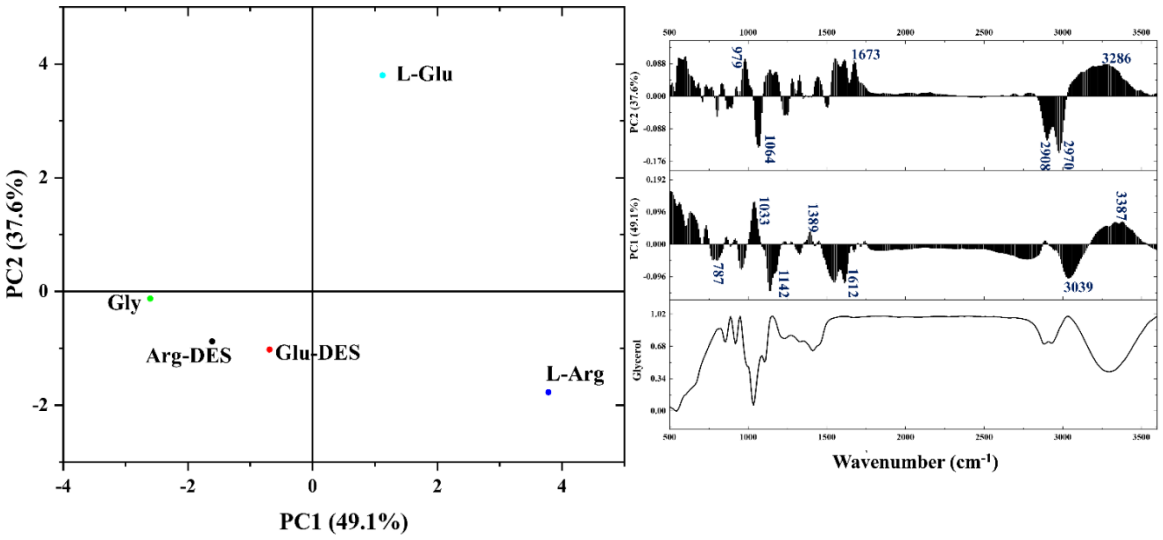

Figure 4.5. Principal component analysis (PCA) on the IR spectral data of the pure components and the AADESs, where L-arginine and L-glutamic acid are observed at right side on the PC1 axis and glycerol at the left side on PC1 axis. The values of AADESs are

in between the values of their corresponding components. Left image is the score plot and the right image is the score plot of the spectral data.

It is observed that the PC1 can successfully separate scores of amino acids and glycerol from their IR spectral data (**Figure 4.5**). It is reasonable as their spectral features are distinct from each other. Scores of the Glu:Gly and Arg:Gly reside close to each other and between the scores of their corresponding components i.e., amino acid and glycerol. Positions of their scores confirm that the spectral features of the AADESs are the combination of their respective components. Score of the Arg:Gly on PC1 axis is closer to the score of glycerol, which indicates that this formation could be dominated by glycerol. However, the score of Glu:Gly is almost in the middle of the scores of its components indicating Glu:Gly DES shares characteristics of both components (**Figure 4.5**). PC1 explains a higher percentage of spectral data because it is driven by O-H, C-O, and C=O stretching vibrations, while PC2 is driven by mainly C-O, C=O, and C-H stretching vibrations of hydrocarbon region. The loading plot (**Figure 4.5**) shows that O-H and C=O frequencies have large and opposing effects on the PC1 and PC2 scores. PC2 is driven by some additional large peaks in the hydrocarbon region at 2900-2980 cm^{-1}, which appear for C-H stretching peaks of amino acids and glycerol.

4.3.3. ^{1}H-NMR characterization

The interactions among the protons of glycerol and the amino acids (e.g., L-glutamic acid and L-(+)-arginine) are characterized using ^{1}H-NMR spectroscopy. From **Figure 4.6** and **4.7**, it can be seen that the AADESs contain protons from both the donor and the acceptor molecules. In **Figure 4.6**, the protons of the glycerol structures are marked by M01, M02,

and M03, respectively. The details of their chemical shift and coupling are δ ppm 3.44 (dd, J=11.71, 6.42 Hz, 2H, M03), 3.53 (dd, J=1.00 Hz, 2 H, M02), 3.67 (tt, J=6.56, 4.39 Hz, 1 H, M01). Overall, five protons are seen on the carbon backbone of the glycerol structure. The same peaks in the Arg:Gly and Glu:Gly spectra have not changed their positions (**Figure 4.6** and **4.7**), but their intensity is reduced drastically indicating that all the C-H protons participate to the form the DESs. **Figure 4.6** shows the peaks corresponding to C-H of L-(+)-arginine, denoted as a, b, c, and d. Their peak positions have also been observed at the same location in the Arg-Gly spectrum, but with reduced peak height. The integration values in the spectrum of Arg:Gly suggest that glycerol has stronger contribution to the formation of this DES. Since no new peaks appeared in the spectrum, this DES produces ester impurities below the detectable limit or do not produce ester at all.

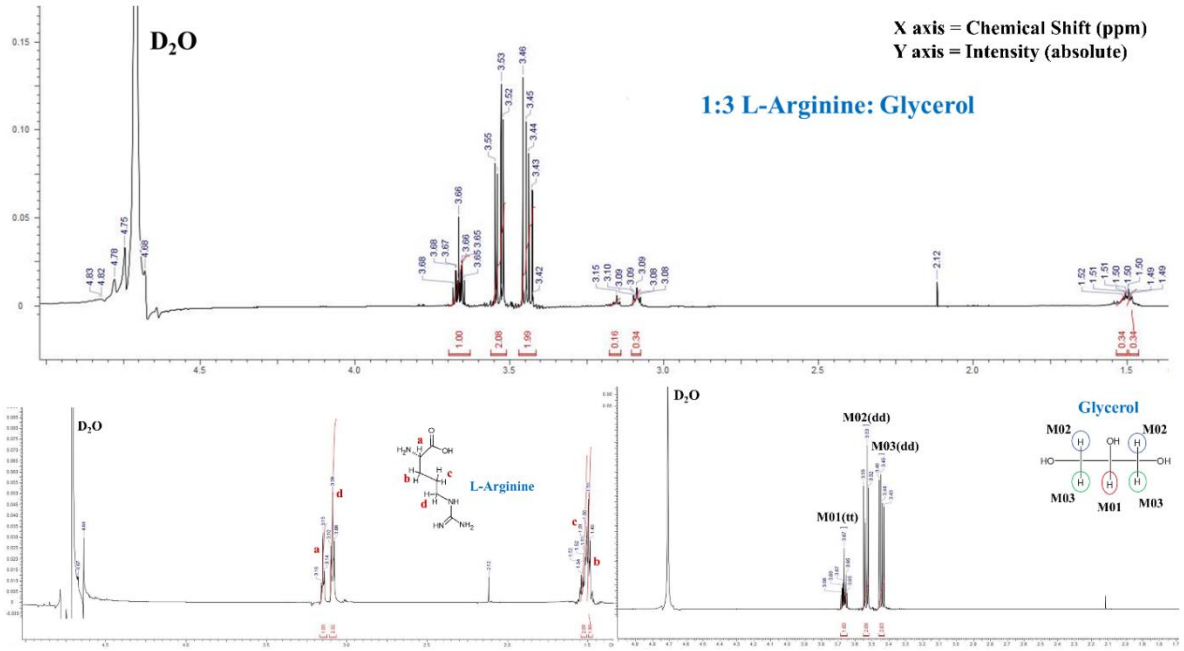

Figure 4.6. [1]H-NMR spectra of 1:3 L-arginine:glycerol, and its components L-arginine and glycerol.

In the spectrum of the Glu:Gly, two interesting phenomena occurred, corresponding peaks of a, b, and c protons of L-glutamic acid shift downfield in the spectrum evidence of the presence of stronger hydrogen bonding network, and peaks at around 2.3, 4.1, 4.2, and 4.4 ppm appeared for the formation of ester impurities (**Figure 4.7**). This is reasonable because L-glutamic acid has higher number of -COOH groups in its structure compared to L-(+)-arginine, which could provide stronger interaction to the -OH groups of glycerol at high mixing temperature.

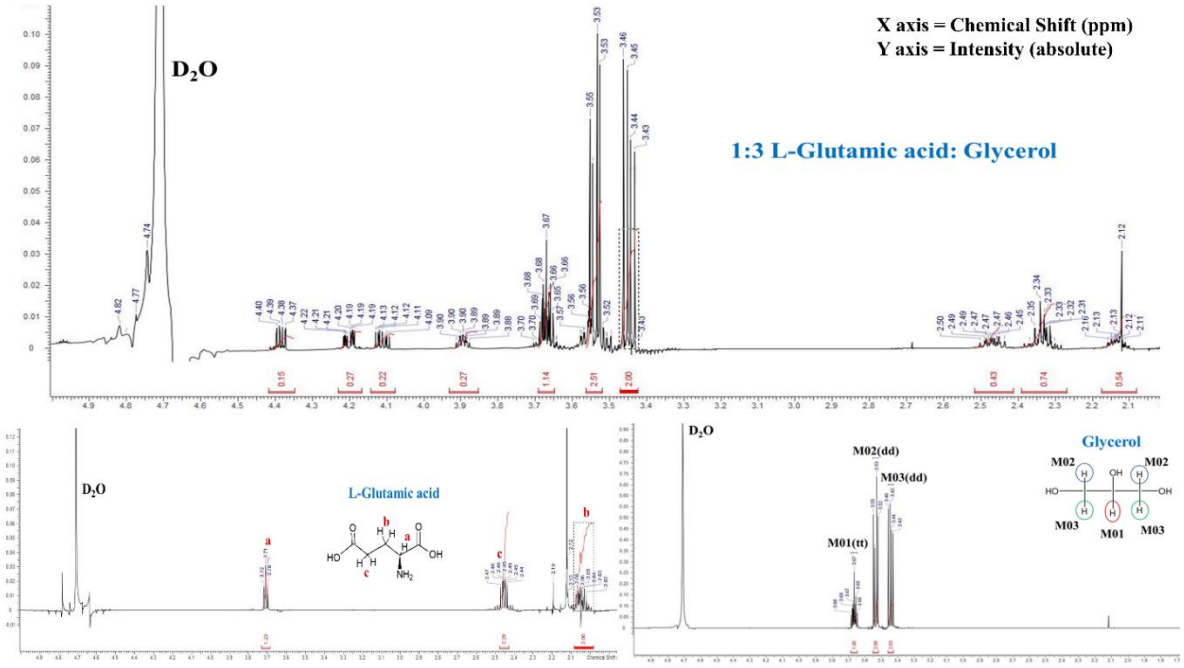

Figure 4.7. ^{1}H-NMR spectra of 1:3 L-glutamic acid:glycerol, L-glutamic acid, and glycerol.

Florindo *et al.* observed the formation of ester impurities when they formed DES using -OH of cholinium cation and -COOH of glutaric acid [203] We previously observed that heat mixing of choline chloride and acid molecules form hydrophobic DESs, but produce

ester impurities simultaneously [331] Those studies verified that ester formation is quite common during if the components contain acid and alcohol groups and they are mixed at higher temperature (>50°C). Therefore, a controlled formulation system should be introduced when synthesizing a DES using -COOH and -OH containing molecules.

4.3.4. Determination of Lignin Monomers. Quantitative monomeric structural characterization of the lignin and its residue are carried out by gas chromatographic analysis. The identified monomers are mostly phenolic compounds, including vanillin, 2,4-di-tert-butylphenol, and methyl salicylate, where o-terphenyl is used as an internal standard.

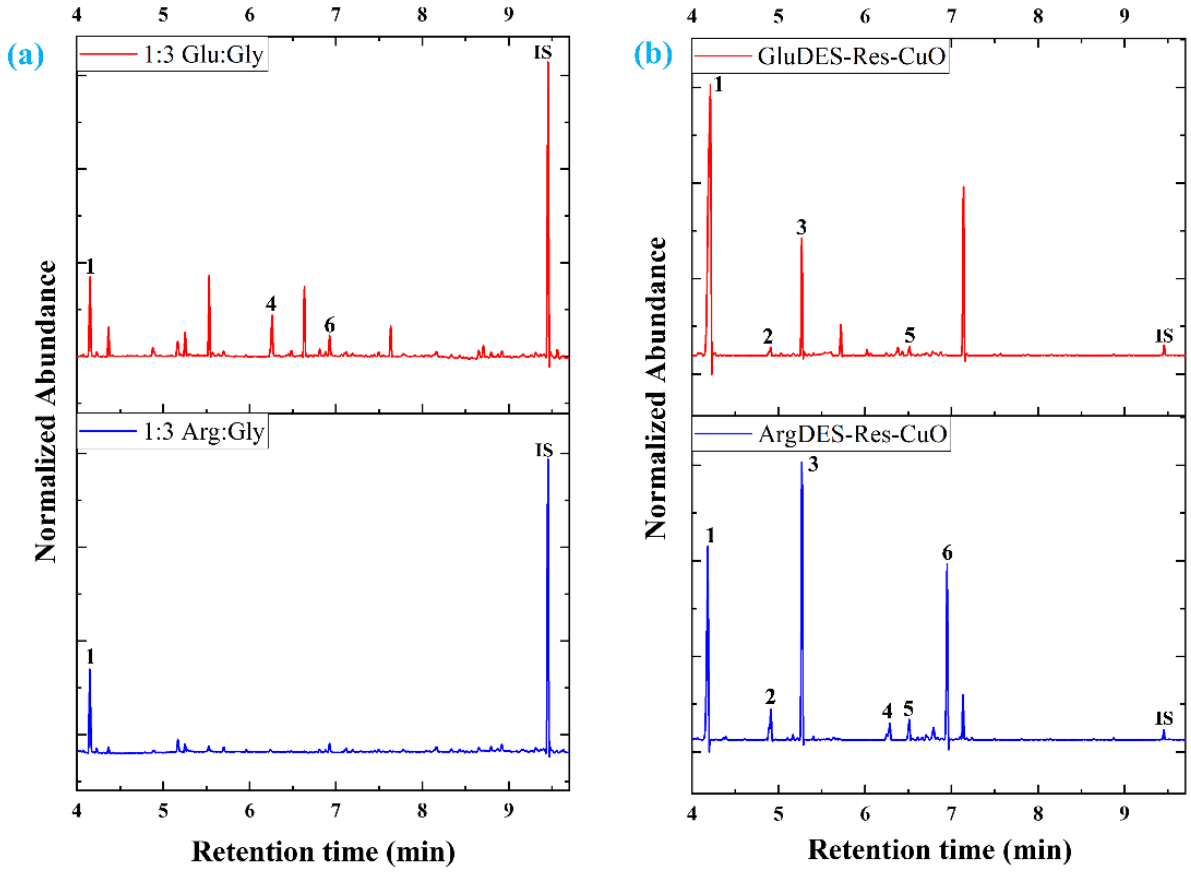

Figure 4.8. GC-MS chromatograms of monomers extracted from the lignin (a) are depolymerized by AADES's (1:3 L-glutamic acid:glycerol and 1:3 L-arginine:glycerol) treatment followed by (b) the monomers extracted from their residues are depolymerized using CuO oxidation.

Lignin depolymerization was conducted using a two-step treatment, depolymerization of lignin using the AADES followed by CuO oxidative depolymerization of their residues. The main aim of this experiment is to see the effect of acidic and basic AADES to the lignin structure. **Figure 4.8** represents the chromatogram of the lignin samples treated by AADESs and their residues. The peaks correspond to certain monomeric compounds which are listed in **Table 4.2**. The figure and table show that lignin and its residue have produced three and four monomeric compounds with Glu:Gly and oxidative treatments, respectively, where 4-methylbenzaldehyde is common in both cases. However, Arg:Gly treatment is highly sensitive, producing only one monomer, while the oxidative reaction produces six monomeric compounds. Between acidic Glu:Gly and basic Arg:Gly, Glu:Gly is found more efficient to depolymerize the lignin sample, while Arg:Gly is more selective.

Table 4.2. Monomeric compounds obtained from the depolymerized lignin and residues analyzed by gas chromatography-mass spectrometry (GC-MS).

Retention time (min)	**Compound number**	**Compound name**
4.17	1	4-Methylbenzaldehyde
4.92	2	Methyl salicylate

5.27	3	1,3-bis-(1,1 dimethylethyl) benzene
6.28	4	Vanillin
6.51	5	1,1´-(1,4-phenylene) bis-Ethanone
6.94	6	2,4-Di-tert-butylphenol

Lignin is a polymer of three monomeric units, which are interconnected through different ether (β-O-4) and C-C bonds [314] The units include p-coumaryl alcohol (H), coniferyl alcohol (G), and sinapyl alcohol (S), which play the major role in its helical structure. Breakdown of those bonds requires selective reaction and the types of monomeric products depend on the reaction conditions. The comparative outcomes of the depolymerization of lignin by the DES treatment followed by CuO oxidation are summarized in **Figure 4.8** and **Table 4.2**. Our study reveals that the acidic-AADES could be more efficient to breakdown of β-O-4 linkages. Oxidative depolymerization of its residue shows no peak for vanillin, which suggests Glu-DES extracted most of the vanillin monomer from the studied lignin. Primary level molecular dynamics simulation was conducted to get insights of the spontaneous interactions among the components of DES and the lignin surface. It suggests that when Glu-DES molecules interact with lignin, its glycerol molecules tend to make stronger interactions with the polar functional groups of lignin compared to the Arg-DES, which could help to turn the H, G, and S moieties apart from each other. Glutamic acid molecules could have helped to make the glycerol interactions stronger.

CHAPTER FIVE

SUMMARY AND FUTURE PERSPECTIVES

Chemical industries are looking for green and sustainable process technologies. One approach is to search for solvents which are alternatives to the inherently toxic and eco-unfriendly organic solvents or the expensive ionic liquids. Therefore, applications of the DESs have drawn considerable interest from the pharmaceutical industry, engineering, and academia, since DESs are safer, nonvolatile, nonflammable, cheaper to formulate, tunable, typically nontoxic, and a lot of them are applicable to biological systems.

Pharmaceuticals primarily rely on oral dosage form, which are mostly solid APIs. Many of the solid APIs have poor solubility, permeability, bioavailability, and thus their therapeutic actions cannot be achieved at the required efficiency in biological systems. These problems could be solved in a less expensive and greener way by formulating them as THEDESs. Depressing the melting point enhances their permeability, intestinal absorption, dissolution rate, and solubility profile. Enhancing their bioavailability could improve the pharmacokinetic and ADMET properties, too. High viscosity of the DESs could be a major hindrance of their wide variety of applications, but addition of glycerol and water or changing the molar ratios of the components could be the easiest ways to overcome the issue. Similar to THEDESs, amino acid-based DESs could also be applicable to improve the bioavailability of various drugs and proteins. Since nonbonding interactions play an important role for the formulation of the DESs, detailed structural insights of the DESs lead to making them more efficient. It is important to know that which compounds have been used for the formulation of the THEDESs and AADESs. Complete knowledge of their

formulation, structures, and applications will certainly help to know the gaps in these research areas. Therefore, in this review, we have studied the formulation conditions, molar ratios, compounds used for the formulations, structural features, and the applications of the THEDESs and AADESs. Although both types of DES have mainly been used for the pharmaceutical applications, AADES have also shown a lot of promise in other fields, such as extraction, synthesis, and separation.

In this thesis work, we have investigated interactions between the HBA and HBD molecules in two types of THEDES by combined computational and experimental techniques. Analyzing RDF data generated from MD simulations demonstrate that there are several hydrogen bonds between ChCl and ASA, specially between the –OH of ASA and Cl^- of ChCl. Density functional theory calculations show that Cl^- is acting as charge transfer bridge between Ch^+ and ASA, which is observed in RDF analysis. The CHELPG partial charge analysis and NBO charge analysis reveal that the positive charge at the cationic core as well as the hydroxyl group of Ch^+ have been decreased and transferred to ASA through chloride bridge. Kamlet-Taft parameters, α, β, and π* experimentally confirmed that Cl^- plays the most important role to transfer charges in the hydrogen bonding network of the THEDES. Thermochemical data acquired from the DFT calculation proved the spontaneity of the formation of its conformers. Experimental Raman and IR spectrum of 1:1 ChCl:ASA is compared with the spectra of ChCl and ASA. Some of the peaks of ChCl and ASA spectra are nearly disappeared or merged in the spectrum of 1:1 ChCl:ASA, which is a clear indication of hydrogen bond formation or the formation of THEDES. The computed Raman and IR showed the similar features; however, computed spectra show more peaks compared to the experimental spectra. Hence, it is difficult to

differentiate the peaks located below 2000 cm^{-1} or specifically the peaks of fingerprint region. Principal component analysis effectively assists to compare not only the spectra of ChCl, ASA, and the four cluster conformers of 1:1 ChCl: ASA of that region, but also demonstrates that the spectral features of ChCl and ASA are totally distinctive and the conformer's spectral features are in between ChCl and ASA. This study was started with three major quests, mentioned at the introduction. The MD simulation generates the representative conformers through which the possible orientations of the micro-structures are determined. Together RDF and spectral data analyses confirm that the hydrogen bonding and the interaction patterns involved in the system cause the depression of the melting point. The DFT calculations and solvatochromic parameters provide the information about charge dislocation, which is the major driving force acting behind the formation of the THEDES. Similar to the ChCl:Aspirin THEDES, experimental mass spectrometry, IR, solvatochromism, and computational approaches helped to elucidate the structural features of the studied 1:1 L-men:AA DES system. Mass spectrometry measurement confirms the formation of 1:1 L-men:AA DES system in ambient temperature. However, such system is not observed when temperature is elevated to 50 °C during the formulation. The most stable cluster conformers of the DES are determined using MD simulation followed by DFT calculation approach. By monitoring the structures and vibrational spectra, it can be concluded that the major nonbonding interactions among menthol and acetic acid are $O(20)_{Men}…H(39)\text{-}O(38)_{AA}$ and $O(20)\text{-}H(21)_{Men}…O(37)_{AA}$, which are mainly responsible for the formation of the studied DES. Radial distribution function calculations showed that along with the classical hydrogen bonds, nonclassical hydrogen bonds (e.g., C-H…O) from alkyl tails of the menthol and acetic acid help to form

strong network throughout the DES system, and help to delocalize the charge cloud from one component to another one. VCD spectroscopy followed by PCA is as an excellent approach to analyze the nonbonding interactions and chirality transfer of a chiral molecule-based DES. These insights could be useful to study the emerging research areas, such as amino acid-based DES[332] and DES-protein interactions [333]

Water-based deep eutectic solvents are sustainable and environment friendly. They are easier to formulate, cheaper, and safer for a wide range of applications. Thermal study proved that the WDESs are applicable from extremely low temperature to high temperature. Although solubilities of the metal halides decreased compared to their solubilities in water, their high polarizability values indicate that they could increase the solubilities of a wide range of compounds (e.g., active pharmaceutical ingredients). The studies of their physicochemical properties will certainly help to understand the role of water molecules in the formation and disruption of a DES. FT-IR and Raman spectroscopy explained how ChCl and water form WDESs by forming strong classical and weak nonclassical hydrogen bonds. Quantum mechanical calculation and RDF by molecular dynamics studies helped to understand their microstructural insights. The RDF analysis shows that Cl^- is performing as a bridge in between Ch^+ and water through hydrogen bonding as well as the structural disruption of ChCl, leading to significant contribution in the special physical properties shown by WDES. Again, there are also other hydrogen bonding present in between the oxygens and hydrogens of water and Ch^+. The interactions lead the WDESs to show their unique physical properties. Cheaper formulations, nontoxic constituents, extremely low melting points, higher polarizability, comparable viscosity to other common DESs, and neutral pH make the DESs as suitable media for the

pharmaceutical applications. Solubility and cell-based experiments proved the formulated WDES as a promising media for biological experiments. Besides, the WDESs could selectively dissolve some important metal ions (e.g., Li^{+} and Co^{2+}) or metallic compounds. Overall, water-based DESs have showed a lot of promise and will need to be explored further in various fields, such as biological, pharmaceutical, and analytical chemistry research.

Amino acid-based deep eutectic solvents were successfully formulated using glycerol, which is sustainable and environment friendly. They are easier to formulate, cheaper, and safer for a wide range of applications. Thermal study proved that the AADESs are easily applicable at the freezing temperature of water and temperatures as high as 150°C. Rigorous spectroscopic study suggests that the formulated DES are pure enough to apply for depolymerization of lignin. Since combination of spectroscopic and spectrometric studies can capture any kind of the formation of ester impurity in AADES, it is crucial to make sure the extent of impurities before going for any further application. The formulation process could be optimized further to keep the formation of ester as less as possible. Depolymerization of lignin using AADESs was studied using comparative analysis of the depolymerization of lignin samples and their residues. This study reveals that acidic, less viscous, and more stable glutamic acid-based AADES can cleave the linkages of the lignin structure. Glycerol might form clusters around the H, G, S moieties and form stronger hydrogen bonds, which helps to cleave the ether and carbon-carbon linkages.

All these outcomes suggest that the advancement and utilization of these emerging DESs could create a safer and greener future for the pharmaceutical, chemical, biochemical,

biotechnology, agricultural, and food industries. Some factors, such as addition of excessive water to adjust the viscosity of a DES could eventually lead to its reduced efficacy, their nonbonding interactions could be disrupted in the biological system, and the hygroscopic nature of their components could damage nanostructures and need to be considered during the formulation and the use of the DESs. Therefore, it is essential to conduct extensive studies to optimize and scale the reported processes from laboratory to pilot scale. It is also important to consider the principles of the green chemistry to make the processes safer and sustainable.

REFERENCES

[1] U. Nations, A/RES/55/2: United Nations Millennium Declaration, 2000.

[2] USEPA, Summary of the Pollution Prevention Act, 42 U.S.C. §13101 et seq. (1990), USEPA. (1990). https://www.epa.gov/laws-regulations/summary-pollution-prevention-act.

[3] P.T. Anastas, J.C. Warner, Green Chemistry: Theory and Practice, Oxford University Press, New York, USA, 1998.

[4] R.K. Henderson, C. Jiménez-González, D.J.C. Constable, S.R. Alston, G.G.A. Inglis, G. Fisher, J. Sherwood, S.P. Binks, A.D. Curzons, Expanding GSK's solvent selection guide – embedding sustainability into solvent selection starting at medicinal chemistry, Green Chemistry. 13 (2011) 854–862. https://doi.org/10.1039/c0gc00918k.

[5] M.K. Tran, M.-T.F. Rodrigues, K. Kato, G. Babu, P.M. Ajayan, Deep eutectic solvents for cathode recycling of Li-ion batteries, Nature Energy. (2019). https://doi.org/10.1038/s41560-019-0368-4.

[6] The Five Domains of Sustainability A Paradigm for Urban Management, (n.d.).

[7] A. Marteel-Parrish, K.M. Newcity, Highlights of the impacts of green and sustainable chemistry on industry, academia and society in the USA, Johnson Matthey Technology Review. 61 (2017) 207–221. https://doi.org/10.1595/205651317X695776.

[8] F. Guthrie, On eutexia, Proceedings of the Physical Society of London. 6 (1884) 124–146. https://doi.org/10.1088/1478-7814/6/1/312.

[9] U.G. Hoang Pham, Pharmaceutical Applications of Eutectic Mixtures, Journal of Developing Drugs. 02 (2013) 2–3. https://doi.org/10.4172/2329-6631.1000e130.

[10] A. Abhat, Low temperature latent heat thermal energy storage: Heat storage materials, Solar Energy. 30 (1983) 313–332. https://doi.org/10.1016/0038-092X(83)90186-X.

[11] S. Kahwaji, M.B. Johnson, A.C. Kheirabadi, D. Groulx, M.A. White, Stable, low-cost phase change material for building applications: The eutectic mixture of decanoic acid and tetradecanoic acid, Applied Energy. 168 (2016) 457–464. https://doi.org/10.1016/j.apenergy.2016.01.115.

[12] A. Sari, K. Kaygusuz, Thermal energy storage characteristics of myristic and stearic acids eutectic mixture for low temperature heating applications, Chinese Journal of Chemical Engineering. 14 (2006) 270–275. https://doi.org/10.1016/S1004-9541(06)60070-0.

[13] F. Guthrie, On eutexia, Proceedings of the Physical Society of London. 6 (1884) 124–146. https://doi.org/10.1088/1478-7814/6/1/312.

[14] A. Paiva, R. Craveiro, I. Aroso, M. Martins, R.L. Reis, A.R.C. Duarte, Natural deep eutectic solvents - Solvents for the 21st century, ACS Sustainable Chemistry and Engineering. 2 (2014) 1063–1071. https://doi.org/10.1021/sc500096j.

[15] M. Francisco, A. Van Den Bruinhorst, M.C. Kroon, Low-transition-temperature mixtures (LTTMs): A new generation of designer solvents, Angewandte Chemie - International Edition. 52 (2013) 3074–3085. https://doi.org/10.1002/anie.201207548.

[16] A. Paiva, R. Craveiro, I. Aroso, M. Martins, R.L. Reis, A.R.C. Duarte, Natural deep eutectic solvents - Solvents for the 21st century, ACS Sustainable Chemistry and Engineering. 2 (2014) 1063–1071. https://doi.org/10.1021/sc500096j.

[17] E.L. Smith, A.P. Abbott, K.S. Ryder, Deep Eutectic Solvents (DESs) and Their Applications, Chemical Reviews. 114 (2014) 11060–11082. https://doi.org/10.1021/cr300162p.

[18] A. Triolo, F. lo Celso, M. Brehm, V. di Lisio, O. Russina, Liquid structure of a choline chloride-water natural deep eutectic solvent: A molecular dynamics characterization, Journal of Molecular Liquids. 331 (2021) 115750. https://doi.org/https://doi.org/10.1016/j.molliq.2021.115750.

[19] M.S. Rahman, D.E. Raynie, Thermal behavior, solvatochromic parameters, and metal halide solvation of the novel water-based deep eutectic solvents, Journal of Molecular Liquids. 324 (2021) 114779. https://doi.org/https://doi.org/10.1016/j.molliq.2020.114779.

[20] Y. Dai, G.J. Witkamp, R. Verpoorte, Y.H. Choi, Tailoring properties of natural deep eutectic solvents with water to facilitate their applications, Food Chemistry. 187 (2015) 14–19. https://doi.org/10.1016/j.foodchem.2015.03.123.

[21] M. Sajjadur Rahman, J. Kyeremateng, M. Saha, S. Asare, N. Uddin, M.A. Halim, D.E. Raynie, Evaluation of the experimental and computed properties of choline chloride-water formulated deep eutectic solvents, Journal of Molecular Liquids. (2022) 118520. https://doi.org/https://doi.org/10.1016/j.molliq.2022.118520.

[22] P.T. Anastas, J.C. Warner, Green Chemistry: Theory and Practice, Oxford University Press, New York. (1998).

[23] C. Capello, U. Fischer, K. Hungerbühler, What is a green solvent? A comprehensive framework for the environmental assessment of solvents, Green Chemistry. (2007). https://doi.org/10.1039/b617536h.

[24] N. V. Plechkova, K.R. Seddon, Applications of ionic liquids in the chemical industry, Chemical Society Reviews. (2008). https://doi.org/10.1039/b006677j.

[25] A. Romero, A. Santos, J. Tojo, A. Rodríguez, Toxicity and biodegradability of imidazolium ionic liquids, Journal of Hazardous Materials. (2008). https://doi.org/10.1016/j.jhazmat.2007.10.079.

[26] P. Nockemann, K. Binnemans, K. Driesen, Purification of imidazolium ionic liquids for spectroscopic applications, Chemical Physics Letters. (2005). https://doi.org/10.1016/j.cplett.2005.08.128.

[27] M. Avalos, R. Babiano, P. Cintas, J.L. Jiménez, J.C. Palacios, Greener media in chemical synthesis and processing, Angewandte Chemie - International Edition. (2006). https://doi.org/10.1002/anie.200504285.

[28] H.R. Lobo, B.S. Singh, G.S. Shankarling, Deep eutectic solvents and glycerol: A simple, environmentally benign and efficient catalyst/reaction media for synthesis of N-aryl phthalimide derivatives, Green Chemistry Letters and Reviews. 5 (2012) 487–533. https://doi.org/10.1080/17518253.2012.669500.

[29] I. Mamajanov, A.E. Engelhart, H.D. Bean, N. V. Hud, DNA and RNA in anhydrous media: Duplex, triplex, and G-quadruplex secondary structures in a deep eutectic solvent, Angewandte Chemie - International Edition. 49 (2010) 6310–6314. https://doi.org/10.1002/anie.201001561.

[30] A.P. Abbott, D. Boothby, G. Capper, D.L. Davies, R.K. Rasheed, Deep Eutectic Solvents formed between choline chloride and carboxylic acids: Versatile alternatives to ionic liquids, J Am Chem Soc. 126 (2004) 9142–9147. https://doi.org/10.1021/ja048266j.

[31] K. El Ttaib, The electrodeposition of composite materials using deep eutectic solvents, (2011).

[32] P.M. Mancini, G.G. Fortunato, L.R. Vottero, Molecular solvent/ionic liquid binary mixtures: Designing solvents based on the determination of their microscopic properties, Physics and Chemistry of Liquids. 42 (2004) 625–632. https://doi.org/10.1080/00319100412331320476.

[33] Q. Zhang, K. De Oliveira Vigier, S. Royer, F. Jérôme, Deep eutectic solvents: Syntheses, properties and applications, Chemical Society Reviews. (2012). https://doi.org/10.1039/c2cs35178a.

[34] O.S. Hammond, D.T. Bowron, K.J. Edler, The Effect of Water upon Deep Eutectic Solvent Nanostructure: An Unusual Transition from Ionic Mixture to Aqueous Solution, Angewandte Chemie - International Edition. 56 (2017) 9782–9785. https://doi.org/10.1002/anie.201702486.

[35] M. Kuddushi, G.S. Nangala, S. Rajput, S.P. Ijardar, N.I. Malek, Understanding the peculiar effect of water on the physicochemical properties of choline chloride based deep eutectic solvents theoretically and experimentally, Journal of Molecular Liquids. 278 (2019) 607–615. https://doi.org/10.1016/j.molliq.2019.01.053.

[36] M. Moghimi, A. Roosta, Physical properties of aqueous mixtures of (choline chloride + glucose) deep eutectic solvents, Journal of Chemical Thermodynamics. 129 (2019) 159–165. https://doi.org/10.1016/j.jct.2018.09.029.

[37] L.K. Savi, D. Carpiné, N. Waszczynskyj, R.H. Ribani, C.W.I. Haminiuk, Influence of temperature, water content and type of organic acid on the formation, stability and properties of functional natural deep eutectic solvents, Fluid Phase Equilibria. 488 (2019) 40–47. https://doi.org/10.1016/j.fluid.2019.01.025.

[38] Y. Marcus, Unconventional Deep Eutectic Solvents: Aqueous Salt Hydrates, ACS Sustainable Chemistry and Engineering. 5 (2017) 11780–11787. https://doi.org/10.1021/acssuschemeng.7b03528.

[39] S. Asare, Synthesis , Characterization and Molecular Dynamic Simulations of Aqueous Choline Deep Eutectic Solvents, (2018).

[40] H.G. Morrison, C.C. Sun, S. Neervannan, Characterization of thermal behavior of deep eutectic solvents and their potential as drug solubilization vehicles, International Journal of Pharmaceutics. 378 (2009) 136–139. https://doi.org/10.1016/j.ijpharm.2009.05.039.

[41] Q. Abbas, L. Binder, Synthesis and characterization of choline chloride based binary mixtures, Journal of the Chemical Society Transactions. 33 (2009) 49–59. https://doi.org/10.1017/CBO9781107415324.004.

[42] A.R. Katritzky, D.C. Fara, H. Yang, K. Tämm, T. Tamm, M. Karelson, Quantitative Measures of Solvent Polarity, Chemical Reviews. (2004). https://doi.org/10.1021/cr020750m.

[43] C. Reichardt, Solvatochromic Dyes as Solvent Polarity Indicators, Chemical Reviews. (1994). https://doi.org/10.1021/cr00032a005.

[44] M.A. Ab Rani, A. Brant, L. Crowhurst, A. Dolan, M. Lui, N.H. Hassan, J.P. Hallett, P.A. Hunt, H. Niedermeyer, J.M. Perez-Arlandis, M. Schrems, T. Welton, R. Wilding, Understanding the polarity of ionic liquids, Physical Chemistry Chemical Physics. (2011). https://doi.org/10.1039/c1cp21262a.

[45] M. Saha, M.S. Rahman, M.N. Hossain, D.E. Raynie, M.A. Halim, Molecular and Spectroscopic Insights of a Choline Chloride Based Therapeutic Deep Eutectic Solvent, J Phys Chem A. 124 (2020) 4690–4699. https://doi.org/10.1021/acs.jpca.0c00851.

[46] M.J. Kamlet, The solvatochromic comparison method. I. The .beta.-scale of solvent hydrogen-bond acceptor (HBA) basicities, J. Am. Chem. Soc. 98 (1976) 377–383. https://doi.org/10.1021/ja00418a009.

[47] M.J. Kamlet, R.W. Taft, The solvatochromic comparison method. 2. The .alpha.-scale of solvent hydrogen-bond donor (HBD) acidities, J Am Chem Soc. 98 (1976) 2886–2894. https://doi.org/10.1021/ja00418a009.

[48] M.J. Kamlet, T.N. Hall, J. Boykin, R.W. Taft, Linear Solvation Energy Relationships. 6. Additions to and Correlations with the .pi.* Scale of Solvent Polarities, Journal of Organic Chemistry. 44 (1979) 2599–2604. https://doi.org/10.1021/jo01329a001.

[49] A.P. Abbott, G. Capper, D.L. Davies, K.J. McKenzie, S.U. Obi, Solubility of metal oxides in deep eutectic solvents based on choline chloride, Journal of Chemical and Engineering Data. 51 (2006) 1280–1282. https://doi.org/10.1021/je060038c.

[50] F.S. Ghareh Bagh, M.K.O. Hadj-Kali, F.S. Mjalli, M.A. Hashim, I.M. Alnashef, Solubility of sodium chloride in phosphonium-based deep eutectic solvents, Journal of Molecular Liquids. 199 (2014) 344–351. https://doi.org/10.1016/j.molliq.2014.09.025.

[51] F.S. Ghareh Bagh, M.K.O. Hadj-Kali, F.S. Mjalli, M.A. Hashim, I.M. Alnashef, Solubility of sodium chloride in phosphonium-based deep eutectic solvents, Journal of Molecular Liquids. 199 (2014) 344–351. https://doi.org/10.1016/j.molliq.2014.09.025.

[52] S. Riaño, M. Petranikova, B. Onghena, T. Vander Hoogerstraete, D. Banerjee, M.R.S. Foreman, C. Ekberg, K. Binnemans, Separation of rare earths and other valuable metals from deep-eutectic solvents: A new alternative for the recycling

of used NdFeB magnets, RSC Advances. (2017). https://doi.org/10.1039/c7ra06540j.

[53] G.R.T. Jenkin, A.Z.M. Al-Bassam, R.C. Harris, A.P. Abbott, D.J. Smith, D.A. Holwell, R.J. Chapman, C.J. Stanley, The application of deep eutectic solvent ionic liquids for environmentally-friendly dissolution and recovery of precious metals, Minerals Engineering. (2016). https://doi.org/10.1016/j.mineng.2015.09.026.

[54] K.R. Seddon, A. Stark, M.J. Torres, Influence of chloride, water, and organic solvents on the physical properties of ionic liquids, Pure and Applied Chemistry. 72 (2000) 2275–2287. https://doi.org/10.1351/pac200072122275.

[55] S. Elderderi, C. Leman-Loubière, L. Wils, S. Henry, D. Bertrand, H.J. Byrne, I. Chourpa, C. Enguehard-Gueiffier, E. Munnier, A.A. Elbashir, L. Boudesocque-Delaye, F. Bonnier, ATR-IR spectroscopy for rapid quantification of water content in deep eutectic solvents, Journal of Molecular Liquids. 311 (2020). https://doi.org/10.1016/j.molliq.2020.113361.

[56] J. Gelpi, A. Hospital, R. Goñi, M. Orozco, Molecular dynamics simulations: advances and applications, Advances and Applications in Bioinformatics and Chemistry. 8 (2015) 37. https://doi.org/10.2147/AABC.S70333.

[57] N. Attig, K. Binder, H. Grubmüller, G. Grubmüller, K. Kremer, Computational Soft Matter: From Synthetic Polymers to Proteins edited by, n.d.

[58] I. Shahriar, M.K. Bin Islam, M. Iqfath, A. Rahman, M.A. Halim, Solvent effect on vibrational circular dichroism of chiral amino acids, Theoretical Chemistry Accounts. 138 (2019). https://doi.org/10.1007/s00214-019-2419-0.

[59] K.T. Savjani, A.K. Gajjar, J.K. Savjani, Drug Solubility: Importance and Enhancement Techniques, ISRN Pharmaceutics. (2012). https://doi.org/10.5402/2012/195727.

[60] S.B. Murdande, M.J. Pikal, R.M. Shanker, R.H. Bogner, Aqueous solubility of crystalline and amorphous drugs: Challenges in measurement, Pharmaceutical Development and Technology. 16 (2011) 187–200. https://doi.org/10.3109/10837451003774377.

[61] M.S. Rahman, R. Roy, B. Jadhav, M.N. Hossain, M.A. Halim, D.E. Raynie, Formulation, Structure, and Applications of Therapeutic and Amino Acid-Based Deep Eutectic Solvents: An Overview, Journal of Molecular Liquids. (2020) 114745. https://doi.org/10.1016/j.molliq.2020.114745.

[62] M.S. Rahman, D.E. Raynie, Thermal behavior, solvatochromic parameters, and metal halide solvation of the novel water-based deep eutectic solvents, Journal of

Molecular Liquids. 324 (2021) 114779. https://doi.org/10.1016/j.molliq.2020.114779.

[63] S. Kalepu, V. Nekkanti, Insoluble drug delivery strategies: Review of recent advances and business prospects, Acta Pharmaceutica Sinica B. (2015). https://doi.org/10.1016/j.apsb.2015.07.003.

[64] N.K. Sachan, A. Bhattacharya, S. Pushkar, A. Mishra, Biopharmaceutical classification system: A strategic tool for oral drug delivery technology, Asian Journal of Pharmaceutics. 3 (2009) 76–81. https://doi.org/10.4103/0973-8398.55042.

[65] K.T. Savjani, A.K. Gajjar, J.K. Savjani, Drug Solubility: Importance and Enhancement Techniques, ISRN Pharmaceutics. (2012). https://doi.org/10.5402/2012/195727.

[66] W.L. Hough, M. Smiglak, H. Rodríguez, R.P. Swatloski, S.K. Spear, D.T. Daly, J. Pernak, J.E. Grisel, R.D. Carliss, M.D. Soutullo, J.H. Davis, Jr., R.D. Rogers, The third evolution of ionic liquids: active pharmaceutical ingredients, New Journal of Chemistry. 31 (2007) 1429. https://doi.org/10.1039/b706677p.

[67] E. Saadi, G. White, Rewarding innovation in drug development, American Health and Drug Benefits. (2014).

[68] M.S. Ku, W. Dulin, A biopharmaceutical classification-based Right-First-Time formulation approach to reduce human pharmacokinetic variability and project cycle time from First-In-Human to clinical Proof-Of-Concept, Pharmaceutical Development and Technology. 17 (2012) 285–302. https://doi.org/10.3109/10837450.2010.535826.

[69] G.L. Amidon, H. Lennernäs, V.P. Shah, J.R. Crison, A Theoretical Basis for a Biopharmaceutic Drug Classification: The Correlation of in Vitro Drug Product Dissolution and in Vivo Bioavailability, Pharmaceutical Research: An Official Journal of the American Association of Pharmaceutical Scientists. 12 (1995) 413–420. https://doi.org/10.1023/A:1016212804288.

[70] J. Dressman, J. Butler, J. Hempenstall, C. Reppas, The BCS: Where do we go from here?, Pharmaceutical Technology. 25 (2001) 68–76.

[71] N.K. Sachan, A. Bhattacharya, S. Pushkar, A. Mishra, Biopharmaceutical classification system: A strategic tool for oral drug delivery technology, Asian Journal of Pharmaceutics. 3 (2009) 76–81. https://doi.org/10.4103/0973-8398.55042.

[72] J.M. Custodio, C.-Y. Wu, L.Z. Benet, PREDICTING DRUG DISPOSITION, ABSORPTION / ELIMINATION / TRANSPORTER INTERPLAY AND THE ROLE OF FOOD ON DRUG ABSORPTION, Adv Drug Deliv Rev. 60 (2008) 717–733. https://doi.org/10.1161/CIRCULATIONAHA.110.956839.

[73] N.A. Kasim, M. Whitehouse, C. Ramachandran, M. Bermejo, H. Lennernäs, A.S. Hussain, H.E. Junginger, S.A. Stavchansky, K.K. Midha, V.P. Shah, G.L. Amidon, Molecular properties of WHO essential drugs and provisional biopharmaceutical classification., Mol Pharm. 1 (2004) 85–96. https://doi.org/10.1021/mp034006h.

[74] Z.X. Liu, C. Artmann, Relative bioavailability comparison of different coenzyme Q10 formulations with a novel delivery system., Altern Ther Health Med. 15 (2009) 42–46.

[75] I.M. Aroso, R. Craveiro, Â. Rocha, M. Dionísio, S. Barreiros, R.L. Reis, A. Paiva, A.R.C. Duarte, Design of controlled release systems for THEDES - Therapeutic deep eutectic solvents, using supercritical fluid technology, International Journal of Pharmaceutics. 492 (2015) 73–9. https://doi.org/10.1016/j.ijpharm.2015.06.038.

[76] P.W. Stott, A.C. Williams, B.W. Barry, Transdermal delivery from eutectic systems: enhanced permeation of a model drug, ibuprofen, Journal of Controlled Release. 50 (1998) 297–308. https://doi.org/10.1016/S0168-3659(97)00153-3.

[77] Q. Shen, X. Li, W. Li, X. Zhao, Enhanced intestinal absorption of daidzein by borneol/menthol eutectic mixture and microemulsion, AAPS PharmSciTech. 12 (2011) 1044–1049. https://doi.org/10.1208/s12249-011-9672-4.

[78] M. Saha, M.S. Rahman, M.N. Hossain, D.E. Raynie, M.A. Halim, Molecular and Spectroscopic Insights of a Choline Chloride Based Therapeutic Deep Eutectic Solvent, The Journal of Physical Chemistry A. 124 (2020) 4690–4699. https://doi.org/10.1021/acs.jpca.0c00851.

[79] I.M. Aroso, J.C. Silva, F. Mano, A.S.D. Ferreira, M. Dionísio, I. Sá-Nogueira, S. Barreiros, R.L. Reis, A. Paiva, A.R.C. Duarte, Dissolution enhancement of active pharmaceutical ingredients by therapeutic deep eutectic systems, European Journal of Pharmaceutics and Biopharmaceutics. 98 (2016) 57–66. https://doi.org/10.1016/j.ejpb.2015.11.002.

[80] A.R.C. Duarte, A.S.D. Ferreira, S. Barreiros, E. Cabrita, R.L. Reis, A. Paiva, A comparison between pure active pharmaceutical ingredients and therapeutic deep eutectic solvents: Solubility and permeability studies, European Journal of Pharmaceutics and Biopharmaceutics. 114 (2017) 296–304. https://doi.org/10.1016/j.ejpb.2017.02.003.

[81] A.P. Golovanov, G.M. Hautbergue, S.A. Wilson, L.Y. Lian, A simple method for improving protein solubility and long-term stability, J Am Chem Soc. 126 (2004) 8933–8939. https://doi.org/10.1021/ja049297h.

[82] Y.C. He, D.P. Zhang, Z.C. Tao, Y. Lu, Y. Ding, F. Liu, Z.Z. Zhu, H. Rui, G.W. Zheng, X. Zhang, Improved biosynthesis of ethyl (S)-4-chloro-3-hydroxybutanoate by adding l-glutamine plus glycine instead of NAD+ in β-cyclodextrin-water system, Bioresource Technology. 182 (2015) 98–102. https://doi.org/10.1016/j.biortech.2015.01.111.

[83] Y. Chen, H. Liang, X. Qin, Y. Liu, S. Tian, Y. Yang, S. Wang, Cheap and biodegradable amino acid-based deep eutectic solvents for radioactive iodine capture via halogen bonds, Journal of Molecular Liquids. 303 (2020) 112615. https://doi.org/10.1016/j.molliq.2020.112615.

[84] L. Duan, L.L. Dou, L. Guo, P. Li, E.H. Liu, Comprehensive Evaluation of Deep Eutectic Solvents in Extraction of Bioactive Natural Products, ACS Sustainable Chemistry and Engineering. 4 (2016) 2405–2411. https://doi.org/10.1021/acssuschemeng.6b00091.

[85] Z. Zhang, N. Kang, J. Wang, H. Sui, L. He, X. Li, Synthesis and application of amino acid ionic liquid-based deep eutectic solvents for oil-carbonate mineral separation, Chemical Engineering Science. 181 (2018) 264–271. https://doi.org/10.1016/j.ces.2018.02.023.

[86] Y. Liang, W. Duan, X. An, Y. Qiao, Y. Tian, H. Zhou, Novel betaine-amino acid based natural deep eutectic solvents for enhancing the enzymatic hydrolysis of corncob, Bioresource Technology. 310 (2020) 123389. https://doi.org/10.1016/j.biortech.2020.123389.

[87] I.M. Aroso, R. Craveiro, Â. Rocha, M. Dionísio, S. Barreiros, R.L. Reis, A. Paiva, A.R.C. Duarte, Design of controlled release systems for THEDES - Therapeutic deep eutectic solvents, using supercritical fluid technology, International Journal of Pharmaceutics. 492 (2015) 73–9. https://doi.org/10.1016/j.ijpharm.2015.06.038.

[88] Q. Shen, X. Li, W. Li, X. Zhao, Enhanced intestinal absorption of daidzein by borneol/menthol eutectic mixture and microemulsion, AAPS PharmSciTech. 12 (2011) 1044–1049. https://doi.org/10.1208/s12249-011-9672-4.

[89] J.M. Silva, R.L. Reis, A. Paiva, A.R.C. Duarte, Design of Functional Therapeutic Deep Eutectic Solvents Based on Choline Chloride and Ascorbic Acid, ACS Sustainable Chemistry and Engineering. 6 (2018) 10355–10363. https://doi.org/10.1021/acssuschemeng.8b01687.

[90] M. Saha, M.S. Rahman, M.N. Hossain, D.E. Raynie, M.A. Halim, Molecular and Spectroscopic Insights of a Choline Chloride Based Therapeutic Deep Eutectic Solvent, The Journal of Physical Chemistry A. 124 (2020) 4690–4699. https://doi.org/10.1021/acs.jpca.0c00851.

[91] S. Nazzal, I.I. Smalyukh, O.D. Lavrentovich, M.A. Khan, Preparation and in vitro characterization of a eutectic based semisolid self-nanoemulsified drug delivery system (SNEDDS) of ubiquinone: Mechanism and progress of emulsion formation, International Journal of Pharmaceutics. 235 (2002) 247–265. https://doi.org/10.1016/S0378-5173(02)00003-0.

[92] B. Tarate, A.K. Bansal, Characterization of CoQ 10-lauric acid eutectic system, Thermochimica Acta. 605 (2015) 100–106. https://doi.org/10.1016/j.tca.2015.01.018.

[93] S. Benessam, K. Khimeche, F. Djellouli, M. Benziane, A. Dahmani, Phase diagram of ibuprofen with fatty acids, Journal of Thermal Analysis and Calorimetry. 112 (2013) 317–320. https://doi.org/10.1007/s10973-012-2831-3.

[94] U. Gala, M.C. Chuong, R. Varanasi, H. Chauhan, Characterization and Comparison of Lidocaine-Tetracaine and Lidocaine-Camphor Eutectic Mixtures Based on Their Crystallization and Hydrogen-Bonding Abilities, AAPS PharmSciTech. 16 (2015) 528–536. https://doi.org/10.1208/s12249-014-0242-4.

[95] WHO, Tetracaine hydrochloride (Tetracaini hydrochloridum), in: The International Pharmacopoeia - Ninth Edition, 2019, WHO Department of Essential Medicines and Health Products, 2019.

[96] W. Wang, Y. Cai, Y. Liu, Y. Zhao, J. Feng, C. Liu, Microemulsions based on paeonol-menthol eutectic mixture for enhanced transdermal delivery: formulation development and in vitro evaluation, Artificial Cells, Nanomedicine and Biotechnology. 45 (2017) 1241–1246. https://doi.org/10.1080/21691401.2016.1226178.

[97] K. Bica, J. Shamshina, W.L. Hough, D.R. MacFarlane, R.D. Rogers, Liquid forms of pharmaceutical co-crystals: Exploring the boundaries of salt formation, Chemical Communications. 47 (2011) 2267–2269. https://doi.org/10.1039/c0cc04485g.

[98] Y. Kaplun-Frischoff, E. Touitou, Testosterone skin permeation enhancement by menthol through formation of eutectic with drug and interaction with skin lipids, Journal of Pharmaceutical Sciences. 86 (1997) 1394–1399. https://doi.org/10.1021/js9701465.

[99] A.P. Abbott, E.I. Ahmed, K. Prasad, I.B. Qader, K.S. Ryder, Liquid pharmaceuticals formulation by eutectic formation, Fluid Phase Equilibria. 448 (2017) 2–8. https://doi.org/10.1016/j.fluid.2017.05.009.

[100] C. V. Pereira, J.M. Silva, L. Rodrigues, R.L. Reis, A. Paiva, A.R.C. Duarte, A. Matias, Unveil the Anticancer Potential of Limomene Based Therapeutic Deep Eutectic Solvents, Scientific Reports. 9 (2019) 1–11. https://doi.org/10.1038/s41598-019-51472-7.

[101] W.L. Chiou, S. Niazi, Phase diagram and dissolution-rate studies on sulfathiazole-urea solid dispersions, Journal of Pharmaceutical Sciences. 60 (1971) 1333–1338. https://doi.org/10.1002/jps.2600600908.

[102] S. Kim, J. Chen, T. Cheng, A. Gindulyte, J. He, S. He, Q. Li, B.A. Shoemaker, P.A. Thiessen, B. Yu, L. Zaslavsky, J. Zhang, E.E. Bolton, PubChem 2019 update: Improved access to chemical data, Nucleic Acids Research. 46 (2019) D1102–D1109. https://doi.org/10.1093/nar/gky1033.

[103] P.W. Stott, A.C. Williams, B.W. Barry, Mechanistic study into the enhanced transdermal permeation of a model β-blocker, propranolol, by fatty acids: A melting point depression effect, International Journal of Pharmaceutics. 219 (2001) 161–176. https://doi.org/10.1016/S0378-5173(01)00645-7.

[104] A.D. Woolfson, R.K. Malcolm, K. Campbell, D.S. Jones, J.A. Russell, Rheological, mechanical and membrane penetration properties of novel dual drug systems for percutaneous delivery, Journal of Controlled Release. 67 (2000) 395–408. https://doi.org/10.1016/S0168-3659(00)00230-3.

[105] P. Berton, K.R. Di Bona, D. Yancey, S.A.A. Rizvi, M. Gray, G. Gurau, J.L. Shamshina, J.F. Rasco, R.D. Rogers, Transdermal Bioavailability in Rats of Lidocaine in the Forms of Ionic Liquids, Salts, and Deep Eutectic, ACS Medicinal Chemistry Letters. 8 (2017) 498–503. https://doi.org/10.1021/acsmedchemlett.6b00504.

[106] H. Wang, G. Gurau, J. Shamshina, O.A. Cojocaru, J. Janikowski, D.R. Macfarlane, J.H. Davis, R.D. Rogers, Simultaneous membrane transport of two active pharmaceutical ingredients by charge assisted hydrogen bond complex formation, Chemical Science. 5 (2014) 3449–3456. https://doi.org/10.1039/c4sc01036a.

[107] C.W. Park, H.M. Mansour, T.O. Oh, J.Y. Kim, J.M. Ha, B.J. Lee, S.C. Chi, Y.S. Rhee, E.S. Park, Phase behavior of itraconazole-phenol mixtures and its pharmaceutical applications, International Journal of Pharmaceutics. 436 (2012) 652–658. https://doi.org/10.1016/j.ijpharm.2012.07.054.

[108] M. Lazerges, P. Espeau, S.S. Crauste-Manciet, D. Brossard, Y. Corvis, F. Agnely, N. Huang, Topical emulsions based on mixtures of local eutectic anaesthetics and fatty acids as analgesics, antalgics, or as sexual retardants, 2015.

[109] A. Brodin, A. Nyqvist-Mayer, F. Broberg, T. Wadsten, B. Forslund, Phase diagram and aqueous solubility of the lidocaine-prilocaine binary system, Journal of Pharmaceutical Sciences. 73 (1984) 481–484. https://doi.org/10.1002/jps.2600730413.

[110] A.A. Nyqvist-Mayer, A.F. Brodin, S.G. Frank, Drug release studies on an oil-water emulsion based on a eutectic mixture of lidocaine and prilocaine as the dispersed phase, Journal of Pharmaceutical Sciences. 75 (1986) 365–373. https://doi.org/10.1002/jps.2600750409.

[111] A.P. Abbott, E.I. Ahmed, K. Prasad, I.B. Qader, K.S. Ryder, Liquid pharmaceuticals formulation by eutectic formation, Fluid Phase Equilibria. 448 (2017) 2–8. https://doi.org/10.1016/j.fluid.2017.05.009.

[112] K. Bica, J. Shamshina, W.L. Hough, D.R. MacFarlane, R.D. Rogers, Liquid forms of pharmaceutical co-crystals: Exploring the boundaries of salt formation, Chemical Communications. 47 (2011) 2267–2269. https://doi.org/10.1039/c0cc04485g.

[113] M. Lazerges, I.B. Rietveld, Y. Corvis, R. Céolin, P. Espeau, Thermodynamic studies of mixtures for topical anesthesia: Lidocaine-salol binary phase diagram, Thermochimica Acta. 497 (2010) 124–128. https://doi.org/10.1016/j.tca.2009.08.016.

[114] F. Al-Akayleh, H.H. Mohammed Ali, M.M. Ghareeb, M. Al-Remawi, Therapeutic deep eutectic system of capric acid and menthol: Characterization and pharmaceutical application, Journal of Drug Delivery Science and Technology. 53 (2019) 101159. https://doi.org/10.1016/j.jddst.2019.101159.

[115] C. V. Pereira, J.M. Silva, L. Rodrigues, R.L. Reis, A. Paiva, A.R.C. Duarte, A. Matias, Unveil the Anticancer Potential of Limomene Based Therapeutic Deep Eutectic Solvents, Scientific Reports. 9 (2019) 1–11. https://doi.org/10.1038/s41598-019-51472-7.

[116] J.M. Silva, R.L. Reis, A. Paiva, A.R.C. Duarte, Design of Functional Therapeutic Deep Eutectic Solvents Based on Choline Chloride and Ascorbic Acid, ACS Sustainable Chemistry and Engineering. 6 (2018) 10355–10363. https://doi.org/10.1021/acssuschemeng.8b01687.

[117] R.J. Sánchez-Leija, J.A. Pojman, G. Luna-Bárcenas, J.D. Mota-Morales, Controlled release of lidocaine hydrochloride from polymerized drug-based deep-eutectic

solvents, Journal of Materials Chemistry B. 2 (2014) 7495–7501. https://doi.org/10.1039/c4tb01407c.

[118] S. Kim, J. Chen, T. Cheng, A. Gindulyte, J. He, S. He, Q. Li, B.A. Shoemaker, P.A. Thiessen, B. Yu, L. Zaslavsky, J. Zhang, E.E. Bolton, PubChem 2019 update: Improved access to chemical data, Nucleic Acids Research. 46 (2019) D1102–D1109. https://doi.org/10.1093/nar/gky1033.

[119] B.D. Ribeiro, C. Florindo, L.C. Iff, M.A.Z. Coelho, I.M. Marrucho, Menthol-based eutectic mixtures: Hydrophobic low viscosity solvents, ACS Sustainable Chemistry and Engineering. 3 (2015) 2469–2477. https://doi.org/10.1021/acssuschemeng.5b00532.

[120] S.T.K. Narishetty, R. Panchagnula, Effect of L-menthol and 1,8-cineole on phase behavior and molecular organization of SC lipids and skin permeation of zidovudine, Journal of Controlled Release. 102 (2005) 59–70. https://doi.org/10.1016/j.jconrel.2004.09.016.

[121] S.T.K. Narishetty, R. Panchagnula, Effect of L-menthol and 1,8-cineole on phase behavior and molecular organization of SC lipids and skin permeation of zidovudine, Journal of Controlled Release. 102 (2005) 59–70. https://doi.org/10.1016/j.jconrel.2004.09.016.

[122] A.A. Nyqvist-Mayer, A.F. Brodin, S.G. Frank, Drug release studies on an oil-water emulsion based on a eutectic mixture of lidocaine and prilocaine as the dispersed phase, Journal of Pharmaceutical Sciences. 75 (1986) 365–373. https://doi.org/10.1002/jps.2600750409.

[123] H. Hermanns, M.W. Hollmann, M.F. Stevens, P. Lirk, T. Brandenburger, T. Piegeler, R. Werdehausen, Molecular mechanisms of action of systemic lidocaine in acute and chronic pain: a narrative review, British Journal of Anaesthesia. 123 (2019) 335–349. https://doi.org/10.1016/j.bja.2019.06.014.

[124] J. Cassens, A. Prudic, F. Ruether, G. Sadowski, Solubility of pharmaceuticals and their salts as a function of pH, Industrial and Engineering Chemistry Research. 52 (2013) 2721–2731. https://doi.org/10.1021/ie302064h.

[125] H. Wang, G. Gurau, J. Shamshina, O.A. Cojocaru, J. Janikowski, D.R. Macfarlane, J.H. Davis, R.D. Rogers, Simultaneous membrane transport of two active pharmaceutical ingredients by charge assisted hydrogen bond complex formation, Chemical Science. 5 (2014) 3449–3456. https://doi.org/10.1039/c4sc01036a.

[126] P. Berton, K.R. Di Bona, D. Yancey, S.A.A. Rizvi, M. Gray, G. Gurau, J.L. Shamshina, J.F. Rasco, R.D. Rogers, Transdermal Bioavailability in Rats of Lidocaine in the

Forms of Ionic Liquids, Salts, and Deep Eutectic, ACS Medicinal Chemistry Letters. 8 (2017) 498–503. https://doi.org/10.1021/acsmedchemlett.6b00504.

[127] C.W. Park, H.M. Mansour, T.O. Oh, J.Y. Kim, J.M. Ha, B.J. Lee, S.C. Chi, Y.S. Rhee, E.S. Park, Phase behavior of itraconazole-phenol mixtures and its pharmaceutical applications, International Journal of Pharmaceutics. 436 (2012) 652–658. https://doi.org/10.1016/j.ijpharm.2012.07.054.

[128] E.R.C. G.B. Kasting, R.L. Smith, Effects of lipid solubility and molecular size on percutaneous absorption, Pharmacol. Skin 1. 26 (2013) 295–301.

[129] A.R.C. Duarte, A.S.D. Ferreira, S. Barreiros, E. Cabrita, R.L. Reis, A. Paiva, A comparison between pure active pharmaceutical ingredients and therapeutic deep eutectic solvents: Solubility and permeability studies, European Journal of Pharmaceutics and Biopharmaceutics. 114 (2017) 296–304. https://doi.org/10.1016/j.ejpb.2017.02.003.

[130] W. Keung, B.L. Vallee, Daidzin and daidzein suppress free-choice ethanol intake by Syrian Golden hamsters, Proc. Natl. Acad. Sci. USA. 90 (1993) 10008–10012.

[131] R.J. Sánchez-Leija, J.A. Pojman, G. Luna-Bárcenas, J.D. Mota-Morales, Controlled release of lidocaine hydrochloride from polymerized drug-based deep-eutectic solvents, Journal of Materials Chemistry B. 2 (2014) 7495–7501. https://doi.org/10.1039/c4tb01407c.

[132] P. Pradeepkumar, N.K. Rajendran, A.A. Alarfaj, M.A. Munusamy, M. Rajan, Deep Eutectic Solvent-Mediated FA-g-β-Alanine-co-PCL Drug Carrier for Sustainable and Site-Specific Drug Delivery, ACS Applied Bio Materials. 1 (2018) 2094–2109. https://doi.org/10.1021/acsabm.8b00554.

[133] P. Pradeepkumar, R. Sangeetha, S. Gunaseelan, P. Varalakshmi, A.A. Chuturgoon, M. Rajan, Folic Acid Conjugated Polyglutamic Acid Drug Vehicle Synthesis through Deep Eutectic Solvent for Targeted Release of Paclitaxel, ChemistrySelect. 4 (2019) 10225–10235. https://doi.org/10.1002/slct.201902256.

[134] A. Roda, F. Santos, A.A. Matias, A. Paiva, A.R.C. Duarte, Design and processing of drug delivery formulations of therapeutic deep eutectic systems for tuberculosis, Journal of Supercritical Fluids. 161 (2020) 104826. https://doi.org/10.1016/j.supflu.2020.104826.

[135] W.L. Chiou, S. Niazi, Phase diagram and dissolution-rate studies on sulfathiazole-urea solid dispersions, Journal of Pharmaceutical Sciences. 60 (1971) 1333–1338. https://doi.org/10.1002/jps.2600600908.

[136] J. Li, P. Wang, J. Huang, J. Sun, Design and application of a novel ionic liquid with the property of strengthening coenzyme regeneration for whole-cell bioreduction in an ionic liquid-distilled water medium, Bioresource Technology. 175 (2015) 42–50. https://doi.org/10.1016/j.biortech.2014.10.059.

[137] M. Cvjetko Bubalo, S. Vidović, I. Radojčić Redovniković, S. Jokić, New perspective in extraction of plant biologically active compounds by green solvents, Food and Bioproducts Processing. 109 (2018) 52–73. https://doi.org/10.1016/j.fbp.2018.03.001.

[138] W. Leuchtenberger, K. Huthmacher, K. Drauz, Biotechnological production of amino acids and derivatives: Current status and prospects, Applied Microbiology and Biotechnology. 69 (2005) 1–8. https://doi.org/10.1007/s00253-005-0155-y.

[139] B.H. Sarmadi, A. Ismail, Antioxidative peptides from food proteins: A review, Peptides (N.Y.). 31 (2010) 1949–1956. https://doi.org/10.1016/j.peptides.2010.06.020.

[140] A.P. Golovanov, G.M. Hautbergue, S.A. Wilson, L.Y. Lian, A simple method for improving protein solubility and long-term stability, J Am Chem Soc. 126 (2004) 8933–8939. https://doi.org/10.1021/ja049297h.

[141] Y.C. He, D.P. Zhang, Z.C. Tao, Y. Lu, Y. Ding, F. Liu, Z.Z. Zhu, H. Rui, G.W. Zheng, X. Zhang, Improved biosynthesis of ethyl (S)-4-chloro-3-hydroxybutanoate by adding l-glutamine plus glycine instead of NAD+ in β-cyclodextrin-water system, Bioresource Technology. 182 (2015) 98–102. https://doi.org/10.1016/j.biortech.2015.01.111.

[142] Y. Chen, H. Liang, X. Qin, Y. Liu, S. Tian, Y. Yang, S. Wang, Cheap and biodegradable amino acid-based deep eutectic solvents for radioactive iodine capture via halogen bonds, Journal of Molecular Liquids. 303 (2020) 112615. https://doi.org/10.1016/j.molliq.2020.112615.

[143] L. Duan, L.L. Dou, L. Guo, P. Li, E.H. Liu, Comprehensive Evaluation of Deep Eutectic Solvents in Extraction of Bioactive Natural Products, ACS Sustainable Chemistry and Engineering. 4 (2016) 2405–2411. https://doi.org/10.1021/acssuschemeng.6b00091.

[144] Z. Zhang, N. Kang, J. Wang, H. Sui, L. He, X. Li, Synthesis and application of amino acid ionic liquid-based deep eutectic solvents for oil-carbonate mineral separation, Chemical Engineering Science. 181 (2018) 264–271. https://doi.org/10.1016/j.ces.2018.02.023.

[145] Y. Liang, W. Duan, X. An, Y. Qiao, Y. Tian, H. Zhou, Novel betaine-amino acid based natural deep eutectic solvents for enhancing the enzymatic hydrolysis of corncob, Bioresource Technology. 310 (2020) 123389. https://doi.org/10.1016/j.biortech.2020.123389.

[146] Y. Liu, J.B. Friesen, J.B. McAlpine, D.C. Lankin, S.N. Chen, G.F. Pauli, Natural Deep Eutectic Solvents: Properties, Applications, and Perspectives, Journal of Natural Products. 81 (2018) 679–690. https://doi.org/10.1021/acs.jnatprod.7b00945.

[147] M. Cvjetko Bubalo, S. Vidović, I. Radojčić Redovniković, S. Jokić, New perspective in extraction of plant biologically active compounds by green solvents, Food and Bioproducts Processing. 109 (2018) 52–73. https://doi.org/10.1016/j.fbp.2018.03.001.

[148] Y. Liu, J.B. Friesen, J.B. McAlpine, D.C. Lankin, S.N. Chen, G.F. Pauli, Natural Deep Eutectic Solvents: Properties, Applications, and Perspectives, Journal of Natural Products. 81 (2018) 679–690. https://doi.org/10.1021/acs.jnatprod.7b00945.

[149] F.S. Mjalli, Novel amino acids based ionic liquids analogues: Acidic and basic amino acids, J Taiwan Inst Chem Eng. 61 (2016) 64–74. https://doi.org/10.1016/j.jtice.2015.12.020.

[150] Q. Liu, X. Zhao, D. Yu, H. Yu, Y. Zhang, Z. Xue, T. Mu, Novel deep eutectic solvents with different functional groups towards highly efficient dissolution of lignin, Green Chemistry. 21 (2019) 5291–5297. https://doi.org/10.1039/c9gc02306b.

[151] Y. He, Q. Huang, P. Wang, Design and evaluation of novel bio-based deep eutectic solvents for highly efficient bioproduction of chiral aryl alcohol, Journal of Chemical Technology and Biotechnology. (2020). https://doi.org/10.1002/jctb.6386.

[152] F.S. Mjalli, Novel amino acids based ionic liquids analogues: Acidic and basic amino acids, J Taiwan Inst Chem Eng. 61 (2016) 64–74. https://doi.org/10.1016/j.jtice.2015.12.020.

[153] Y. Marcus, Estimation of the Critical Temperatures of Some More Deep Eutectic Solvents from Their Surface Tensions, Advances in Materials Science and Engineering. 2018 (2018) 5749479. https://doi.org/10.1155/2018/5749479.

[154] Y. Dai, J. van Spronsen, G.J. Witkamp, R. Verpoorte, Y.H. Choi, Natural deep eutectic solvents as new potential media for green technology, Analytica Chimica Acta. 766 (2013) 61–68. https://doi.org/10.1016/j.aca.2012.12.019.

[155] G. Li, C. Yan, B. Cao, J. Jiang, W. Zhao, J. Wang, T. Mu, Highly efficient I2 capture by simple and low-cost deep eutectic solvents, Green Chemistry. 18 (2016) 2522–2527. https://doi.org/10.1039/c5gc02691a.

[156] A. Gutiérrez, S. Aparicio, M. Atilhan, Design of arginine-based therapeutic deep eutectic solvents as drug solubilization vehicles for active pharmaceutical ingredients, Physical Chemistry Chemical Physics. 21 (2019) 10621–10634. https://doi.org/10.1039/c9cp01408j.

[157] D. Chandam, A. Mulik, P. Patil, S. Jagdale, D. Patil, S. Sankpal, M. Deshmukh, Oxalic acid dihydrate: Proline (LTTM) as a new generation solvent for synthesis of 3,3-diaryloxindole and chromone based bis(indolyl)alkanes: Green, chromatography free protocol, Journal of Molecular Liquids. 207 (2015) 14–20. https://doi.org/10.1016/j.molliq.2015.02.036.

[158] M.C. Gutiérrez, M.L. Ferrer, C.R. Mateo, F. Del Monte, Freeze-drying of aqueous solutions of deep eutectic solvents: A suitable approach to deep eutectic suspensions of self-assembled structures, Langmuir. 25 (2009) 5509–5515. https://doi.org/10.1021/la900552b.

[159] M. Francisco, A. Van Den Bruinhorst, M.C. Kroon, Low-transition-temperature mixtures (LTTMs): A new generation of designer solvents, Angewandte Chemie - International Edition. 52 (2013) 3074–3085. https://doi.org/10.1002/anie.201207548.

[160] T. Altamash, M.S. Nasser, Y. Elhamarnah, M. Magzoub, R. Ullah, H. Qiblawey, S. Aparicio, M. Atilhan, Gas solubility and rheological behavior study of betaine and alanine based natural deep eutectic solvents (NADES), Journal of Molecular Liquids. 256 (2018) 286–295. https://doi.org/10.1016/j.molliq.2018.02.049.

[161] A. Faraone, D. V. Wagle, G.A. Baker, E.C. Novak, M. Ohl, D. Reuter, P. Lunkenheimer, A. Loidl, E. Mamontov, Glycerol Hydrogen-Bonding Network Dominates Structure and Collective Dynamics in a Deep Eutectic Solvent, Journal of Physical Chemistry B. 122 (2018) 1261–1267. https://doi.org/10.1021/acs.jpcb.7b11224.

[162] Y. He, Q. Huang, P. Wang, Design and evaluation of novel bio-based deep eutectic solvents for highly efficient bioproduction of chiral aryl alcohol, Journal of Chemical Technology and Biotechnology. (2020). https://doi.org/10.1002/jctb.6386.

[163] M.C. Manning, D.K. Chou, B.M. Murphy, R.W. Payne, D.S. Katayama, Stability of protein pharmaceuticals: An update, Pharmaceutical Research. 27 (2010) 544–575. https://doi.org/10.1007/s11095-009-0045-6.

[164] B.M. Baynes, D.I.C. Wang, B.L. Trout, Role of arginine in the stabilization of proteins against aggregation, Biochemistry. 44 (2005) 4919–4925. https://doi.org/10.1021/bi047528r.

[165] D. Shukla, B.L. Trout, Interaction of arginine with proteins and the mechanism by which it inhibits aggregation, Journal of Physical Chemistry B. 114 (2010) 13426–13438. https://doi.org/10.1021/jp108399g.

[166] D. Shukla, B.L. Trout, Understanding the synergistic effect of arginine and glutamic acid mixtures on protein solubility, Journal of Physical Chemistry B. 115 (2011) 11831–11839. https://doi.org/10.1021/jp204462t.

[167] E. Petrova, Innovation in the Pharmaceutical Industry: The Process of Drug Discovery and Development, in: M. Ding et al. (Ed.), Innovation in the Pharmaceutical Industry: The Process of Drug Discovery and Development, Springer Science+Business Media, New York, USA, 2014: pp. 19–81. https://doi.org/10.1007/978-1-4614-7801-0_2.

[168] R.A. Sheldon, The: E factor 25 years on: The rise of green chemistry and sustainability, Green Chemistry. 19 (2017) 18–43. https://doi.org/10.1039/c6gc02157c.

[169] A. M, I. M., Effect of thyroid irradiation on the release of labelled protein-bound iodine in rats, NATURE. 197 (1963) 302–304.

[170] G. Steinhauser, Fukushimas forgotten radionuclides: A review of the understudied radioactive emissions, Environmental Science and Technology. 48 (2014) 4649–4663. https://doi.org/10.1021/es405654c.

[171] S. Xu, S.P.H.T. Freeman, X. Hou, A. Watanabe, K. Yamaguchi, L. Zhang, Iodine isotopes in precipitation: Temporal responses to 129I emissions from the fukushima nuclear accident, Environmental Science and Technology. 47 (2013) 10851–10859. https://doi.org/10.1021/es401527q.

[172] G. Brunner, Supercritical fluids: Technology and application to food processing, Journal of Food Engineering. 67 (2005) 21–33. https://doi.org/10.1016/j.jfoodeng.2004.05.060.

[173] A. Aiyejina, D.P. Chakrabarti, A. Pilgrim, M.K.S. Sastry, Wax formation in oil pipelines: A critical review, International Journal of Multiphase Flow. 37 (2011) 671–694. https://doi.org/10.1016/j.ijmultiphaseflow.2011.02.007.

[174] S. Vashisth, C.P.J. Bennington, J.R. Grace, R.J. Kerekes, Column Flotation Deinking: State-of-the-art and opportunities, Resources, Conservation and Recycling. 55 (2011) 1154–1177. https://doi.org/10.1016/j.resconrec.2011.06.013.

[175] L. He, F. Lin, X. Li, H. Sui, Z. Xu, Interfacial sciences in unconventional petroleum production: from fundamentals to applications, Chemical Society Reviews. 44 (2015) 5446–5494. https://doi.org/10.1039/c5cs00102a.

[176] G. Joana Gil-Chávez, J.A. Villa, J. Fernando Ayala-Zavala, J. Basilio Heredia, D. Sepulveda, E.M. Yahia, G.A. González-Aguilar, Technologies for Extraction and Production of Bioactive Compounds to be Used as Nutraceuticals and Food Ingredients: An Overview, Comprehensive Reviews in Food Science and Food Safety. 12 (2013) 5–23. https://doi.org/10.1111/1541-4337.12005.

[177] C. Manach, A. Scalbert, C. Morand, C. Rémésy, L. Jiménez, Polyphenols: Food sources and bioavailability, American Journal of Clinical Nutrition. 79 (2004) 727–747. https://doi.org/10.1093/ajcn/79.5.727.

[178] L. Marín, E.M. Miguélez, C.J. Villar, F. Lombó, Bioavailability of dietary polyphenols and gut microbiota metabolism: Antimicrobial properties, BioMed Research International. 2015 (2015) 905215. https://doi.org/10.1155/2015/905215.

[179] A. Casapullo, G. Bifulco, I. Bruno, R. Riccio, New bisindole alkaloids of the topsentin and hamacanthin classes from the Mediterranean marine sponge Rhaphisia lacazei, Journal of Natural Products. 63 (2000) 447–451. https://doi.org/10.1021/np9903292.

[180] P. Hazarika, S. Das Sharma, D. Konwar, Efficient synthesis of bis- and tris-indolylalkanes catalyzed by a Brønsted acid-surfactant catalyst in water, Synthetic Communications. 38 (2008) 2870–2880. https://doi.org/10.1080/00397910801979387.

[181] J. Azizian, A.A. Mohammadi, N. Karimi, M.R. Mohammadizadeh, A.R. Karimi, Silica sulfuric acid a novel and heterogeneous catalyst for the synthesis of some new oxindole derivatives, Catalysis Communications. 7 (2006) 752–755. https://doi.org/10.1016/j.catcom.2006.01.026.

[182] P. Paira, A. Hazra, S. Kumar, R. Paira, K.B. Sahu, S. Naskar, P. Saha, S. Mondal, A. Maity, S. Banerjee, N.B. Mondal, Efficient synthesis of 3,3-diheteroaromatic oxindole analogues and their in vitro evaluation for spermicidal potential, Bioorganic and Medicinal Chemistry Letters. 19 (2009) 4786–4789. https://doi.org/10.1016/j.bmcl.2009.06.049.

[183] D. Chandam, A. Mulik, P. Patil, S. Jagdale, D. Patil, S. Sankpal, M. Deshmukh, Oxalic acid dihydrate: Proline (LTTM) as a new generation solvent for synthesis of 3,3-diaryloxindole and chromone based bis(indolyl)alkanes: Green, chromatography free protocol, Journal of Molecular Liquids. 207 (2015) 14–20. https://doi.org/10.1016/j.molliq.2015.02.036.

[184] S. Kalepu, V. Nekkanti, Insoluble drug delivery strategies: review of recent advances and business prospects., Acta Pharm Sin B. 5 (2015) 442–53. https://doi.org/10.1016/j.apsb.2015.07.003.

[185] K.T. Savjani, A.K. Gajjar, J.K. Savjani, Drug Solubility: Importance and Enhancement Techniques, ISRN Pharmaceutics. 2012 (2012) 1–10. https://doi.org/10.5402/2012/195727.

[186] W.L. Hough, M. Smiglak, H. Rodríguez, R.P. Swatloski, S.K. Spear, D.T. Daly, J. Pernak, J.E. Grisel, R.D. Carliss, M.D. Soutullo, J.H. Davis, Jr., R.D. Rogers, The third evolution of ionic liquids: active pharmaceutical ingredients, New Journal of Chemistry. 31 (2007) 1429. https://doi.org/10.1039/b706677p.

[187] E. Saadi, G. White, Rewarding innovation in drug development, American Health and Drug Benefits. 7(7) (2014) 373–374.

[188] M. Moniruzzaman, M. Tamura, Y. Tahara, N. Kamiya, M. Goto, Ionic liquid-in-oil microemulsion as a potential carrier of sparingly soluble drug: Characterization and cytotoxicity evaluation, International Journal of Pharmaceutics. 400 (2010) 243–250. https://doi.org/10.1016/j.ijpharm.2010.08.034.

[189] M. Moniruzzaman, N. Kamiya, M. Goto, Ionic liquid based microemulsion with pharmaceutically accepted components: Formulation and potential applications., J Colloid Interface Sci. 352 (2010) 136–42. https://doi.org/10.1016/j.jcis.2010.08.035.

[190] A. Paiva, R. Craveiro, I. Aroso, M. Martins, R.L. Reis, A.R.C. Duarte, Natural Deep Eutectic Solvents – Solvents for the 21st Century, ACS Sustainable Chemistry & Engineering. 2 (2014) 1063–1071. https://doi.org/10.1021/sc500096j.

[191] A.P. Abbott, D. Boothby, G. Capper, D.L. Davies, R.K. Rasheed, Deep Eutectic Solvents Formed between Choline Chloride and Carboxylic Acids: Versatile Alternatives to Ionic Liquids, J Am Chem Soc. 126 (2004) 9142–9147. https://doi.org/10.1021/ja048266j.

[192] E.L. Smith, A.P. Abbott, K.S. Ryder, Deep Eutectic Solvents (DESs) and Their Applications, Chemical Reviews. 114 (2014) 11060–11082. https://doi.org/10.1021/cr300162p.

[193] P.W. Stott, A.C. Williams, B.W. Barry, Transdermal delivery from eutectic systems: enhanced permeation of a model drug, ibuprofen, Journal of Controlled Release. 50 (1998) 297–308. https://doi.org/10.1016/S0168-3659(97)00153-3.

[194] I.M. Aroso, J.C. Silva, F. Mano, A.S.D. Ferreira, M. Dionísio, I. Sá-Nogueira, S. Barreiros, R.L. Reis, A. Paiva, A.R.C. Duarte, Dissolution enhancement of active pharmaceutical ingredients by therapeutic deep eutectic systems, European Journal of Pharmaceutics and Biopharmaceutics. 98 (2016) 57–66. https://doi.org/10.1016/j.ejpb.2015.11.002.

[195] S.L. Perkins, P. Painter, C.M. Colina, Molecular Dynamic Simulations and Vibrational Analysis of an Ionic Liquid Analogue, The Journal of Physical Chemistry B. 117 (2013) 10250–10260. https://doi.org/10.1021/jp404619x.

[196] S. L. Perkins, P. Painter, C. M. Colina, Experimental and Computational Studies of Choline Chloride-Based Deep Eutectic Solvents, Journal of Chemical & Engineering Data. 59 (2014) 3652–3662. https://doi.org/10.1021/je500520h.

[197] H. Sun, Y. Li, X. Wu, G. Li, Theoretical study on the structures and properties of mixtures of urea and choline chloride, Journal of Molecular Modeling. 19 (2013) 2433–2441. https://doi.org/10.1007/s00894-013-1791-2.

[198] O.S. Hammond, D.T. Bowron, K.J. Edler, Liquid structure of the choline chloride-urea deep eutectic solvent (reline) from neutron diffraction and atomistic modelling, Green Chemistry. 18 (2016) 2736–2744. https://doi.org/10.1039/c5gc02914g.

[199] E. O. Fetisov, D. B. Harwood, I.-F. William Kuo, S. E. E. Warrag, M. C. Kroon, C. J. Peters, J. Ilja Siepmann, First-Principles Molecular Dynamics Study of a Deep Eutectic Solvent: Choline Chloride/Urea and Its Mixture with Water, The Journal of Physical Chemistry B. 122 (2018) 1245–1254. https://doi.org/10.1021/acs.jpcb.7b10422.

[200] D. Shah, F.S. Mjalli, Effect of water on the thermo-physical properties of Reline: An experimental and molecular simulation based approach, Physical Chemistry Chemical Physics. 16 (2014) 23900–23907. https://doi.org/10.1039/c4cp02600d.

[201] M.S. Rahman, R. Roy, B. Jadhav, M.N. Hossain, M.A. Halim, D.E. Raynie, Formulation, Structure, and Applications of Therapeutic and Amino Acid-Based Deep Eutectic Solvents: An Overview, Journal of Molecular Liquids. (2020) 114745. https://doi.org/10.1016/j.molliq.2020.114745.

[202] I.M. Aroso, J.C. Silva, F. Mano, A.S.D. Ferreira, M. Dionísio, I. Sá-Nogueira, S. Barreiros, R.L. Reis, A. Paiva, A.R.C. Duarte, Dissolution enhancement of active

pharmaceutical ingredients by therapeutic deep eutectic systems, European Journal of Pharmaceutics and Biopharmaceutics. 98 (2016) 57–66. https://doi.org/10.1016/j.ejpb.2015.11.002.

[203] C. Florindo, F.S. Oliveira, L.P.N. Rebelo, A.M. Fernandes, I.M. Marrucho, Insights into the synthesis and properties of deep eutectic solvents based on cholinium chloride and carboxylic acids, ACS Sustainable Chemistry and Engineering. 2 (2014) 2416–2425. https://doi.org/10.1021/sc500439w.

[204] J. Wang, Y. Zhou, M. Wang, W. Bi, H. Li, D.D.Y. Chen, High-Throughput Analysis for Artemisinins with Deep Eutectic Solvents Mechanochemical Extraction and Direct Analysis in Real Time Mass Spectrometry, Analytical Chemistry. 90 (2018) 3109–3117. https://doi.org/10.1021/acs.analchem.7b04060.

[205] N. Delgado-Mellado, M. Larriba, P. Navarro, V. Rigual, M. Ayuso, J. García, F. Rodríguez, Thermal stability of choline chloride deep eutectic solvents by TGA/FTIR-ATR analysis, Journal of Molecular Liquids. 260 (2018) 37–43. https://doi.org/10.1016/j.molliq.2018.03.076.

[206] B.D. Ribeiro, C. Florindo, L.C. Iff, M.A.Z. Coelho, I.M. Marrucho, Menthol-based eutectic mixtures: Hydrophobic low viscosity solvents, ACS Sustainable Chemistry and Engineering. 3 (2015) 2469–2477. https://doi.org/10.1021/acssuschemeng.5b00532.

[207] J. Sadlej, J.C. Dobrowolski, J.E. Rode, VCD spectroscopy as a novel probe for chirality transfer in molecular interactions, Chemical Society Reviews. 39 (2010) 1478–1488. https://doi.org/10.1039/b915178h.

[208] L.A. Nafie, Vibrational CD spectrometers, in: Encyclopedia of Spectroscopy and Spectrometry, Elsevier Ltd., 2010: pp. 2899–2909. https://doi.org/10.1016/B978-0-12-803224-4.00081-9.

[209] S. Góbi, E. Vass, G. Magyarfalvi, G. Tarczay, Effects of strong and weak hydrogen bond formation on VCD spectra: A case study of 2-chloropropionic acid, Physical Chemistry Chemical Physics. 13 (2011) 13972–13984. https://doi.org/10.1039/c1cp20797k.

[210] J. Kessler, V. Andrushchenko, J. Kapitán, P. Bouř, Insight into vibrational circular dichroism of proteins by density functional modeling, Physical Chemistry Chemical Physics. 20 (2018) 4926–4935. https://doi.org/10.1039/c7cp08016f.

[211] Q. Wang, Q. Gao, X. Gao, F. Nie, Angle principal component analysis, in: IJCAI International Joint Conference on Artificial Intelligence, International Joint

Conferences on Artificial Intelligence Organization, 2017: pp. 2936–2942. https://doi.org/10.5455/ijlr.20170415115235.

[212] H. Martens, T. Næs, Multivariate Calibration, John Wiley & Sons, Inc, New Jersey, USA, 1992.

[213] P. Yu, Applications of hierarchical cluster analysis (CLA) and principal component analysis (PCA) in feed structure and feed molecular chemistry research, using synchrotron-based fourier transform infrared (FTIR) microspectroscopy, Journal of Agricultural and Food Chemistry. 53 (2005) 7115–7127. https://doi.org/10.1021/jf050959b.

[214] M.S. Rahman, D.E. Raynie, Thermal behavior, solvatochromic parameters, and metal halide solvation of the novel water-based deep eutectic solvents, Journal of Molecular Liquids. (2020) 114779. https://doi.org/10.1016/j.molliq.2020.114779.

[215] M. Saha, M.S. Rahman, M.N. Hossain, D.E. Raynie, M.A. Halim, M.A. Halim, Molecular and Spectroscopic Insights of a Choline Chloride Based Therapeutic Deep Eutectic Solvent, Journal of Physical Chemistry A. 124 (2020) 4690–4699. https://doi.org/10.1021/acs.jpca.0c00851.

[216] S.J. Allen, A.R. Curran, R.H. Templer, W. Meijberg, P.J. Booth, Controlling the folding efficiency of an integral membrane protein, J. Mol. Biol. 342 (2004) 1293–1304.

[217] X. Wu, S. Gao, J.-S. Wang, H. Wang, Y.-W. Huang, Y. Zhao, The surface-enhanced Raman spectra of aflatoxins: spectral analysis, density functional theory calculation, detection and differentiation, Analyst. 137 (2012) 4226. https://doi.org/10.1039/c2an35378d.

[218] C.R. Ashworth, R.P. Matthews, T. Welton, P.A. Hunt, Doubly ionic hydrogen bond interactions within the choline chloride-urea deep eutectic solvent, Physical Chemistry Chemical Physics. 18 (2016) 18145–18160. https://doi.org/10.1039/c6cp02815b.

[219] E.R. Lindahl, Molecular dynamics simulations, Methods in Molecular Biology. 443 (2008) 3–23. https://doi.org/10.1007/978-1-59745-177-2_1.

[220] Q. Wang, Q. Gao, X. Gao, F. Nie, Angle principal component analysis, IJCAI International Joint Conference on Artificial Intelligence. 2 (2017) 2936–2942.

[221] E. Krieger, G. Vriend, New ways to boost molecular dynamics simulations, Journal of Computational Chemistry. 36 (2015) 996–1007. https://doi.org/10.1002/jcc.23899.

[222] J.A. Maier, C. Martinez, K. Kasavajhala, L. Wickstrom, K.E. Hauser, C. Simmerling, ff14SB: Improving the Accuracy of Protein Side Chain and Backbone Parameters from ff99SB, Journal of Chemical Theory and Computation. 11 (2015) 3696–3713. https://doi.org/10.1021/acs.jctc.5b00255.

[223] D. Tom, Y. Darrin, L. Pedersen, Particle mesh Ewald: An N·log(N) method for Ewald sums in large systems, The Journal of Chemical Physics. 98 (1993) 10089–10092. https://doi.org/10.1063/1.464397.

[224] T. Darden, D. York, L. Pedersen, Particle mesh Ewald: An *N* ·log(*N*) method for Ewald sums in large systems, The Journal of Chemical Physics. 98 (1993) 10089–10092. https://doi.org/10.1063/1.464397.

[225] M.J. Frisch, G.W. T., H.B. Schlegel, G.E. Scuseria, M.A. Robb, J.R. Cheeseman, G. Scalmani, V. Barone, B. Mennucci, G.A. Petersson, H. Nakatsuji, M. Caricato, X. Li, H.P. Hratchian, A.F. Izmaylov, J. Bloino, G. Zheng, Sonnenberg, J.L. Hada, F.D. J., Gaussian 09, revision A. 02, Gaussian, Inc., Wallingford, CT, 2009. (1988).

[226] E.D. Glendening, C.R. Landis, F. Weinhold, Natural bond orbital methods, Wiley Interdisciplinary Reviews: Computational Molecular Science. 2 (2012) 1–42. https://doi.org/10.1002/wcms.51.

[227] C.M. Breneman, K.B. Wiberg, Determining atom-centered monopoles from molecular electrostatic potentials. The need for high sampling density in formamide conformational analysis, Journal of Computational Chemistry. 11 (1990) 361–373. https://doi.org/10.1002/jcc.540110311.

[228] M. Basire, P. Parneix, F. Calvo, Finite-temperature IR spectroscopy of polyatomic molecules: A theoretical assessment of scaling factors, Journal of Physical Chemistry A. 114 (2010) 3139–3146. https://doi.org/10.1021/jp9088639.

[229] J. Sanchez, Martens, Harald; Naes, Tormod: Multivariate Calibration. John Wiley & Sons, Chichester 1989, 419+xvii pp., ISBN 0471 90979 3, Biometrical Journal. 33 (1991) 418–418. https://doi.org/10.1002/bimj.4710330407.

[230] B. Igne, S. Talwar, H. Feng, J.K. Drennen, C.A. Anderson, Near-Infrared Spatially Resolved Spectroscopy for Tablet Quality Determination, Journal of Pharmaceutical Sciences. 104 (2015) 4074–4081. https://doi.org/10.1002/jps.24618.

[231] R. Stefanovic, M. Ludwig, G.B. Webber, R. Atkin, A.J. Page, Nanostructure, hydrogen bonding and rheology in choline chloride deep eutectic solvents as a function of the hydrogen bond donor, Physical Chemistry Chemical Physics. 19 (2017) 3297–3306. https://doi.org/10.1039/c6cp07932f.

[232] K. Wendler, J. Thar, S. Zahn, B. Kirchner, Estimating the Hydrogen Bond Energy, The Journal of Physical Chemistry A. 114 (2010) 9529–9536. https://doi.org/10.1021/jp103470e.

[233] M.E. Senko, D.H. Templeton, Unit cells of choline halides and structure of choline chloride, Acta Crystallographica. 13 (1960) 281–285. https://doi.org/10.1107/S0365110X60000728.

[234] D. Carriazo, M.C. Serrano, M.C. Gutiérrez, M.L. Ferrer, F. del Monte, Deep-eutectic solvents playing multiple roles in the synthesis of polymers and related materials, Chemical Society Reviews. 41 (2012) 4996. https://doi.org/10.1039/c2cs15353j.

[235] M. Meot-Ner (Mautner), The Ionic Hydrogen Bond, Chemical Reviews. 105 (2005) 213–284. https://doi.org/10.1021/cr9411785.

[236] I.G. Binev, B.A. Stamboliyska, Y.I. Binev, The infrared spectra and structure of acetylsalicylic acid (aspirin) and its oxyanion: an ab initio force field treatment, Journal of Molecular Structure: THEOCHEM. 378 (2004) 189–197. https://doi.org/10.1016/s0166-1280(96)90972-0.

[237] A.J. Mendoza, T.B. Tighe, G. Chen, L. Wang, M.A. Hickner, In-situ electrochemical degradation of anion exchange membranes, ACS National Meeting Book of Abstracts. (2011).

[238] A.J. Mendoza, T.B. Tighe, G. Chen, L. Wang, M.A. Hickner, In-situ electrochemical degradation of anion exchange membranes, ACS National Meeting Book of Abstracts. (2011).

[239] C.R. Ashworth, R.P. Matthews, T. Welton, P.A. Hunt, Doubly ionic hydrogen bond interactions within the choline chloride-urea deep eutectic solvent, Physical Chemistry Chemical Physics. 18 (2016) 18145–18160. https://doi.org/10.1039/c6cp02815b.

[240] R. Szostak, S. Mazurek, Quantitative determination of acetylsalicylic acid and acetaminophen in tablets by FT-Raman spectroscopy, Analyst. 127 (2002) 144–148. https://doi.org/10.1039/B108240J.

[241] C.F. Araujo, J.A.P. Coutinho, M.M. Nolasco, S.F. Parker, P.J.A. Ribeiro-Claro, S. Rudić, B.I.G. Soares, P.D. Vaz, Inelastic neutron scattering study of reline: Shedding light on the hydrogen bonding network of deep eutectic solvents, Physical Chemistry Chemical Physics. 19 (2017) 17998–18009. https://doi.org/10.1039/c7cp01286a.

[242] S. Zhu, H. Li, W. Zhu, W. Jiang, C. Wang, P. Wu, Q. Zhang, H. Li, Vibrational analysis and formation mechanism of typical deep eutectic solvents: An experimental and theoretical study, Journal of Molecular Graphics and Modelling. 68 (2016) 158–175. https://doi.org/10.1016/j.jmgm.2016.05.003.

[243] Precomputed vibrational scaling factors, Computational Chemistry Comparison and Benchmark DataBase, National Institute of Standards and Technology. (n.d.).

[244] M.J. Kamlet, J.L. Abboud, R.W. Taft, The solvatochromic comparison method. 6. The .pi.* scale of solvent polarities, J Am Chem Soc. 99 (1977) 6027–6038. https://doi.org/10.1021/ja00460a031.

[245] H.G. Hertz, Y. Marcus: Introduction to Liquid State Chemistry . John Wiley & Sons, London, New York, Sidney, Toronto 1977. 357 Seiten, Preis: $ 12,50, $ 24,00, Berichte Der Bunsengesellschaft Für Physikalische Chemie. 82 (1978) 665–665. https://doi.org/10.1002/bbpc.197800140.

[246] Y. Wu, T. Sasaki, K. Kazushi, T. Seo, K. Sakurai, Interactions between Spiropyrans and Room-Temperature Ionic Liquids: Photochromism and Solvatochromism, The Journal of Physical Chemistry B. 112 (2008) 7530–7536. https://doi.org/10.1021/jp800957c.

[247] S. Zhang, X. Qi, X. Ma, L. Lu, Y. Deng, Hydroxyl Ionic Liquids: The Differentiating Effect of Hydroxyl on Polarity due to Ionic Hydrogen Bonds between Hydroxyl and Anions, The Journal of Physical Chemistry B. 114 (2010) 3912–3920. https://doi.org/10.1021/jp911430t.

[248] B.R. Mellein, S.N.V.K. Aki, R.L. Ladewski, J.F. Brennecke, Solvatochromic studies of ionic liquid/organic mixtures., J Phys Chem B. 111 (2007) 131–8. https://doi.org/10.1021/jp0653353.

[249] N.D. Khupse, A. Kumar, Delineating Solute−Solvent Interactions in Binary Mixtures of Ionic Liquids in Molecular Solvents and Preferential Solvation Approach, The Journal of Physical Chemistry B. 115 (2011) 711–718. https://doi.org/10.1021/jp110040a.

[250] C. Chiappe, D. Pieraccini, Determination of Ionic Liquids Solvent Properties Using an Unusual Probe: The Electron Donor−Acceptor Complex between 4,4‘-bis(Dimethylamino)-benzophenone and Tetracyanoethene, The Journal of Physical Chemistry A. 110 (2006) 4937–4941. https://doi.org/10.1021/jp057236f.

[251] L. Crowhurst, P.R. Mawdsley, J.M. Perez-Arlandis, P.A. Salter, T. Welton, Solvent–solute interactions in ionic liquids, Phys. Chem. Chem. Phys. 5 (2003) 2790–2794. https://doi.org/10.1039/B303095D.

[252] G. Degam, Deep Eutectic Solvents Synthesis, Characterization and Applications in Pretreatment of Lignocellulosic Biomass, n.d.

[253] L.R. Snyder, Classification off the Solvent Properties of Common Liquids, Journal of Chromatographic Science. 16 (1978) 223–234. https://doi.org/10.1093/chromsci/16.6.223.

[254] C. Ortega-Zamora, J. González-Sálamo, J. González-Sálamo, C. Hernández-Sánchez, C. Hernández-Sánchez, J. Hernández-Borges, J. Hernández-Borges, Menthol-Based Deep Eutectic Solvent Dispersive Liquid-Liquid Microextraction: A Simple and Quick Approach for the Analysis of Phthalic Acid Esters from Water and Beverage Samples, ACS Sustainable Chemistry and Engineering. 8 (2020) 8783–8794. https://doi.org/10.1021/acssuschemeng.0c02603.

[255] J.L. McCann, A. Rauk, H. Wieser, A conformational study of (1S, 2R, 5S)-(+)-menthol using vibrational circular dichroism spectroscopy, Canadian Journal of Chemistry. 76 (1998) 274–283. https://doi.org/10.1139/v98-014.

[256] J.R. Avilés Moreno, F. Partal Ureña, J.J. López González, Hydrogen bonding network in a chiral alcohol: (1R,2S,5R)-(-)-menthol. Conformational preference studied by IR-Raman-VCD spectroscopies and quantum chemical calculations, Structural Chemistry. 24 (2013) 671–680. https://doi.org/10.1007/s11224-012-0118-8.

[257] I. Shahriar, M.K. Bin Islam, M. Iqfath, A. Rahman, M.A. Halim, Solvent effect on vibrational circular dichroism of chiral amino acids, Theoretical Chemistry Accounts. 138 (2019). https://doi.org/10.1007/s00214-019-2419-0.

[258] S. Rahman, S.M. Hossain, M.T. Rahman, M. Kabir, Analysis of Iron , Scandium , Samarium , and Zinc in Commercial Fertilizers and the Chemistry behind the Stability of These Metals in the Fertilizers, Journal of Agricultural Chemistry and Environment. (2019) 155–171. https://doi.org/10.4236/jacen.2019.83013.

[259] M.S. Rahman, S.M. Hossain, M.T. Rahman, M.A. Halim, M.N. Ishtiak, M. Kabir, Determination of trace metal concentration in compost, DAP, and TSP fertilizers by neutron activation analysis (NAA) and insights from density functional theory calculations, Environmental Monitoring and Assessment. (2017). https://doi.org/10.1007/s10661-017-6328-1.

[260] M. Losada, Y. Xu, Chirality transfer through hydrogen-bonding: Experimental and ab initio analyses of vibrational circular dichroism spectra of methyl lactate in water, Physical Chemistry Chemical Physics. 24 (2007) 3127–3135. https://doi.org/10.1039/b703368k.

[261] V.P. Nicu, J. Autschbach, E.J. Baerends, Enhancement of IR and VCD intensities due to charge transfer, Physical Chemistry Chemical Physics. 10 (2009) 1526–1538. https://doi.org/10.1039/b816151h.

[262] J.F. Deye, T.A. Berger, A.G. Anderson, Nile Red as a Solvatochromic Dye for Measuring Solvent Strength in Normal Liquids and Mixtures of Normal Liquids with Supercritical and Near Critical Fluids, Analytical Chemistry. (1990). https://doi.org/10.1021/ac00205a015.

[263] N.D. Khupse, A. Kumar, Delineating solute-solvent interactions in binary mixtures of ionic liquids in molecular solvents and preferential solvation approach, Journal of Physical Chemistry B. 115 (2011) 711–718. https://doi.org/10.1021/jp110040a.

[264] S. Emami, A. Shayanfar, Deep eutectic solvents for pharmaceutical formulation and drug delivery applications, Pharmaceutical Development and Technology. 25 (2020) 779–796. https://doi.org/10.1080/10837450.2020.1735414.

[265] J. Alsenz, M. Kansy, High throughput solubility measurement in drug discovery and development, Advanced Drug Delivery Reviews. 59 (2007) 546–567. https://doi.org/10.1016/j.addr.2007.05.007.

[266] A. Triolo, F. LoCelso, M. Brehm, V. Di Lisio, O. Russina, Liquid structure of a choline chloride-water natural deep eutectic solvent: A molecular dynamics characterization, Journal of Molecular Liquids. 331 (2021) 115750.

[267] M.J. et al Frisch, Gaussian 09, Revision A.02, Gaussian 09, Revision A.02. (2009).

[268] A. Ali, M.S. Rahman, R. Roy, P. Gambill, D.E. Raynie, M.A. Halim, Structure Elucidation of Menthol-Based Deep Eutectic Solvent using Experimental and Computational Techniques, The Journal of Physical Chemistry A. (2021). https://doi.org/10.1021/acs.jpca.0c10735.

[269] K. Remya, C.H. Suresh, Which density functional is close to CCSD accuracy to describe geometry and interaction energy of small non-covalent dimers? A benchmark study using gaussian09, Journal of Computational Chemistry. 34 (2013) 1341–1353. https://doi.org/10.1002/jcc.23263.

[270] S.A. Smith, K.E. Hand, M.L. Love, G. Hill, D.H. Magers, Conventional strain energies of azetidine and phosphetane: Can density functional theory yield reliable results?, Journal of Computational Chemistry. 34 (2013) 558–565. https://doi.org/10.1002/jcc.23165.

[271] C.R. Ashworth, R.P. Matthews, T. Welton, P.A. Hunt, Doubly ionic hydrogen bond interactions within the choline chloride-urea deep eutectic solvent, Physical

Chemistry Chemical Physics. 18 (2016) 18145–18160. https://doi.org/10.1039/c6cp02815b.

[272] R.L. McCreery, Raman Spectroscopy for Chemical Analysis, 2001. https://doi.org/10.1088/0957-0233/12/5/704.

[273] Origin Lab, Origin(Pro), Version 2021. OriginLab Corporation, Northampton, MA, USA, (2021).

[274] Y. Gu, F. Jérôme, Glycerol as a sustainable solvent for green chemistry, Green Chemistry. (2010). https://doi.org/10.1039/c001628d.

[275] A.E. Díaz-Álvarez, J. Francos, B. Lastra-Barreira, P. Crochet, V. Cadierno, Glycerol and derived solvents: New sustainable reaction media for organic synthesis, Chemical Communications. (2011). https://doi.org/10.1039/c1cc10620a.

[276] A. Pandey, R. Rai, M. Pal, S. Pandey, How polar are choline chloride-based deep eutectic solvents?, Physical Chemistry Chemical Physics. (2014). https://doi.org/10.1039/c3cp53456a.

[277] G. Imperato, New organic solvents based on Carbohydrates, (2006) 1–107.

[278] Origin Lab, Origin(Pro), Version 2020. OriginLab Corporation, Northampton, MA, USA, (n.d.). https://www.originlab.com/index.aspx?go=Company&pid=1130.

[279] L.R. Snyder, Changing reversed-phase high performance liquid chromatography selectivity. Which variables should be tried first?, in: Journal of Chromatography B: Biomedical Applications, 1997. https://doi.org/10.1016/S0378-4347(96)00351-9.

[280] L.R. Snyder, Classification off the solvent properties of common liquids, Journal of Chromatographic Science. (1978). https://doi.org/10.1093/chromsci/16.6.223.

[281] G. Degam, Deep Eutectic Solvents Synthesis, Characterization and Applications in Pretreatment of Lignocellulosic Biomass (Ph.D. Dissertation), South Dakota State University, 2017.

[282] M.C. Gutiérrez, M.L. Ferrer, C.R. Mateo, F. del Monte, Freeze-Drying of Aqueous Solutions of Deep Eutectic Solvents: A Suitable Approach to Deep Eutectic Suspensions of Self-Assembled Structures, Langmuir. 25 (2009) 5509–5515. https://doi.org/10.1021/la900552b.

[283] P.F. Mcmillan, A.M. Hofmeister, Infrared and Raman spectroscopy, VCH Publishers. Inc., New York, USA, 2019. https://doi.org/10.1117/1.1906246.

[284] P.F. Mcmillan, A.M. Hofmeister, Infrared and Raman spectroscopy, VCH Publishers. Inc., New York, USA, 2019. https://doi.org/10.1117/1.1906246.

[285] S. Elderderi, C. Leman-Loubière, L. Wils, S. Henry, D. Bertrand, H.J. Byrne, I. Chourpa, C. Enguehard-Gueiffier, E. Munnier, A.A. Elbashir, L. Boudesocque-Delaye, F. Bonnier, ATR-IR spectroscopy for rapid quantification of water content in deep eutectic solvents, Journal of Molecular Liquids. 311 (2020). https://doi.org/10.1016/j.molliq.2020.113361.

[286] E. Arunan, G.R. Desiraju, R.A. Klein, J. Sadlej, S. Scheiner, I. Alkorta, D.C. Clary, R.H. Crabtree, J.J. Dannenberg, P. Hobza, H.G. Kjaergaard, A.C. Legon, B. Mennucci, D.J. Nesbitt, Defining the hydrogen bond: An account (IUPAC Technical Report), Pure and Applied Chemistry. 83 (2011) 1619–1636. https://doi.org/10.1351/PAC-REP-10-01-01.

[287] Merck, The Merck Index: An Encyclopedia of Chemicals, Drugs, and Biologicals, 13th Ed., Merck Sharp & Dohme Corp., Whitehouse Station, N.J., USA, 2001.

[288] W. M. Haynes, CRC Handbook of Chemistry and Physics, 94th Edition, 2013-2014, 2013. https://doi.org/10.1136/oem.53.7.504.

[289] D.R. Lide, CRC Handbook of Chemistry and Physics, 88th, 2007. https://doi.org/10.1021/ja077011d.

[290] J. Burgess, Metal Ions in Solution, Ellis Horwood Series in Chemical Sciences. New York: Ellis Horwood, 1978.

[291] D.R. Lide, CRC Handbook of Chemistry and Physics 86TH Edition 2005-2006. CRC Press, Taylor & Francis, Boca Raton, FL 2005, p. 3-140, in: CRC Handbook of Chemistry and Physics, 2005. https://doi.org/10.1159/000333116.

[292] W. M. Haynes, CRC Handbook of Chemistry and Physics, 94th Edition, 2013-2014, 2013. https://doi.org/10.1136/oem.53.7.504.

[293] W.M. Haynes, CRC Handbook of Chemistry and Physics, 95th Ed., CRC Press, Taylor & Francis, Boca Raton, FL, USA, 2014. https://doi.org/10.1136/oem.53.7.504.

[294] International group of experts on behalf of ILO and WHO, with the financial assistance of the European Commission. Cobalt (II) Chloride, Physical & Chemical Information., (n.d.).

[295] K.R. Seddon, A. Stark, M.J. Torres, Influence of chloride, water, and organic solvents on the physical properties of ionic liquids, Pure and Applied Chemistry. 72 (2000) 2275–2287. https://doi.org/10.1351/pac200072122275.

[296] Drug Bank, Solubility of salicyclic acid, (n.d.). https://go.drugbank.com/drugs/DB00936 (accessed August 29, 2021).

[297] ILO, Solubility of Acetylsalicylic Acid, (n.d.). https://www.ilo.org/dyn/icsc/showcard.display?p_version=2&p_card_id=0822 (accessed August 29, 2021).

[298] S.H. Yalkowsky, Y. He, P. Jain, Handbook of Aqueous Solubility Data, 2nd ed., CRC Press, Taylor & Francis, Boca Raton, FL, 2010.

[299] Drug Bank, Solubility of 4-Ethoxyacetanilide, (n.d.). https://go.drugbank.com/drugs/DB03783 (accessed August 29, 2021).

[300] R.-M. Dannenfelser, S.H. Yalkowsky, Data base of aqueous solubility for organic non-electrolytes, Science of The Total Environment. 109–110 (1991) 625–628. https://doi.org/https://doi.org/10.1016/0048-9697(91)90214-Y.

[301] HMDB, Solubility of O-toluic acid, (n.d.). https://hmdb.ca/metabolites/HMDB0002340 (accessed August 29, 2021).

[302] E.G. Worthley, C.D. Schott, The toxicity of four concentrations of DMSO, Toxicology and Applied Pharmacology. 15 (1969) 275–281. https://doi.org/10.1016/0041-008X(69)90027-1.

[303] G. Da Violante, N. Zerrouk, I. Richard, G. Provot, J.C. Chaumeil, P. Arnaud, Evaluation of the cytotoxicity effect of dimethyl sulfoxide (DMSO) on Caco2/TC7 colon tumor cell cultures, Biological and Pharmaceutical Bulletin. 25 (2002) 1600–1603. https://doi.org/10.1248/bpb.25.1600.

[304] L. O'Driscoll, N. Walsh, A. Larkin, J. Ballot, W.S. Ooi, G. Gullo, R. O'Connor, M. Clynes, J. Crown, S. Kennedy, MDR1/P-glycoprotein and MRP-1 drug efflux pumps in pancreatic carcinoma, Anticancer Research. 27 (2007) 2115–2120.

[305] J. König, M. Hartel, A.T. Nies, M.E. Martignoni, J. Guo, M.W. Büchler, H. Friess, D. Keppler, Expression and localization of human multidrug resistance protein (ABCC) family members in pancreatic carcinoma, International Journal of Cancer. 115 (2005) 359–367. https://doi.org/10.1002/ijc.20831.

[306] N. Walsh, A. Larkin, S. Kennedy, L. Connolly, J. Ballot, W. Ooi, G. Gullo, J. Crown, M. Clynes, L. O'Driscoll, Expression of multidrug resistance markers ABCB1 (MDR-1/P-gp) and ABCC1 (MRP-1) in renal cell carcinoma, BMC Urology. 9 (2009) 1–7. https://doi.org/10.1186/1471-2490-9-6.

[307] S. Asare, Characterization and Molecular Dynamic Simulations of Aqueous Choline Deep Eutectic Solvents, South Dakota State University, 2018.

[308] M.S. Rahman, R. Roy, B. Jadhav, M.N. Hossain, M.A. Halim, D.E. Raynie, Formulation, structure, and applications of therapeutic and amino acid-based deep eutectic solvents: An overview, Journal of Molecular Liquids. 321 (2020) 114745. https://doi.org/10.1016/j.molliq.2020.114745.

[309] A. Paiva, R. Craveiro, I. Aroso, M. Martins, R.L. Reis, A.R.C. Duarte, Natural Deep Eutectic Solvents – Solvents for the 21st Century, ACS Sustainable Chemistry & Engineering. 2 (2014) 1063–1071. https://doi.org/10.1021/sc500096j.

[310] A. Skulcova, A. Russ, M. Jablonsky, J. Sima, The pH Behavior of Seventeen Deep Eutectic Solvents, BioResources. 13 (2018) 5042–5051.

[311] L. Percevault, T. Delhaye, A. Chaumont, R. Schurhammer, L. Paquin, D. Rondeau, Cold-Spray Ionization Mass Spectrometry of the Choline Chloride-Urea Deep Eutectic Solvent (Reline), Journal of Mass Spectrometry. 56 (2021) e4725. https://doi.org/10.1002/jms.4725.

[312] R. Roy, M.S. Rahman, D.E. Raynie, Recent advances of greener pretreatment technologies of lignocellulose, Current Research in Green and Sustainable Chemistry. 3 (2020). https://doi.org/10.1016/j.crgsc.2020.100035.

[313] W. Den, V.K. Sharma, M. Lee, G. Nadadur, R.S. Varma, Lignocellulosic biomass transformations via greener oxidative pretreatment processes: Access to energy and value added chemicals, Frontiers in Chemistry. 6 (2018) 141. https://doi.org/10.3389/fchem.2018.00141.

[314] R. Roy, J. Balawanthrao, M.S. Rahman, D.E. Raynie, Characterization of Residue from Catalytic Hydrothermal Depolymerization of Lignin, Current Research in Green and Sustainable Chemistry. (2020).

[315] J.A. Onwudili, P.T. Williams, Catalytic depolymerization of alkali lignin in subcritical water: Influence of formic acid and Pd/C catalyst on the yields of liquid monomeric aromatic products, Green Chemistry. 16 (2014) 4740–4748. https://doi.org/10.1039/c4gc00854e.

[316] D. L. Klass, Biomass for renewable energy, fuels, and chemicals, Academic press, 1998.

[317] H. Martens, T. Næs, Multivariate Calibration, John Wiley & Sons, Inc, New Jersey, USA, 1992.

[318] I.A.; Pearl, D.L. Beyer, Studies on lignin and related products, Tappi. 33 (1950) 544–548.

[319] A.W. Rudie, P.W. Hart, Catalysis: A potential alternative to kraft pulping. A synthesis of the literature, PEERS Conference 2014. (2014) 33–46.

[320] R. Roy, B. Jadhav, M.S. Rahman, D.E. Raynie, Characterization of Residue from Catalytic Hydrothermal Depolymerization of Lignin, Current Research in Green and Sustainable Chemistry. (2020). https://doi.org/10.1016/j.crgsc.2020.100052.

[321] L. Dhar, S. Hossain, M.S. Rahman, S.B. Quraishi, K. Saha, F. Rahman, M.T. Rahman, Adsorption Mechanism of Methylene Blue by Graphene Oxide-Shielded Mg-Al-Layered Double Hydroxide from Synthetic Wastewater, Journal of Physical Chemistry A. 125 (2021) 954–965. https://doi.org/10.1021/acs.jpca.0c09124.

[322] E. Krieger, G. Koraimann, G. Vriend, Increasing the precision of comparative models with YASARA NOVA - A self-parameterizing force field, Proteins: Structure, Function and Genetics. 47 (2002) 393–402. https://doi.org/10.1002/prot.10104.

[323] S. Wang, X. Peng, L. Zhong, S. Jing, X. Cao, F. Lu, R. Sun, Choline chloride/urea as an effective plasticizer for production of cellulose films, Carbohydrate Polymers. 117 (2015) 133–139. https://doi.org/10.1016/j.carbpol.2014.08.113.

[324] A.* Haz, P. Strizincova, V. Majova, Skulcova, Jablonsky M, Thermal stability of selected deep eutectic solvents, International Journal of Recent Scientific Research. 7 (2016) 14441–14444.

[325] N. Delgado-Mellado, M. Larriba, P. Navarro, V. Rigual, M. Ayuso, J. García, F. Rodríguez, Thermal stability of choline chloride deep eutectic solvents by TGA/FTIR-ATR analysis, Journal of Molecular Liquids. 260 (2018) 37–43. https://doi.org/10.1016/j.molliq.2018.03.076.

[326] S. Salehpour, M.A. Dubé, Reaction Monitoring of Glycerol Step-Growth Polymerization Using ATR-FTIR Spectroscopy, Macromolecular Reaction Engineering. 6 (2012) 85–92. https://doi.org/10.1002/mren.201100071.

[327] J.L. Guimarães, A.C.T. Cursino, C.K. Saul, M.R. Sierrakowski, L.P. Ramos, K.G. Satyanarayana, Evaluation of castor oil cake starch and recovered glycerol and development of “green” composites based on those with plant fibers, Materials. 9 (2016). https://doi.org/10.3390/ma9020076.

[328] C. Ortega-Zamora, J. González-Sálamo, C. Hernández-Sánchez, J. Hernández-Borges, Menthol-Based Deep Eutectic Solvent Dispersive Liquid–Liquid Microextraction: A Simple and Quick Approach for the Analysis of Phthalic Acid Esters from Water and Beverage Samples, ACS Sustainable Chemistry & Engineering. 8 (2020) 8783–8794. https://doi.org/10.1021/acssuschemeng.0c02603.

[329] A. Cuevas, I. Viera, M.H. Torre, E. Kremer, S.B. Etcheverry, E.J. Baran, Infrared spectra of the copper (II) complexes of amino acids with hydroxylic residues, Afinidad. 56 (1999) 263–265.

[330] A. Ebrahiminezhad, Y. Ghasemi, S. Rasoul-Amini, J. Barar, S. Davaran, Impact of amino-acid coating on the synthesis and characteristics of iron-oxide nanoparticles (IONs), Bull Korean Chem Soc. 33 (2012) 3957–3962. https://doi.org/10.5012/bkcs.2012.33.12.3957.

[331] A.K. Dwamena, Investigating Anions and Hydrophobicity of Deep Eutectic Solvents by Experiment and Computational Simulation (Ph.D. Dissertation), South Dakota State University, 2019.

[332] R. Roy, M.S. Rahman, D.E. Raynie, Recent Advances of Greener Pretreatment Technologies of Lignocellulose, Current Research in Green and Sustainable Chemistry. (2020) 100035. https://doi.org/10.1016/j.crgsc.2020.100035.

[333] A. Sanchez-Fernandez, K.J. Edler, T. Arnold, D. Alba Venero, A.J. Jackson, Protein conformation in pure and hydrated deep eutectic solvents, Physical Chemistry Chemical Physics. 19 (2017) 8667–8670. https://doi.org/10.1039/c7cp00459a.